ABSTRACT

SHANKAR, RAVI. Electroactive Behavior of Nanostructured Polymers. (Under the direction of Professors Tushar K. Ghosh and Richard J. Spontak.)

Electroactive polymers (EAPs) offer a new class of actuator materials, which display physical response to electrical excitation. EAPs can be classified into two groups based on their response mechanism: electronic EAPs and ionic EAPs. Electronic EAPs respond due to electrostatic or Coulomb forces developed on application of an electric field, whereas ionic EAPs are driven by mobility or diffusion of ions. Electronic EAPs display better properties than ionic EAPs in terms of their high actuation strain, reliability and durability, efficiency, and response time. Dielectric electroactive polymers or D-EAPs produce large actuation strain on application of an electric field due to Maxwell stress effect. D-EAPs have superior performance than other EAPs, which is ascribed to their high actuation strain, fast response time, high energy density, and high efficiency. Acrylic elastomer is known to be superior amongst electric EAPs due to its highest areal actuation strain (~160 %), highest elastic energy density (3.4 MJ/m^3), and highest pressure (7 MPa). Generally, all the D-EAPs require very high electric field for actuation.

In this work, we demonstrate that incorporation of a low-volatility, aliphatic-rich solvent (mineral oil) into a nanostructured poly [styrene-b-(ethylene-co-butylene)-b-styrene] (SEBS) triblock copolymer yields physically cross-linked micellar networks, known as thermoplastic elastomer gels (TPEG). This nanostructured material exhibits excellent displacement under an external electric field, therefore refers as electroactive nanostructured polymers (ENP). Comparison of the ENPs investigated here with EAPs previously reported, confirms that the ENP217 system with 5 wt% copolymer yields the highest areal actuation amongst all D-EAPs currently known. Dielectric strength of both ENPs (ENP of 217kDa and 161kDa molecular weights) increases with increasing copolymer fraction. The ENPs introduced here exhibit coupling efficiencies that are comparable, if not superior, to existing EAPs. The mechanical hysteresis behavior of the ENPs reveals that under cyclic loading/unloading at constant strain (100 cycles at 400% strain) these materials exhibit far less nonrecoverable strain unlike acrylic elastomers, which suffer from high viscoelastic losses. In fact, ENPs with 5 wt% copolymer do not posses nonrecoverable strain.

Comparison of ENPs with homopolymer based EAPs demonstrates that these ENPs exhibit a broad range of composition-tunable electromechanical behavior. An increase in copolymer molecular weight (i.e., the population of polarizable phenyl rings within each micelle and correspondingly the length of the swollen EB midblock) or, conversely, a reduction in copolymer concentration significantly improves actuation strain at low electric field in both ENP series.

ENPs investigated in the present work exhibit highly tunable alternatives to conventional homopolymer-based dielectric elastomers. However, these polymeric actuators currently require mechanical prestrain prior to actuation, which restricts their practical application. In this work, we demonstrate that ENPs of a relatively low-molecular-weight SEBS75 triblock copolymer, swollen in the presence of a primarily aliphatic mineral oil, are energy-efficient materials with no (0%) mechanical prestrain. This ENP converts a large fraction of input energy into useful mechanical work more effectively than either (i) ENPs containing high-molecular-weight copolymers of comparable composition or (ii) EAPs based on acrylic dielectric elastomers under no mechanical pre-strain condition. One such ENP exhibits a high elastic energy density (26 kJ/m^3) at 0% prestrain relative to other dielectric EAPs identified so far. Under these conditions, the ENPs afford higher electromechanical coupling efficiencies than the benchmark acrylic elastomers. Mechanical and actuation response of these ENP systems is determined under quasi-static, dynamic and electromechanical loading conditions. Quasi-static properties under tensile and compressive loading, which yield similar results also depend on copolymer concentration and triblock molecular weight. We anticipate that this type of EAP would prove useful in moving the appendages of microrobots, covering/uncovering pixels on video displays or shifting the position of buttons on haptic devices (for smart Braille devices).

Electroactive Behavior of Nanostructured Polymers

By

RAVI SHANKAR

A dissertation submitted to the Graduate Faculty of
North Carolina State University
in partial fulfillment of the
requirements for the Degree of
Doctor of Philosophy

FIBER AND POLYMER SCIENCE

&

MATERIALS SCIENCE AND ENGINEERING

Raleigh
2007

APPROVED BY:

Dr. Saad A. Khan	Dr. Russell E. Gorga	Dr. Stephen Michielsen

Dr. Richard J. Spontak	Dr. Tushar K. Ghosh
(Co-chair of Advisor Committee)	(Co-chair of Advisor Committee)

DEDICATION

This is dedicated to my parents,

whose support and encouragement made all this possible…….

BIOGRAPHY

Ravi Shankar was born in Ghaziabad, in Uttar Pradesh, India. He completed his high school from Government Composite Model School, New Delhi, India in the year 1996. He pursued his undergraduate degree from one of India's renowned institutes of engineering, The National Institute of Technology (NIT), Rourkela. He completed his Bachelor of Engineering degree in the department of Ceramic Engineering with honours from NIT in May 2002. After that, he joined the 'Indian Institute of Science' (IISc), which is the most prestigious research institute in India, for his degree of Master of Science (M.S.) in Materials Engineering. Following his M.S. in 2004, he joined North Carolina State University to pursue his Ph.D. in 'Fiber & Polymer Science' and 'Materials Science & Engineering' with minor in 'Chemical and Biomolecular Engineering'.

ACKNOWLEDGEMENTS

I am eternally grateful to both of my advisors, Professors Tushar Ghosh and Richard Spontak, who have made this foray back to study rich and rewarding. I have learned tremendously from them during these three years at NC State, which helped me to improve my writing, presentation, and technical skills as well as methodologies for solving problems. Additionally, the other members of my committee were also influential for the success of this work. Dr. Khan provided tremendous support and direction in the rheological aspect of this project, permitting full use of the rheometers in his lab.

I would also like to thank several other people for their extensive support and assistance throughout the project. These include Dr. Rudy Bukovnik and Maigan Shrum (Tyco Electronics, Fuquay Varina) for helping me in sample preparation and Dr. John Muth (North Carolina State University) for helping me in dielectric measurements.

My hear felt appreciation to the lab members of the Rheology Group and Polymer Morphology Group who taught me the techniques needed to analyze my data. Additionally, I would also like to thank 'National Textile Centre' for funding this research project.

Last but certainly not the least, I thank my family and my fiancé for their continuous support and encouragement and for showing confidence in me. Big thanks also go out to my friends at NC State, Indian Institute of Science, Bangalore and National Institute of Technology, Rourkela, India. You all know I could not have done this without you. Thank you for all the support and encouragement.

TABLE OF CONTENTS

LIST OF FIGURES ixx
LIST OF TABLES xix
1 Introduction 1
1.1 References 4
2 Dielectric Elastomers as Next-Generation Polymeric Actuators 7
2.1 Abstract 7
2.2 Introduction to Electroactive Polymers 7
2.3 Ionic EAPs 10
2.3.1 Carbon nanotubes (CNTs) 10
2.3.2 Conductive polymers (CPs) 13
2.3.3 Ionic polymer-metal composites (IPMCs) 14
2.4 Electronic EAPs 15
2.4.1 Ferroelectric polymers 16
2.4.2 Dielectric elastomers 17
2.5 Actuation mechanism 20
2.6 Actuation characteristics 21
2.6.1 Actuation stress and blocking force 21
2.6.2 Actuation displacement 22
2.7 Actuation performance 26
2.8 Homogeneous dielectric elastomers 27
2.8.1 Acrylic elastomers 27
2.8.2 Silicone elastomers 28
2.9 Nanostructured dielectric elastomers 29
2.10 Comparison of EAPs 32
2.11 Technological opportunities 35
2.12 Summary 36
2.13 Acknowledgments 37
2.14 Related websites 37

2.15 Notes 37
2.16 References 38
3 Thermoplastic Elastomer Gels –Reinventing the Wheel 43
3.1 Abstract 43
3.2 Introduction 43
3.3 Networks 45
3.4 Gels 46
3.5 Gelation 46
3.6 Classification of Gels 47
3.6.1 Chemical gels 47
3.6.2 Physical Gels 50
3.7 Micellization and Phase Behavior 51
3.8 Types of TPEG 54
3.8.1 Symmetric Styrenic Triblock (ABA) Copolymers based TPEG 55
3.8.2 Non-Symmetric Styrenic Triblock (ABC) and Multiblock Copolymers 62
3.8.3 Symmetric Non-Styrenic Triblock Copolymers 65
3.9 Nanocomposites 66
3.9.1 Organic/Inorganic 67
3.9.2 Organic/Organic 67
3.10 Conclusions 69
3.11 Notes 69
3.12 References 70
4 Electroactive Nanostructured Polymers as Tunable Actuators 81
4.1 Abstract 81
4.2 Introduction 81
4.3 Result and Discussion 84
4.4 Experimental 91
4.5 Acknowledgments 93
4.6 Supplementary Information 93
4.7 Notes 94
4.8 References 95

5 Electromechanical Response of Nanostructured Polymer Systems with No Mechanical Pre-strain 99
5.1 Abstract 99
5.2 Introduction 99
5.3 Experimental 101
5.4 Results and Discussion 102
5.5 Conclusions 108
5.6 Acknowledgments 109
5.7 Notes 109
5.8 References 109
6 Electrical and Mechanical Behavior of Electroactive Nanostructured Polymers 112
6.1 Abstract 112
6.2 Introduction 112
6.3 Experimental 114
6.4 Results and Discussion 117
6.5 Conclusions 125
6.6 Acknowledgments 125
6.7 Notes 125
6.8 References 126
7 Triblock Copolymer Organogels as High-Performance Dielectric Elastomers 130
7.1 Abstract 130
7.2 Introduction 130
7.3 Theoretical Background 133
7.4 Experimental 135
7.4.1 Materials 135
7.4.2 Methods 135
7.5 Results and Discussion 137
7.5.1 Nonlinear Mechanical Behavior 138
7.5.2 Electromechanical Behavior 145
7.6 Conclusions 157
7.7 Acknowledgments 157

7.8 Notes 158
7.9 References 158
8 Conclusions and Future Work 164
8.1 Summary of Present Work 164
8.2 Future work 167
8.2.1 Fundamental behavior of nanostructured EAPs 168
8.2.2 Physical Modification of ENPs 168
8.2.3 Design of novel polar blocks containing EAPs 169
8.3 References 169

LIST OF FIGURES

Figure 2.1 Contemporary examples of state-of-the-art robotic systems: (a) *Albert Hubo* designed on the basis of hydraulics by KAIST and Hanson Robotics, Inc., (adapted from ref. 10 and used with permission from IEEE) and (b) *FLEX 2* designed on the basis of electroactive polymers (EAPs) by SRI International (reprinted from ref. 67 and used with permission from SPIE)..... 9

Figure 2.2 Demonstration of single-wall carbon nanotubes (CNTs) as electroactive materials. High-resolution transmission electron microscopy (HRTEM) image of a lone CNT (adapted from ref. 21 and used with permission from Springer) and an illustration of a single-wall CNT(reprinted from en.wikipedia.org/wiki/Wikipedia:Featured_picture_candidates/ February-2006 and used with permission) are displayed in (a). In (b), the mechanism by which CNT-based actuators operate is illustrated (reprinted from ref. 11 with permission from Elsevier). In (c), experimental data confirm that electrically-driven CNT "paper" (15 □m thick) can bend a polymer film measuring ~0.2 mm thick (adapted from ref. 4 and used with permission from the American Association for the Advancement of Science)..... 12

Figure 2.3 Schematic diagram showing the operational principle of IPMCs. Prior to actuation, the aqueous IPMC is flat (a). Application of an electrical potential promotes migration of cations, thereby causing the IPMC to curve or bend (b). The system eventually adjusts to the applied electrical potential (c) and can return to (a) upon removal of the potential (reprinted from ref. 3 with permission from IEEE). 15

Figure 2.4 In (a), molecular depictions of PVDF, an electrostrictive ferroelectric polymer. The □ phase (with an all-T conformation) is responsible for ferroelectricity, whereas the □ phase (with both T and G conformations) promotes paraelectricity (adapted from ref. 11 and used with permission from Elsevier). In (b), the transverse strain is presented as a function of electric field for PVDF-TrFE modified[36] with 40 wt% CuPc (X, see inset for the chemical structure) and PVDF-TrFE-CTFE (○) modified[38] with two different concentrations of PANi (in vol%): 13 (▲) and 23 (●). The solid line verifies that the strain scales as E^2 in accord with Eq. 3, whereas the dashed and dotted lines (power-law regressions to the data) deviate from this expected behavior and thus serve only as guides for the eye. 18

Figure 2.5 Schematic illustration showing the operational principle of D-EAPs. Prior to actuation, the elastomer film of initial thickness z_0 is coated on each side with a compliant electrode. An applied electric field promotes attraction of the oppositely charged electrodes, thereby introducing a compressive Maxwell stress (σ_M) along the transverse (z) direction. Actuation is normally measured in terms of the lateral (in-plane) dimensional change, and the blocking force along the y-direction (F_y), for example, is identified..... 21
Figure 2.6 Circular experimental setup used to measure the electromechanical behavior of D-EAPs in the presence of an electric field and corresponding optical images. An elastomeric film is commonly subjected to a mechanical prestrain and subsequently fixed to a frame prior to coating the active area on both film surfaces with a compliant electrode. Actuation upon electrical stimulation results in an increase in the active area, which is digitally measured and quantified. 25
Figure 2.7 TEM image of an ENP composed of a microphase-separated SEBS triblock copolymer swollen with a midblock-selective oligomeric oil. The micellar morphology in this 10/90 w/w SEBS/oil system consists of swollen EB midblocks that form a molecular network stabilized by glassy S micelles, which appear electron-opaque (dark) due to selective staining with the vapor of RuO_4(aq). The copolymer network illustrated in the inset displays only bridged midblocks for the sake of clarity (the midblocks may also form loops and dangling ends). 32
Figure 2.8 Comparison of the actuation strain levels achieved for (a) various EAPs as a function of electric potential and (b, c) D-EAPs and a ferroelectric polymer as a function of electric field. The actuation strains are labeled in each part and include (a) lateral area or length, (b) lateral area and (c) transverse. The dotted lines serve as guides for the eye..... 33
Figure 2.9 Dependence of blocking stress on actuation strain for various electroactive materials and systems: inorganic (green), ionic and ferroelectric EAPs (black) and D-EAPs (red). The dotted diagonal lines correspond to different energy densities (blue, labeled), and the red area signifies the characteristics of human muscle. (Modified from the SRI International document at http://ndeaa.jpl.nasa.gov/nasa-nde/lommas/eap/actuators-comp.pdf and used with permission). 35
Figure 3.1 Schematic of $(A\text{-}B)_n$ block copolymers[2]. 44

Figure 3.2 Phase behavior of symmetric diblock (A-B) copolymer based on self consistent mean field theory[23, 24] 45
Figure 3.3 Schematic illustration of percolation theory of network formation.[42] 47
Figure 3.4 Schematic representations of gels (a) Flory III type, (b) Flory II, (C) Flory IV.[32] 49
Figure 3.5 Schematic illustrating chemical and physical crosslinking.[30] 50
Figure 3.6 Schematic representation of critical micelles concentration (CMC) and critical gel concentration (CGC) in BCP solution.[26] 52
Figure 3.7 Possible micelles and aggregates formed by diblock and triblock copolymers in selective solvents. (a) Solvent is selective towards end blocks or B block in case of AB and BAB block copolymers. (b) For high loop/bridge ratio, Flower like micelles in case of BAB triblock copolymer where solvent is selective towards A block. (c) A block selective BAB triblock with some free B block extending into solution. (d) A block selective BAB triblock, branched structure formation where strands of B block extending into the cores of different micelles.[83, 84] 53
Figure 3.8 Chain topologies of (a) diblock and (b) ABA triblock copolymers in selective solvents.[81] 53
Figure 3.9 Stress-strain plot of SBS copolymers diluted with mineral oil varying from 0 to 140 wt%.[119] 56
Figure 3.10 Long period (L) of SBS copolymers diluted with (+) low molecular weight PB (lithane PM), (x) paraffinic oil, and (●) aromatic oil.[121] 56
Figure 3.11 Experimental morphology diagram for SIS (filled symbol) and SEPS (open symbol) triblocks, diluted with mineral oil, displaying composition ranges over which different morphology lamellar (● and ○), cylindrical (▲ and Δ), and micellar (◆ and ◊) have been observed.[109] 57
Figure 3.12 SANS pattern of 12% SEPS (A and B) and SEBS (C and D) TPEGs. A and C original undeformed states. B and D after 100% deformation.[128] 58
Figure 3.13 The position of structure factor maxima q^* plotted as a function of the deformation ratio λ. Solid line indicates the affine deformation. Extension rates were (a) 4E-4 s^{-1} and (b) 1E-2 s^{-1}.[133] 60

Figure 3.14 Phase diagram displaying texture development for normalized shear amplitude and angular frequency where normalized frequency (ω_0) and shear amplitude (γ_0) are 2 s^{-1} and 20%, respectively.[134] 60
Figure 3.15 Compressive stress relaxation plots on a double logarithmic scale for SEBS gels at 25^0C and 15 wt% copolymer at different deformation (λ).[135] (B) Stress relaxation rate [m = -d(log σ)/d(log t)] as a function of temperature for SEBS (87.3 Kg/mol with 32 % S) at 8.5 (□), 11.2 (Δ), and 17.5 wt% (○) and SEBS (260 Kg/mol with 30 % S) at 4.9 ($\Diamond$) and 6.8 wt% ($\triangledown$) at deformation 0.7.[114] 61
Figure 3.16 TEM micrograph of SEBS TPEG with 30, 20, 10 wt% copolymer quenched from 180 to 0^0C.[89] 63
Figure 3.17 TEM micrograph of an annealed SBM/oil blend of (50/50 g/g). (a) RuO_2 stained gels showing hexagonally array of cylinders of M endblocks. (b) OsO_4 stained gels showing both S and M cylinders. (c) Circle in the (b) zoomed here showing PMMA hexagon in the centre and dotted lines showing hexagon of S. (d) schematic illustration of proposed twinned hexagonal structure.[103] 64
Figure 3.18 Schematic illustration of temperature dependent structure of PMMA triblock copolymer gels in alcohols.[141] 66
Figure 4.1 In (A), the operational principle of a conventional elastomeric EAP before and after actuation. Development of a Maxwell stress (labeled) between oppositely charged compliant electrodes squeezes the elastomer, thereby causing lateral displacement of the specimen. The morphology of a midblock-swollen triblock copolymer that self-organizes into glassy micelles connected by a midblock network before and after actuation is schematically depicted in (B). A TEM image (scale marker = 50 nm) of a solvated copolymer system containing 10 wt% SEBS161, with the S-rich micelles selectively stained by the vapor of RuO_4(aq), is included to confirm the existence of the micellar morphology in the inset of (B). 83
Figure 4.2 In (A), a series of digital images showing the effect of electric field (listed values in V/□m) on areal activation in the ENP containing 5 wt% SEBS217. The dependence of areal actuation on electric field is provided in (B) and (C) for ENP systems composed of the SEBS161 and SEBS217 copolymers, respectively, at various concentrations (in wt%): 5

(○), 10 (●), 15 (△), 20 (▲), 25 (◇) and 30 (◆). The solid lines represent exponential fits to the data. 85

Figure 4.3 In (A), the maximum areal actuation strain measured for ENPs varying in SEBS161 (●) or SEBS217 (○) copolymer concentration as a function of near-breakdown electric field at 300% biaxial prestrain. The dependence of the electromechanical coupling factor (K^2) on copolymer concentration is provided in the inset, with K^2 values for other dielectric EAPs (dashed lines) labeled for comparison. The solid lines connect the data in (A). The low-strain tensile behavior (displaying engineering stress) of select ENPs at different copolymer concentrations (in wt%) — 30 (solid lines) and 10 (dashed lines) — at ambient temperature is presented in (B). Results obtained from the VHB 4910 acrylic (heavy dotted line) are included for comparison. The dependence of tensile modulus on copolymer concentration and molecular weight, using the same symbols as in (A), is shown in the inset of (B). The solid lines connect the data. In all cases, the extension rate is 127 mm/min. 88

Figure 4.4Maximum actuation strain presented as a function of electric field for several promising classes of dielectric organic materials: an acrylic,[1] two silicone elastomers[1] (see Table 4.1), a ferroelectric polymer,[9] a single-crystal ferroelectric ceramic,[4] and the ranges of the two series of ENPs under investigation in this work (SEBS161, green; SEBS217, blue). Values shown for polyurethane, as well as natural and synthetic rubber, are calculated from actuation measurements reported in refs. 43 and 44. Data displayed here for dielectric elastomers refer to areal strains, whereas linear strains are included for the two classes of ferroelectric materials. 92

Figure 4.5Low-strain tensile data acquired after 1, 50 and 100 cycles from the SEBS161 (A,B) and SEBS217 (C,D) series at concentrations of 10 (A,C) and 30 (B,D) wt% copolymer. All tests were performed at a constant uniaxial extension rate of 500 mm/min at ambient temperature..... 93

Figure 4.6 Thickness strain due to electrical actuation (s_z) presented as a function of electric field for the dielectric and ferroelectric organic materials displayed in Fig. 4.4 in the text. The cited reference sources are the same as those listed in the caption of Fig. 4.4 with the exception of the ferroelectric polymer.[45] On the basis of its definition, the thickness strain is an inherently negative quantity. The negative sign is routinely omitted in literature reports, and so we adopt this convention here. 94

Figure 5.1Schematic illustration of a dielectric elastomer before and after application of an external electrical potential across the film. The development of a Maxwell stress compresses the film from t_0 to t_a, which depends on the magnitude of the electric field [E in Equation (1)], as well as on several material properties (e.g., ε and compressive modulus). 101
Figure 5.2 (a) Maximum areal actuation strain measured just below the breakdown field presented as a function of SEBS molecular weight for three different ENP systems: 5 wt.-% copolymer biaxially pre-strained to 300% (□), 30 wt.-% copolymer biaxially pre-strained to 300% (▲), and 30 wt.-% copolymer with no pre-strain (●). Values of VHB acrylics under the same conditions (labeled, dashed lines) are included for comparison. The solid line serves as a guide for the eye, and the inset shows the dependence of the maximum areal actuation strain on the extent of biaxial pre-strain for the SEBS217/MO ENP with 5 wt.-% copolymer (the solid line connects the data). (b) Corresponding elastic energy density (US) values of the ENPs with no pre-strain(●) and nonstrained VHB acrylics (dashed lines). The solid line serves to connect the data 104
Figure 5.3 The frequency dependence of the real component of the complex dielectric constant (e0) measured for the VHB acrylic (●) and three SEBS75/MO ENPs varying in concentration (in wt.-% copolymer): 25 (◊), 35 (Δ), and 45 (○). The dashed lines signify the range over which e0 does not vary with frequency 105
Figure 5.4 The dependence of (a) compressive modulus (Y), (b) maximum areal and thickness actuation strain, (c) elastic energy density (U_S), and (d) electromechanical coupling efficiency (K^2) on copolymer concentration for ENPs with no mechanical pre-strain and containing the following copolymers: SEBS75 (○,□), SEBS161 (●,×), and SEBS217 (▲,+). Note that the secondary symbols are only used to denote areal actuation strains in (b). The dashed (and dotted, as labeled) lines identify values measured for the VHB acrylic EAPs in the absence of pre-strain. The solid line in each part serves to connect data displayed for the SEBS75/MO ENP series. 107
Figure 6.1 Schematic illustration of a D-EAP before (left) and after (right) electrical actuation. Electrostatic attraction between the negatively charged compliant electrodes applied to opposing surfaces of the D-EAP generates a normal Maxwell stress upon actuation and compresses the film in the transverse (z) direction. Under isochoric conditions, the film extends laterally along the x and y directions. 114

Figure 6.2 Process diagram depicting measurement of the blocking force generated by a D-EAP upon electrical actuation. In (a), a film is prestrained (an)isotropically along x and y at predetermined strain increments ($\Delta\varepsilon = 25\%$) up to $\varepsilon_{max} = 275\%$. The plastic fixture shown in (b) is bolted on both sides of the prestrained film to lock-in the biaxial deformation, and the fixture is then subjected to uniaxial tensile loading along y to achieve a predetermined final anisotropic prestrain in (c). The specimen is then coated with a compliant electrode on both sides (d) and subsequently subjected to an external potential (e) to induce transverse compression and lateral actuation, which results in a measurable force reduction in the y direction. 116

Figure 6.3 Stress-strain curves generated during uniaxial compression and tension loading, identified by the solid and dashed lines, respectively, at ambient temperature. The dotted lines in (a) identify the regions of the curves from which the compressive (E_C) and tensile (E_T) moduli are determined. Data acquired from the VHB 4910 acrylic elastomer are shown in (a), whereas the compositions of ENPs composed of the SEBS217 and SEBS161 copolymers are labeled in (b) and (c), respectively. 119

Figure 6.4 Engineering (filled symbols) and true (open symbols) tensile moduli (E_T) presented as a function of the compressive modulus (E_C) for several D-EAPs (in wt% copolymer where appropriate): SEBS217 ENP (5, circles; 30, squares), SEBS161 ENP (5, triangles; 30, inverted triangles) and VHB 4910 (diamonds). The dashed line identifies where $E_T = E_C$, and the E_C values were measured by the indirect-contact method described in the text..... 120

Figure 6.5 Values of E_C measured according to different testing protocols and specimen prestrain conditions: no prestrain, direct contact (red), no prestrain, indirect contact (green), 300% biaxial prestrain, direct contact (blue) and 300% biaxial prestrain, indirect contact (white). 120

Figure 6.6 Stress-strain curves generated during uniaxial compression loading of D-EAPs before (filled symbols) and after (open symbols) 300% biaxial prestrain. The VHB 4910 acrylic elastomer is shown as circles, whereas the ENPs containing 5 and 30 wt% SEBS217 (b) and SEBS161 (c) are denoted by triangles and squares, respectively. The solid lines serve to connect the data. 121

Figure 6.7 Force-time curves of (a) the VHB 4910 acrylic elastomer and (b) the ENP composed of 30 wt% SEBS217 upon final prestrain before and after electrical actuation. Regressions of the Zener stress-relaxation model to the data are shown by the dotted lines. Noise in the data reflects hand application of the compliant electrode on each side of the D-EAP film. Sharp downward spikes correspond to the blocking force (F_y, identified in each part) during actuation under an external electric field. 123
Figure 7.1 In (a), a schematic diagram of the mechanism by which a dielectric elastomer actuates upon electrical stimulation. The electric field-induced Maxwell stress and resulting in-plane actuation (along x and y) are labeled. Included are pre- and post-actuation illustrations of the micellar morphology present in selectively swollen triblock copolymer organogels introduced as electroactive nanostructured polymers (ENPs). In (b), a TEM image of the micellar morphology generated in a 10/90 w/w SEBS/MO blend. The styrenic units comprising the micellar core are stained with the vapor of RuO_4(aq) and appear dark. 132
Figure 7.2 In (a), nominal (engineering) tensile stress-strain curves of three ENP systems — ENP75 (◇), ENP161 (△) and ENP217 (○) — evaluated at two copolymer concentrations: 10 and 30 wt% (labeled). In all cases, the extension rate was constant at 127 mm/min. The light solid lines correspond to regressed fits of the modified Mooney-Rivlin model (Eq. 10) to the data, whereas the heavy solid line denotes the stress-strain response of the acrylic dielectric elastomer. In (b), parameters extracted from the modified Mooney-Rivlin and slip-tube network models (labeled) as functions of copolymer molecular weight at a constant copolymer concentration of 30 wt%. The solid and dashed lines serve to connect the data. 141
Figure 7.3 Dependence of the tensile modulus (Y_T) on copolymer concentration in the ENP75 (◇), ENP161 (△) and ENP217 (○) systems at ambient temperature. The solid lines connect the data, whereas the dashed line identifies the modulus for the acrylic elastomer. 142
Figure 7.4 Nominal (engineering) tensile stress-strain curves measured from the ENP161 and ENP217 systems at 10 and 30 wt% copolymer concentrations (labeled) upon cycling 100 times to 400% strain. The degree of hysteresis is given by the nonrecoverable strain, the permanent deformation (shown as a shift in the data along the abscissa) introduced upon repeated extension. 143
Figure 7.5 In (a), the compressive modulus (Y_C) presented as a function of copolymer concentration for the ENP75 (◇), ENP161 (△) and ENP217 (○) series. The solid lines are

power-law fits to the data (with a scaling exponent of 2). The dashed line corresponds to the modulus measured for the acrylic dielectric elastomer. In (b), the compressive modulus is displayed in terms of the nominal (engineering) tensile modulus for the same ENP series as in (a). The solid lines serve to connect the data, whereas the dashed and dotted lines identify the best linear fit of the data and the condition where $Y_C = Y_T$, respectively. Included for comparison is a single datum point measured for the acrylic elastomer (x)..... 144
Figure 7.6 Dependence of the dielectric constant ($\in$) measured for the ENP161 (●) and ENP217 (○) series as a function of copolymer concentration. Included are data previously reported[50] and measured here for the acrylic dielectric elastomer, as well as data provided elsewhere[50] for silicone elastomers..... 146
Figure 7.7 Cross-sectional BSE image of the ENP75 system with 35 wt% copolymer coated with a compliant electrode (Ag particles embedded in silicone). The MO-swollen copolymer is completely carbonaceous (dark), whereas the more electron-dense compliant electrode (arrow) appears light and the Ag particles within the electrode are bright. During fracture under liquid nitrogen, the pliable silicone layer formed protrusions, an example of which is seen in this image (arrowheads)..... 147
Figure 7.8 Actuation strain (s_{act}) measured for the ENP217 series (300% biaxial pre-strain) as functions of applied electric field and copolymer concentration (labeled). The solid lines serve as guides for the eye. The images of the ENP217 systems containing 5 wt% copolymer correspond to pre-actuation (0 V/μm, bottom) and maximum actuation (22 V/μm, top). The active and inactive actuation areas, as well as a reference feature to facilitate comparison between the two images, are displayed in the bottom image..... 149
Figure 7.9 Dependence of the actuation strain (s_{act}) measured for the ENP217 series (300% biaxial pre-strain) with 5 and 30 wt% copolymer (circles and triangles, respectively) at opposite electric polarities (labeled). The solid lines serve as guides for the eye. 150
Figure 7.10 The Maxwell stress (σ_M) as a function of copolymer concentration for the ENP161 (△, ◇) and ENP217 (○, ■) series (300% biaxial pre-strain) evaluated at the dielectric breakdown field computed in terms of the initial specimen thickness (△, ○) and the true specimen thickness (◇, ■). Corresponding values measured for the acrylic elastomer (300% biaxial pre-strain) are displayed as dashed and dotted lines, respectively. 151

Figure 7.11 Maximum actuation and transverse strains (s_{act} and $|s_z|$, respectively) presented as functions of copolymer concentration for the ENP161/MO (△), ENP217/MO (○) and ENP217/αO (●) series (300% biaxial pre-strain) in (a) and (b), respectively. The solid and dashed lines serve to connect the data, whereas the dotted line and shaded region correspond to acrylic (300% biaxial pre-strain) and silicone[39] dielectric elastomers, respectively. 152
Figure 7.12 In (a), the dielectric breakdown field (relative to the initial specimen thickness) displayed as a function of copolymer concentration for the ENP161/MO (△), ENP217/MO (○) and ENP217/αO (●) series (300% biaxial pre-strain). The solid and dashed lines serve to connect the data, whereas the dotted line and shaded region correspond to acrylic (300% biaxial pre-strain) and silicone[39] dielectric elastomers, respectively. In (b), the maximum actuation strain shown in terms of the dielectric breakdown field for the same series as in (a). The acrylic (x) and silicone (+) elastomers are included for comparison..... 153
Figure 7.13 Dependence of the electromechanical coupling efficiency (K^2) on copolymer concentration for the ENP161/MO (△), ENP217/MO (○) and ENP217/αO (●) series (300% biaxial pre-strain). The solid and dashed lines serve to connect the data, whereas the dotted line and shaded region correspond to acrylic (300% biaxial pre-strain) and silicone[39] dielectric elastomers, respectively. 155
Figure 7.14 Energy density (F) values displayed as a function of copolymer concentration for the ENP161/MO (△) and ENP217/MO (○) series. The light dashed and dotted lines (labeled) and the shaded region correspond to acrylic and silicone[39] dielectric elastomers, respectively. Dielectric elastomers shown above the heavy dashed line have been subjected to mechanical pre-strain (300% biaxial for both the ENP and acrylic elastomers) prior to actuation. At conditions included below the heavy dashed line, the ENP75 (◇) and acrylic elastomers are relaxed (0% pre-strain) prior to actuation. The solid lines serve to connect the data..... 156

LIST OF TABLES

Table 2.1 Comparison of various inorganic and organic electroactive materials.[a] 11
Table 2.2 Common electrical and mechanical properties of homogeneous D-EAPs.[a] 19
Table 2.3 Common electrical and mechanical properties of homogeneous D-EAPs.[a] 31
Table 3.1Gels classifications[*] 48
Table 3.2Flory's structural classification of gels 49
Table 3.3 Diblock vs Triblock copolymers gels 54
Table 4.1Actuation Behavior of ENPs Varying in Composition and Other Dielectric EAPs[a] 90
Table 6.1D-EAP Blocking Stresses Measured in this Study. 124

CHAPTER 1

1 Introduction

The history of human civilization has been, arguably, most deeply influenced by contemporary materials technologies. As a result historians have defined distinct periods of human history as "stone age," "iron age," etc. Polymers and polymer-composites are proving to be the "materials" of current time. Many new polymer-based innovative material technologies, labeled as "smart materials", are capable of autonomous response to changing environmental stimuli, through embedded sensing and response capabilities. In many instances these capabilities match or surpass those that are found in nature. In the last decade, a new class of materials called Electroactive polymers (EAP) has emerged that respond to external electrical stimulation by displaying a significant shape or size displacement[1,2]. EAPs can be generally classified into two categories based on their mechanism of response namely electronic EAP and ionic EAP[1]. Electronic EAPs respond due to electrostatic or Coulomb forces developed on application of an electric field, however ionic EAPs are driven by mobility or diffusion of ions. Common EAPs are ionic polymer-metal composites (IPMC),[3,4] ferroelectric polymers,[5-7] single-wall carbon nanotubes,[8,9] conducting polymers[10,11] and electroelastomers, also known as dielectric elastomers.[1,12] Electronic EAPs exhibit superior properties than ionic EAPs in terms of their high actuation strain, reliability and durability, efficiency, and response time[1,13]. Among electronic EAPs, dielectric elastomers have shown the most promising properties. Dielectric electroactive polymers or D-EAPs have better performance than other EAPs in terms of their actuation strain, response time, high energy density, and high efficiency. Various elastomeric materials such as acrylic foams, various silicone, polyurethane, ethylene propylene, fluroelastomer, and isoprene have been investigated and reported in the literature as D-EAP. In general, acrylic elastomer is known to be superior in terms of its highest areal actuation strain (~160 %), highest elastic energy density (3.4 MJ/m^3), and highest pressure (7 MPa)[2]. However, almost all the D-EAPs reported thus far are derived form homopolymers such as acrylic, silicone, and polyurethane[1,2,13]. Generally, all of the D-EAPs require very high electric field for actuation relative to ionic EAPs. Some are not easily processable or shapeable into useful devices. In

addition, a large uniaxial or biaxial prestrain (often >100%) is commonly required in conjunction with the use of dielectric EAPs to enhance their actuation performance[2]. Common dielectric EAP actuator are typically used in tube, rolled, bow, bowtie, frame-supported and laminated configurations that are designed to support the required prestrain.[14,15] These prestrain fixtures occupy substantial space and weigh considerably more than the dielectric polymer films.[15] Performance parameters of dielectric elastomer actuators, such as the elastic energy density, are consequently reduced by an order of magnitude or two due to overhead (e.g., packaging) or additional required structures associated with them.[16] In addition, the performance of dielectric elastomers can vary with time since stress relaxation of the viscoelastic matrix eventually serves to release the initial prestrain applied.[17] Furthermore, stress concentration located at the interface between the dielectric elastomer film and the rigid support limits the life span of these actuators. Until now, efforts to improve the electromechanical response of D-EAPs have been restricted to addition of fillers or design refinements[15-17]. There is hardly any published report on material development toward better electroactive behavior of polymers. Zhang et al. altered the actuation response of silicone from materials standpoint that is by changing the type and concentration of hardener[18,19]. Only silicone and polyurethane properties are modified, and these generally exhibit lower electromechanical response compared to acrylic[1,2,13,16,19]. Zhang et al. observed that variation of the hardener concentration has small effect on the dielectric constant of the silicones[19]. Superior electromechanical response was achieved with silicones of lowest modulus.

The research described here is aimed at developing EAP materials with widely tunable electromechanical properties and improved response at low electrical fields. The innovative approach involves use of thermoplastic elastomer gels whose properties can be tailored to a large extent by changing the composition of the homopolymers as well as that of the solvents.

The dissertation is presented as a collection of papers. All of the chapters, with the exception of 1 and 8, is written in the form of review or research papers that are either in press or have been submitted or being prepared for submission to appropriate peer-reviewed journals. As a result the reader may notice some redundancy of introductory information

because the papers are intended to be sufficiently independent. A short description of each is provided below to help readers navigate.

Chapter 1. Introduction to EAPs and outline of thesis.

Chapter 2. Includes review of pertinent literature. It gives detailed account of different EAPs: their principle of actuation, advantage, and limitations. Primary focus of this review is dielectric EAPs. Dielectric elastomers based on homopolymers are discussed in details here. In addition, important materials and performance parameters of D-EAPs are compared. This chapter has been accepted for publication in *Soft Matter* and is currently in press.

Chapter 3. Details of thermoplastic elastomer gels (TPEGs) is discussed here. Micellization of block copolymers and gel types (both physical and chemical gels) are discussed with particular emphasis on physical gels. Thermoplastic elastomer gels are broadly classified as styrenic and non-styrenic based gels. Styrenic gels are considered more relevant to the current work and are therefore discussed in more detail. This chapter will be submitted to *Macromolecular Rapid Communication* for publication.

Chapter 4. Describes the fabrication of tunable nanostructured electroactive polymers (ENPs). These ENPs are based on poly[styrene-*b*-(ethylene-*co*-butylene)-*b*-styrene] (SEBS) triblock copolymers. Tunability of ENPs is achieved by either selecting SEBS of different molecular weights or changing the copolymer fraction. Electromechanical behavior of ENPs is determined and compared with current dielectric elastomers. This chapter is slated to be published in *Advanced Materials* and is currently in press.

Chapter 5. Electromechanical behavior of ENPs of under no-prestrain condition is explored here. In addition, an attempt is made to make actuator material exhibiting high energy density under no-prestrain. The focus of this chapter is lower molecular weight triblock ENPs. Behavior of these ENP systems is compared with other D-EAPs. This chapter is published in *Macromolecular Rapid Communication*.

Chapter 6. Mechanical and electrical properties of ENPs of three different molecular weight is investigated and compared with acrylic foam. Mechanical properties of acrylic and ENPs are investigaed under tensile and compressive loading conditions. Compressive properties of ENPs are evaluated under various levels of in-plane prestrains . The ENPs are also evaluated for blocking stress under isometric conditions. This chapter has been submitted to *Sensors and Actuators A* for publication.

Chapter 7 Electromechanical behavior of SEBS triblock copolymers of three different molecular weights is explained. A comparison between both material and performance properties of ENPs is made as a function of molecular weights and copolymer fractions. Effect of midblock selective oil type on actuation behavior also presented. In addition, results of both electrical and mechanical cycling on ENPs are investigated. This chapter is submitted to *Macromolecules* for publication.

Chapter 8 Includes summary of the present study and recommendations for future work.

1.1 References

1. Bar-Cohen, Y. in Electroactive Polymer (EAP) Actuators as Artificial Muscles: Reality, Potential, and Challenges (ed Bar-Cohen, Y.) (SPIE Press, Bellingham, WA, 2004).
2. Pelrine, R., Kornbluh, R., Pei, Q. & Joseph, J. High-Speed Electrically Actuated Elastomers with Strain Greater Than 100%. *Science* **287**, 836-839 (2000).
3. Zhang, S., Randall, C. A. & Shrout, T. R. Electromechanical properties in rhombohedral bisco[sub 3]-pbtio[sub 3] single crystals as a function of temperature. *Jpn. J. Appl. Phys.*, Part 2 **42**, L1152 (2003).
4. Park, S. & Shrout, T. R. Ultrahigh strain and piezoelectric behavior in relaxor based ferroelectric single crystals. *J. Appl. Phys.* **82**, 1804-1811 (1997).

5. Zhang, Q. M. *et al*. An all-organic composite actuator material with a high dielectric constant. *Nature* **419**, 284-287 (2002).

6. Huang, C., Zhang, Q.M., deBotton, G. & Bhattacharya, K. All-organic dielectric-percolative three-component composite materials with high electromechanical response. *Appl. Phys. Lett.* **84**, 4391-4393 (2004).

7. Chu,B., Zhou,X., Ren,K., Neese,B., Lin,M., Wang,Q., Bauer,F. & Zhang,Q.M. A dielectric polymer with high electric energy density and fast discharge speed. *Science* **313**, 334-336 (2006).

8. Baughman, R. H. Playing nature's game with artificial muscles. *Science* **308**, 63-65 (2005).

9. Baughman, R. H. *et al*. Carbon nanotube actuators. *Science* **284**, 1340-1344 (1999).

10. Berdichevsky, Y. & Lo, Y. H. Polypyrrole nanowire actuators. *Adv. Mater.* **18**, 122-125 (2006).

11. Vozzi, G., Carpi, F. & Mazzoldi, A. Realization of conducting polymer actuators using a controlled volume microsyringe system. *Smart Mater. Struct.* **15**, 279 (2006).

12. Ha, S. M., Yuan, W., Pei, Q., Pelrine, R. & Stanford, S. Interpenetrating polymer networks for high-performance electroelastomer artificial muscles. *Adv. Mater.* **18**, 887-891 (2006).

13. Madden, J. D. W. *et al*. Artificial muscle technology: physical principles and naval prospects. *IEEE J. Oceanic Eng.* **29**, 706-728 (2004).

14. Pei, Q., Rosenthal, M., Stanford, S., Prahlad, H. & Pelrine, R. Multiple-degrees-of-freedom electroelastomer roll actuators. *Smart Mater. Struct.* **13**, N86-N92 (2004).

15. Pei, Q., Pelrine, R., Stanford, S., Kornbluh, R., Rosenthal, M., Meijer, K. & Full, R. J. Multifunctional electroelastomer rolls and their application for biomimetic walking robots. *Proc. SPIE Int. Soc. Opt. Eng.* **4698**, 246-253 (2002).

16. Pons, J. L. *Emerging Actuator Technologies A Micromechatronic Approach* (Wiley, Chichester, England , Hoboken, NJ, 2005), 2, p. 731.

17. Choi, H.R., Jung, K., Chuc, N.H., Jung, M., Koo, I., Koo, J., Lee, J., Lee, J., Nam, J. & Cho, M. Effects of prestrain on behavior of dielectric elastomer actuator. *Proc. SPIE.* **5759**, 283-291 (2005).

18. Zhang, X., Löwe, C., Wissler, M., Jähne, B. & Kovacs, G. Dielectric Elastomers in Actuator Technology. *Adv. Eng. Mater.* 7, 361-367 (2005).

19. Zhang, X. Q., Wissler, M., Jaehne, B. Broennimannm R.,& Kovacs, G. Effect of Crosslinking, Prestrain and Dielectric Filler on the Electromechanical Response of a New Silicone and Comparision with Acrylic Elastomer. *Proc. SPIE.* **5385**, 78-86 (2004).

CHAPTER 2

2 Dielectric Elastomers as Next-Generation Polymeric Actuators

2.1 Abstract

Due to their versatile properties, robust behavior, facile processability and low cost, organic polymers have become the material of choice for an increasing number of mature and cutting-edge technologies. In the last decade or so, a new class of polymers capable of responding to external electrical stimulation by displaying significant size or shape change has emerged. These responsive materials, collectively referred to as electroactive polymers (EAPs), are broadly classified as electronic or ionic according to their operational mechanism. Electronic EAPs generally exhibit superior performance relative to ionic EAPs in terms of actuation strain, reliability, durability and response time. Among electronic EAPs, dielectric elastomers exhibit the most promising properties that mimic natural muscle for use in advanced robotics and smart prosthetics, as well as in haptic and microfluidic devices. Elastomers derived from homopolymers such as acrylics and silicones have received considerable attention as dielectric EAPs, whereas novel dielectric EAPs based on selectively swollen nanostructured block copolymers with composition-tailorable properties have only recently been reported. Here, we provide an overview of various EAPs in terms of their operational mechanisms, uses and shortcomings, as well as a detailed account of dielectric elastomers as next-generation actuators.

2.2 Introduction to Electroactive Polymers

Fundamental and technological interest in electroactive polymers (EAPs), representing a broad class of organic actuators that exhibit large dimensional changes relative to their inorganic counterparts upon electrical stimulation, has grown tremendously over the past decade or so. Electroactive polymers can best be described as soft, flexible materials that are capable of converting electrical energy to mechanical energy and thus imparting a force and/or motion.[1-4] For this reason, EAPs are considered "smart" materials due to their responsive and often tunable properties. These polymers can be uniquely considered as

examples of both sensors and transducers.[2] A sensor is a material or device that is capable of monitoring changes in a specific system parameter without altering the parameter, whereas a transducer transforms energy from one form to another. More specifically, EAPs behave as actuators since they convert electrical energy into mechanical energy much in the same fashion as an electric motor can be used to generate torque. Vast improvements in actuator performance are becoming increasingly important in growing fields such as mechatronics, microrobotics, microfluidics and bionics so that high efficiencies at small scales, high power-to-weight ratios and large degrees of compliance can be ultimately realized.[5-7]

Since EAPs are capable of mechanical actuation induced by an external electrical potential and since they are also lightweight, flexible, tough, shape-processable and inexpensive (unlike their rigid and often fragile inorganic counterparts), they afford tremendous promise in emerging technologies ranging from micro air vehicles (MAVs) and flat-panel speakers[2] to active video displays, switchable optics and haptic devices.[2,8] In some cases, the electroresponsive properties of EAPs mimic biological muscle, which explains why EAPs are often referred to as *artificial muscle*. Key material attributes such as resilience, toughness, actuation strain and stress, non-hysteretic cycling and vibration damping, coupled with high fatigue resistance, scalability and reliability,[2,3] constitute critically important considerations in biomimetic efforts designed to emulate the inherent muscular behavior of animals and insects. For reasons such as these, EAPs constitute an exciting class of intelligent materials for use in conjunction with medical implants, responsive prosthetics and, more generally, the human-machine interface.[9] Unveiled at the Asia-Pacific Economic Cooperation (APEC) Summit in Seoul, South Korea, in 2005, an impressive humanoid robot constructed by the Korea Advanced Institute of Science and Technology (KAIST) and Hanson Robotics, Inc., to resemble Albert Einstein ("Albert Hubo" displayed in Fig. 2.1a) exhibits fine facial and hand movement using hydraulics.[10] Replacement of cumbersome hydraulic systems by responsive materials, such as EAPs, would result in more compact and lightweight products. Included in Fig. 2.1b is an example of an insectoid robot containing an EAP fabricated in the form of "spring roll actuators" (*i.e.*, EAP films wound around compression springs).[11] Some EAPs are capable of not only mimicking human expressions but also emulating the mechanical response of human skin and underlying tissue.

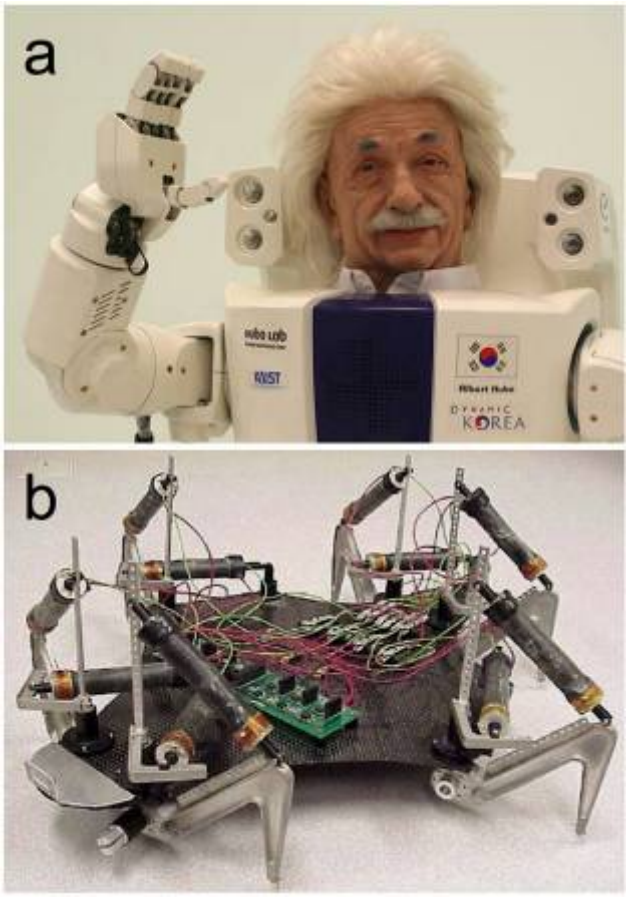

Figure 2.1 Contemporary examples of state-of-the-art robotic systems: (a) *Albert Hubo* designed on the basis of hydraulics by KAIST and Hanson Robotics, Inc., (adapted from ref. 10 and used with permission from IEEE) and (b) *FLEX 2* designed on the basis of electroactive polymers (EAPs) by SRI International (reprinted from ref. 67 and used with permission from SPIE).

Electroresponsive inorganic materials, including, but not limited to, electroactive ceramics (EACs) and shape memory alloys (SMAs), have been available for use in applications requiring electrical actuation for several decades. Rigid materials such as nickel-titanium alloys, for instance, have found extensive use in diverse technologies ranging from hydraulic line couplers on jet fighters to catheter guides in the medical field, but they are severely limited by shortcomings that do not plague EAPs. While SMAs can generate high forces and displacements, they tend to suffer from slow response times, large mechanical hysteresis and short cycle life.[6] Ongoing efforts[12] aimed at surmounting these limitations employ an external fuel source that serves to quickly change surface temperature and thus

induce actuation. Similarly, EACs are effective as compact, rapidly responsive materials, but they offer relatively little mechanical actuation (< 1% strain) and are typically fragile and expensive.[7,13] A comparison among EAC, SMA and EAP properties has been reported by Bar-Cohen[2] and is reproduced in Table 2.1. Since EAPs encompass a broad range of materials,[1,2] they are routinely divided into two general categories on the basis of their physical state or actuation mechanism: *ionic* (or wet), wherein the EAPs may require the presence of a liquid medium to function by ion transport, and *electronic* (or dry), wherein the EAPs intrinsically actuate due to Coulombic forces.[2] In the following sections, both EAP categories will be explored on the bases of mechanism and merit.

2.3 Ionic EAPs

In this section, three important types of ionic EAPs — carbon nanotubes (CNTs), conductive polymers (CPs) and ionic polymer-metal composites (IPMCs) — are introduced. In some cases, these materials are more accurately described as either nanostructured carbons (without the presence of a macromolecular species) or hybrid organic/inorganic materials composed of nanoscale particulates dispersed within a continuous polymeric matrix. The latter type of EAP may likewise be considered a polymer nanocomposite, depending on the characteristic size of the particulates employed.[14] Details regarding other ionic EAPs (***e.g.***, electrorheological fluids and ionic polymer gels) may be found elsewhere.[1,2,15,16]

2.3.1 Carbon nanotubes (CNTs)

With the discovery of CNTs over a decade ago by Iijima,[17] this family of nanostructured carbon remains a subject of considerable and broad interest due to the intrinsic properties and functionalization potential of CNTs, as well as materials containing them. Carbon nanotubes are differentiated on the basis of their nanostructure as either single-wall (SWNT), composed of a single graphene layer, or multi-wall (MWNT), with the former frequently measuring 1 to 20 nm in diameter.[4,18] In the case of MWNTs, the diameter can be significantly larger and likewise exhibit considerable dispersity, depending on process conditions and the number of walls/nanotube thus generated. Excellent reviews[18-20] are available on the subject of CNTs, and a high-resolution transmission electron microscopy (TEM) image[21] and corresponding

schematic of an isolated SWNT are shown for illustrative purposes in Fig. 2.2a. Even though CNTs exhibit a wide array of interesting properties ranging from gas storage to molecular catalysis, our focus in this work is restricted to the efficacy of CNTs as actuators. Electrical activation[3] of CNTs is based on double-layer charge injection in which individual CNTs or CNT macrostructures (usually in the form of sheets) are immersed in an electrolyte solution, and a potential is applied between the CNTs and a counter electrode, as depicted in Fig. 2.2b. Ions residing in a CNT attract oppositely charged electrolyte ions on the outer CNT surface, which induces a rearrangement of the CNT electronic structure and accompanying Coulombic forces. Taken together, these factors yield a dimensional change in the CNT.

Table 2.1 Comparison of various inorganic and organic electroactive materials.[a]

Property	EAC	SMA	EAP
Actuation strain (%)	0.1 – 0.3	< 8%	> 1 (up to > 200)
Blocking force (MPa)	30 – 40	~700	0.1 – 3
Actuation speed magnitude (s)	10^{-6} – 1	1 – 10^{2}	10^{-6} – 10^{2}
Mass density (g/cm^3)	6 – 8	5 – 6	0.9 – 2.5
Drive voltage (V) / field (V/μm)	50 – 800	—	2 – 7 / 10 – 150
Consumed power magnitude[b] (W)	1	1	10^{-3}
Fracture toughness	Fragile	Elastic	Elastic, resilient

[a] Reproduced with minor alteration from ref. 2.
[b] Power consumption is based on devices that are driven by the actuators.

Baughman *et al.*[4] report that CNTs can be used as bimorph cantilever actuators capable of electrically-stimulated bending (*cf.* Fig. 2.2c). They have also shown that "bucky paper," consisting of randomly distributed CNTs, can generate actuated strains > 0.2%, whereas oriented CNT fibers can exhibit strains ranging from 0.5 to 1%.[22]

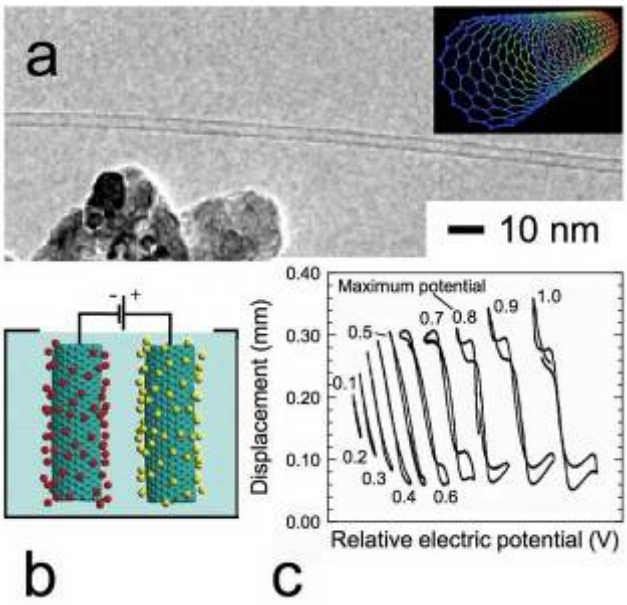

Figure 2.2 Demonstration of single-wall carbon nanotubes (CNTs) as electroactive materials. High-resolution transmission electron microscopy (HRTEM) image of a lone CNT (adapted from ref. 21 and used with permission from Springer) and an illustration of a single-wall CNT(reprinted from en.wikipedia.org/wiki/Wikipedia:Featured_picture_candidates/ February-2006 and used with permission) are displayed in (a). In (b), the mechanism by which CNT-based actuators operate is illustrated (reprinted from ref. 11 with permission from Elsevier). In (c), experimental data confirm that electrically-driven CNT "paper" (15 □m thick) can bend a polymer film measuring ~0.2 mm thick (adapted from ref. 4 and used with permission from the American Association for the Advancement of Science).

While MWNTs may be expected to be less effective than SWNTs as actuators due to lower solvent-accessible area and, hence, less exposed surface area for ion capture,[3] recent results provided by Hughes and Spinks[23] indicate that (~0.2%). Actuators fabricated on the basis of CNTs possess the greatest likelihood of achieving a high work density, that is, the mechanical work per unit mass of actuator generated upon electrical actuation.[4] In fact, the work density of CNTs can be 30x greater than any other actuator technology at the present time due to their incredibly high modulus (the Young's moduli, Y, of single SWNTs[3] and MWNTs[1] are reported to be ~640 GPa and ~1 TPa, respectively), because the work density is directly proportional to the modulus. In the case of actuators fabricated from CNT assemblies, work densities of up to 0.95 GPa and 4.5 kJ/kg have been experimentally realized.[24] Another attractive feature of CNT actuators is the low voltage (~1 V) required for actuation. Although CNT actuators suffer from poor electromechanical coupling (*i.e.*, the conversion from electrical to mechanical work), high manufacturing costs (especially for

SWNTs) and low mass production, ongoing efforts[25,26] designed to grow and harvest highly oriented CNTs into designer yarns and sheets keep this actuator technology on the research forefront. Of particular interest is the use of CNT actuators as active noise and vibration reduction materials at low frequencies.[3,4]

2.3.2 Conductive polymers (CPs)

Inganäs and co-workers[27,28] have provided the first evidence that CPs possessing a conjugated organic backbone and arranged in two layers of conducting electrodes separated by an electrolyte solution could function as actuators. While two of the most common CPs presently available are polypyrrole (PPy) and polyaniline (PANi), other CP candidates identified to date include polythiophene, poly(*p*-phenylene vinylene) (PPV), and *trans*-polyacetylene (*t*-PAc).[1,3] The mechanism by which actuation occurs in CP systems proceeds on the basis of reversible counter-ion uptake and expulsion that occurs during redox cycling.[1-3,11] Electrochemically induced changes in oxidation state promote a corresponding charge flux along the polymer backbone, which then triggers a responsive flux of ions to balance the charge. This ion flux causes the CP to expand if it is oxidized or contract if it is subsequently reduced, thereby yielding controllable and cyclic electrical actuation.[29] Electrochemical reactions required to initiate this response commonly require low voltages (1-2 V),[3] and resultant actuation strains range from 1 to *ca*. 40%.[11,30] A promising aspect of CP actuators is that their achievable force density, while measured[31] up to ~100 MPa, is anticipated[29] to be as high as 450 MPa. However, CP actuators suffer from several serious drawbacks. They exhibit low efficiencies (on the order of 1%) and electromechanical coupling (< 1%),[3] in addition to moderately low linear actuation strain levels (~12%).[32] Actuation strain rates are likewise slow due to the diffusion process required for ions to be absorbed in and expelled from the polymer,[1] as well as internal resistance between the polymer and electrolyte solution.[3] Because of the need for an electrolyte solution, most CP actuators must be isolated from the environment through the use of encapsulating materials.[33] Further development of solid-state electrolytes,[34] however, precludes the need for encapsulation. Lastly, sputtered metal films applied to the CP surface are prone to delaminate over time and repeated use. With these shortcomings notwithstanding, CP actuators represent viable candidates for technologies requiring low applied voltages and a high energy

density/cycle, examples of which include catheters, as well as automotive and prosthetic devices.

2.3.3 Ionic polymer-metal composites (IPMCs)

Several studies[27-29] have demonstrated that ionic polymer-metal composites, also referred to as IPMCs, are ideally suited as soft actuators for bending and sensing applications. The materials comprising this class of EAPs are routinely described as composite laminates, each consisting of a thin (200 - 300 μm), water-swollen ion exchange membrane with thin metal (Pt, Pd, Ag or Au) or carbon electrodes plated on both faces, as illustrated in Fig. 2.3a. Examples of suitable ion exchange membranes include perfluorinated ionomers, such as Nafion® and Flemion® with anionic-terminated side groups, or polystyrene ionomers with anionic-substituted phenyl rings.[2] Prior to application of an electric potential, ion clustering occurs uniformly throughout the IPMC, because the solvated polymer matrix consists of a hydrophobic polymer backbone and hydrophilic anionic side groups in the presence of water. In the case of IPMC actuators, the polymer matrix is normally negatively charged, in which case counterions (*i.e.*, cations) are introduced into the matrix. The mobile cations initially aggregate as clusters in discrete pockets of water throughout the membrane. As an electrical potential is applied across the IPMC actuator, however, the cations spatially redistribute as they diffuse toward the cathode, thereby forming a cation-rich layer along the cathode side and depleting cations from the anode side (*cf*. Figs. 2.3b and 2.3c).

The result of this process is fast bending of the IPMC toward the anode, followed by slow relaxation toward the cathode, due to unequal charge accumulation.[28,29] As with the previously described ionic EAPs, IPMC actuators require relatively low actuation voltages (~1 V).[3] In fact, the applied electromechanical potential must not exceed 2.23 V to avoid water electrolysis.[1,4] Due to their inherent need for water to control cation transport and the swollen nature of the membranes, these actuators lack rigidity and exhibit a low work density[3] (~10 W/kg *versus* 10^3 W/kg for natural muscle[2]). With these limitations notwithstanding, IPMC actuators can be used as catheters and elliptical friction drive elements, peristaltic pumps and bionic devices for augmenting muscle.

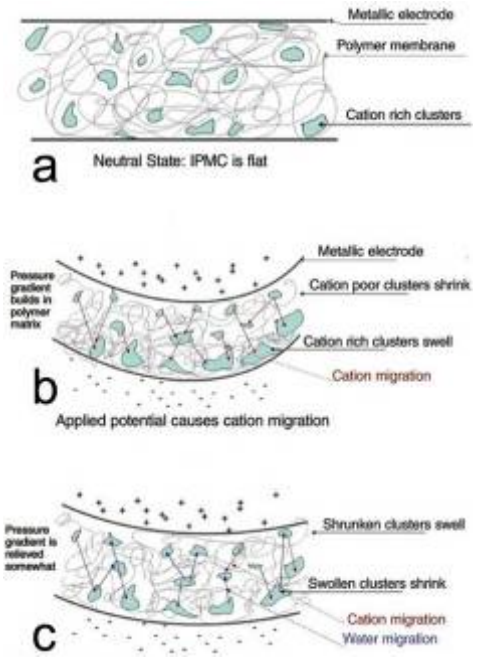

Figure 2.3 Schematic diagram showing the operational principle of IPMCs. Prior to actuation, the aqueous IPMC is flat (a). Application of an electrical potential promotes migration of cations, thereby causing the IPMC to curve or bend (b). The system eventually adjusts to the applied electrical potential (c) and can return to (a) upon removal of the potential (reprinted from ref. 3 with permission from IEEE).

2.4 Electronic EAPs

In the previous section, the operational mechanisms and potential applications associated with ionic EAPs have been explored. This section now focuses on EAPs that respond directly, without the use of added charge carriers (*e.g.*, electrolyte solutions), to an external electric field. Such materials, referred to as electronic EAPs, do not require mass transport and are therefore not diffusion-limited. The consequence is that electronic EAPs, commonly distinguished on the basis of their actuation mechanism as either electrostrictive (ferroelectric polymers) or electrostatic (dielectric elastomers), generally possess fast response times. These two EAP categories are discussed below.

2.4.1 Ferroelectric polymers

Electrostriction occurs when the dielectric properties of a material change with strain.[1,2] Examples of electrostrictive polymer actuators include ferroelectric macromolecules such as polyvinylidene fluoride (PVDF), poly(vinylidene fluoride-*co*-trifluoroethylene) (PVDF-TrFE), polyvinyl fluoride (PVF), odd-numbered nylons (with an odd number of carbon atoms between amide groups) and polyurethane.[1,2] One of the most extensively investigated materials, PVDF, as well as its copolymers and terpolymers, is semicrystalline, composed of crystals dispersed in an amorphous, molten matrix. Reported[30] values of the normal melting and glass transition temperatures for commercial-grade PVDF are 176 and 60°C, but copolymerization of PVDF commonly induces a reduction in these transition temperatures. Upon application of an external electric field, domains of amorphous polymer become polarized and align in the direction of the applied field. This field-induced polarization is permanent, remaining after cessation of the field.[3] A molecular-level representation of field-induced actuation is provided for PVDF-TrFE in Fig. 2.4a, which depicts the all-*trans* (T) conformation constituting the β phase. The electromechanical response of PVDF-TrFE is attributed to a phase transformation from ferroelectric (all T) to paraelectric (a mixture of T and gauche, G).[31] It is evident from this figure that the transformation to the α phase promotes a large change in the lattice constant, which has been experimentally confirmed by Tashiro *et al.*[32] The large molecular strains induced by such a transition are often accompanied by relatively large strain hysteresis.

Zhang *et al.*[33] have proposed that this problem can be overcome further by reducing the energy barrier associated with the conformational transition (polarization switching). To achieve this, they have used high-energy electron radiation to introduce defects into the crystalline structure of the PVDF-TrFE copolymer. Such radiation treatment breaks down domains of coherent polarization and transforms the polymer into a nanostructured material consisting of nanoscale polar regions (β phase) embedded in a nonpolar matrix (α phase).[2] The dimensional changes generated by the polar regions under an applied electric field, coupled with a large lattice strain (due to the difference between the lattice constants of the polar and nonpolar regions), are responsible for a macroscopically large electrostrictive strain. More recently, Zhang and co-workers[34] have adopted several other approaches to enhance the actuation performance of PVDF-based actuators.

A terpolymer composed of PVDF-TrFE with a small quantity (~4 mol%) of chlorofluoroethylene (CFE, -CH_2-CFCl-) has been found to exhibit superior electromechanical properties relative to the parent PVDF-TrFE copolymer. A thickness strain of 4.5% with a coupling efficiency of 55% has been achieved at a relatively low electric field (130 V/μm). Starting with an elastomer, Su *et al.*[35] have chemically grafted polarizable sequences onto flexible polymer backbones to generate electrostrictive graft elastomers that can attain strains of ~4% upon actuation. In another strategy,[36] the dielectric constant (ε) of the PVDF-TrFE copolymer has been greatly improved through the physical addition of a high-ε organometallic filler, namely, copper phthalocyanine (CuPc, with $\varepsilon > 10^6$). In this case, addition of 40 wt% CuPc, a highly planar compound (depicted in the inset of Fig. 2.4b), is observed to increase ε of the hybrid material from 40 to 225. The composition dependence of ε in a PVDF-TrFE copolymer modified with CuPc is shown in Fig. 2.4b. Bobnar *et al.*[37] have likewise investigated a multicomponent composite consisting of PVDF-TrFE-CFE modified with CuPc, whereas Huang *et al.*[38] have studied the electromechanical behavior of PVDF-TrFE-chlorotrifluoroethylene (CTFE) terpolymer modified with different concentrations of PANi (included for comparison in Fig. 2.4b).

Generally speaking, the advantages of such electrostrictive EAPs is that moderate strains (up to ~7%) can be achieved under low-frequency fields, but they can also be operated at frequencies in excess of 100 kHz.[3]

They can likewise generate high stresses[1] (*ca.* 45 MPa) due to their high Young's modulus[34] (> 0.4 GPa) and thus produce higher energy densities relative to piezoelectric ceramics.[1] A severe drawback of electrostrictive EAPs is the high voltage (> 1 kV) or, alternatively, electric field (~150 V/μm) required for actuation. Due to the relatively high strains that are routinely achieved with these materials, surface electrodes tend to fatigue, and the EAPs show signs of considerable hysteresis, upon cycling.[2]

2.4.2 Dielectric elastomers

In dielectric elastomers (D-EAPs, also referred[1-3] to as electroelastomers or elecrostatically stricted polymers, ESSPs), the electric field-induced actuation response is initiated by the electrostatic attraction between oppositely charged conductive layers applied

to the opposing surfaces of a thin elastomeric film.[39-42] This attraction induces a compressive stress, the magnitude of which is dictated by the magnitude of the electric field (E) and ε. The level of corresponding strain achieved upon actuation, on the other hand, depends on Y. To ensure high actuation and cyclic displacement, these EAPs must (*i*) possess shape memory due to chemical or physical cross-linking, (*ii*) be flexible with a relatively low Y and (*iii*) possess a moderate-to-high dielectric constant (typical ε values range from *ca*. 3 to 7).[2,3]

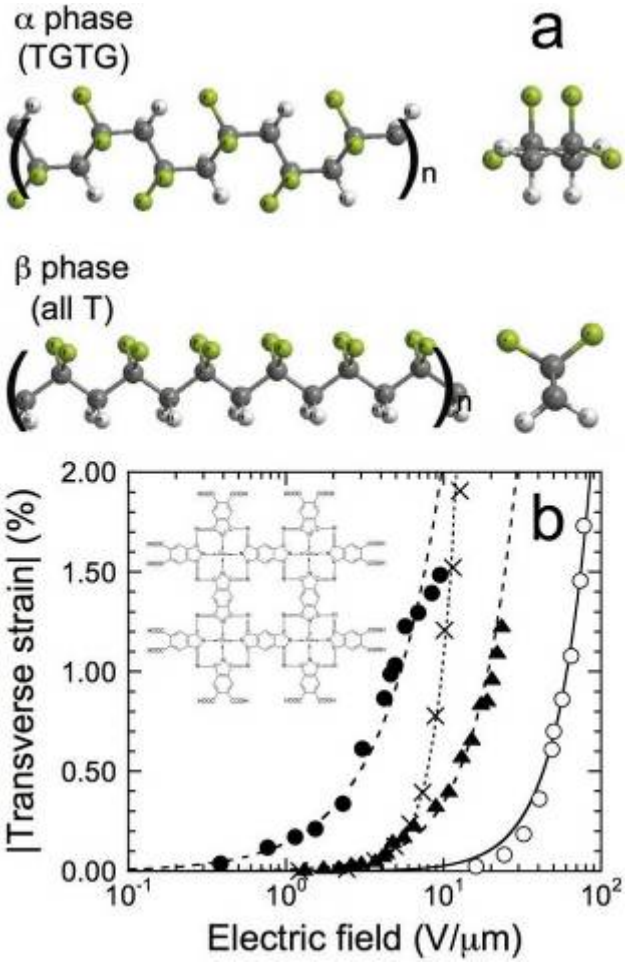

Figure 2.4 In (a), molecular depictions of PVDF, an electrostrictive ferroelectric polymer. The phase (with an all-T conformation) is responsible for ferroelectricity, whereas the phase (with both T and G conformations) promotes paraelectricity (adapted from ref. 11 and used with permission from Elsevier). In (b), the transverse strain is presented as a function of electric field for PVDF-TrFE modified[36] with 40 wt% CuPc (X, see inset for the chemical structure) and PVDF-TrFE-CTFE (○) modified[38] with two different concentrations of PANi (in vol%): 13 (▲) and 23 (●). The solid line verifies that the strain scales as E^2 in accord

with Eq. 3, whereas the dashed and dotted lines (power-law regressions to the data) deviate from this expected behavior and thus serve only as guides for the eye.

Table 2.2 Common electrical and mechanical properties of homogeneous D-EAPs.[a]

Elastomer	Dielectric constant, ε (evaluated at 1 Hz)	Modulus, Y (MPa)	Reference(s)
Fluoroelastomer[b]	13	2.5	43
Polyurethane[c]	7.0	17	43
Fluorosilicone[d]	6.9	0.50	43
Acrylic[e]	4.8	1.0 – 3.0	39
		0.80	65
		0.50	66
Polybutadiene[f]	4.0	1.7	43
Silicone[g]	3.3 – 3.7	0.35 – 0.56	66
(Silicone-C)[h]	2.8	1.0	49
(Silicone-H)[i]	2.8	0.13	49
Polyisoprene	2.7	0.85	43

[a] Values are expressed to two significant figures for consistency. [b] LaurenL143HC. [c] Deerfield PT6100S.
[d] Dow-Corning 730. [e] 3M VHB 4910. [f] Aldrich PBD. [g] Dow-Corning DC3481. [h] NuSil CF19-2186.
[i] Dow-Corning HS3.

Representative material properties of previously investigated D-EAPs are listed in Table 2.1, whereas corresponding metrics of electromechanical actuation (defined in the

following sections) are provided in Table 2.2. Introduction of polar functionalities along the polymer backbone generally tends to increase the value of □, but does not necessarily ensure that the electrical actuation response will be improved. Accompanying changes in Y (due to the extent of cross-linking) and chain entanglement, as well as the propensity for specific inter/intramolecular interactions, may adversely affect the ability of an elastomer to respond to electrical stimulation. Pelrine et al.39 have reported that a commercial acrylic elastomer with moderate values of □ and Y can exhibit very high displacements when subjected to an external electric field. While a large number of elastomers derived from homopolymers (e.g., silicones,39 fluoropolymers43 and natural or synthetic rubber43) have been evaluated as D-EAPs, this acrylic elastomer has set the benchmark against which the performance efficacy of this family of materials is commonly assessed. Recent efforts41,42 have demonstrated that electro¬active nanostructured polymers (ENPs) composed of a microphase-separated triblock copolymer in a nonpolar midblock-selective solvent can likewise achieve high actuation strains at much lower electric fields than the acrylic elastomer. A detailed description of each of these materials is provided in a later section.

2.5 Actuation mechanism

As alluded to above, the electromechanical response of dielectric EAPs is attributed to the development of a Maxwell stress (σ_M) upon application of an external electrical field.[11,39,41,42] In the context of continuum mechanics, the Maxwell stress, schematically depicted in Fig. 2.5, acts normal to the film surface and thus serves to compress the film along its thickness (z) and stretch the film laterally (in x and y). Depending on material properties identified earlier (ε and Y) and the magnitude of E, the resultant Maxwell stress can induce a significant compressive strain in a D-EAP (*e.g.*, ~70% in the acrylic elastomer[39]). Most D-EAP applications exploit this large dimensional change normal to the applied electric field. To improve the extent of strain achieved upon actuation for a given voltage (V), D-EAPs are routinely pre-strained biaxially or uniaxially to reduce the initial film thickness (z_0) and therefore increase E (= V/z_0).[42] Conversely, a desired thickness strain can be achieved at a lower applied voltage. While mechanical pre-strain has also been observed[44] to enhance the dielectric strength of D-EAPs by promoting molecular alignment, it requires a rigid support frame for application purposes and suffers from elastomer

relaxation and adhesive failure over time. Some D-EAPs have recently been found[42] to exhibit adequate electrical actuation without pre-strain.

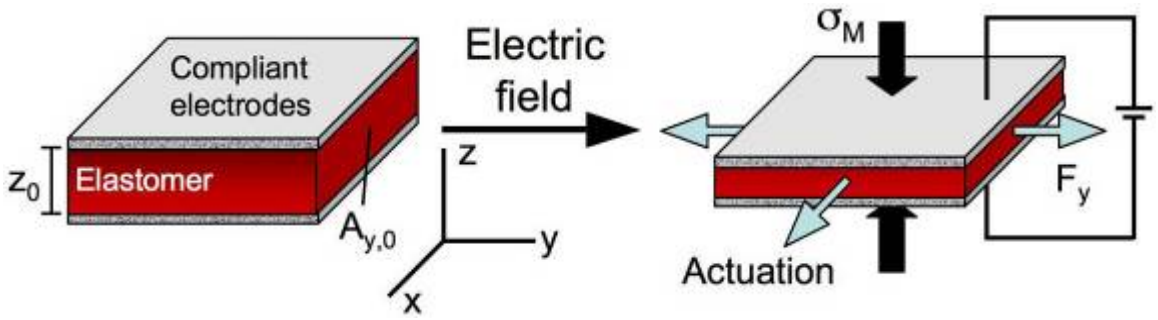

Figure 2.5 Schematic illustration showing the operational principle of D-EAPs. Prior to actuation, the elastomer film of initial thickness z_0 is coated on each side with a compliant electrode. An applied electric field promotes attraction of the oppositely charged electrodes, thereby introducing a compressive Maxwell stress (σ_M) along the transverse (z) direction. Actuation is normally measured in terms of the lateral (in-plane) dimensional change, and the blocking force along the y-direction (F_y), for example, is identified.

2.6 Actuation characteristics

The key parameters that are commonly employed to characterize actuators must be fully understood prior to a detailed comparison of D-EAP actuators. It is important to recognize that, despite their attractively large actuation strains, high energy densities, fast response times and high coupling efficiencies, not all D-EAPs may provide the best performance required in all actuator applications. For this reason, a systematic description of the metrics needed to evaluate actuation efficacy is required. In this section, we present and discuss the common characteristic parameters used to describe D-EAP performance.

2.6.1 Actuation stress and blocking force

The Maxwell stress, commonly regarded as an electrostatic pressure acting perpendicular to the D-EAP film surface, describes the mechanical response of a D-EAP to electrical stimulation.[1-3] Upon application of a transverse electric field via compliant electrodes coated on opposing film surfaces (*cf*. Fig. 2.5), the D-EAP film compresses along the z-direction and expands laterally due to attractive electrostatic charges across the electrodes and repulsive

like charges along each electrode. According to Pelrine *et al.*,[39] the Maxwell stress acting along z can be expressed as

$$\sigma_M = \varepsilon\varepsilon_o E^2 \quad (1)$$

where ε_o is the permittivity of free space. Equation 6 establishes that the electric field-induced normal stress introduced during actuation is proportional to the square of the applied field and the dielectric constant of the D-EAP, which distinguishes D-EAP actuators from other electrostatic materials because ε of a polymer can be easily altered (by chemical or physical means) to increase σ_M without increasing the operating voltage. Along a lateral dimension, the blocking force constitutes the force required to return a fully energized actuator to zero displacement. In other words, it is the force generated by a linear actuator under the constraint of constant length. Kofod *et al.*[45] have derived a relationship between the blocking force along the y-direction (F_y) and other relevant actuator attributes for D-EAPs, *viz.*,

$$F_y = (x_0 z_0/\alpha_y)\varepsilon\varepsilon_o E^2 \quad (2)$$

where α_y (= y/y_0) is the film displacement in the y-direction, while the orthogonal lateral dimension (x_0) is held constant. The blocking stress (σ_B) is therefore given by F_y/A_y, where A_y is the cross-sectional area over which F_y acts (*cf.* Fig. 2.5). Spinks *et al.*[46] have examined the effect of preload tension on F_y in PPy ionic actuators and provide an analysis by which to explain their observation that F_y decreases with increasing preload tension.

2.6.2 Actuation displacement

The magnitude and type of strain or displacement generated by EAPs upon electrical stimulation constitute critically important design considerations. Different classes of EAPs exhibit distinct types of strain (*e.g.*, tensile or bending) with displacements varying by orders of magnitude. Therefore, it is imperative that the strain be unambiguously classified on the basis of an EAP's response to stimulation. As previously discussed, some EAPs including, but not limited to, IPMCs, CPs and CNTs undergo a bending strain upon actuation,[1-3] in which case their response must be expressed accordingly. For D-EAPs, however, the actuation-induced transverse strain promotes a large in-plane strain, which is easily measured and often reported.[2,3,39] Differences such as these provide a potential source of confusion,

since published reports tend to compare the actuation performance of different EAPs on the basis of strain without precisely delineating the type of actuation strain actually measured. Comparisons must therefore be made with caution, since areal or in-plane strains are typically an order or magnitude greater than transverse (or thickness) strain.[39,41]

2.6.2.1 Transverse or thickness strain

This actuation strain reflects a dimensional change in the thickness direction of an EAP film due to the normal pressure induced by an electrostatic Maxwell stress or electrostriction or combination of both.[43] Because D-EAPs, in particular, significantly change their dimensions upon electrical stimulation, this strain establishes a characteristic signature of a given D-EAP material, and it is used to determine many other important actuation parameters. Since bulk D-EAP films evaluated for actuation efficacy are usually thin (often on the order of 1 mm), direct measurement of strain along the z-direction can be challenging. For this reason, the thickness, or transverse, strain is routinely calculated from experimental measurements of in-plane (lateral) actuation strain under the assumption of isochoric deformation. Yang *et al.*,[47] however, have experimentally measured the transverse strain of silicone and polyurethane elastomers using laser Doppler interferometer. In most D-EAPs, the transverse strain, denoted as s_z where s_z is defined as $(z - z_0)/z_0$, arises due to the Maxwell stress discussed earlier. If the strain is sufficiently small (< 20%) so that the deformation due to actuation can be presumed to be linearly elastic, Hooke's law in compression ($\sigma_M = - Ys_z$) can be used to directly relate the transverse strain to the applied electric field:

$$s_z = - \varepsilon\varepsilon_o E^2/Y \qquad (3)$$

While Eq. 3 provides a straightforward means by which to determine the transverse strain from material properties (ε and Y) and field conditions (E) under small strains due to electrostatic compressive stress, two other scenarios must be addressed. At large strains, Y itself becomes a function of strain, in which case Eq. 3 is no longer valid. In the limit of D-EAPs exhibiting large in-plane (lateral) strains, s_z can be discerned from constitutive relations. Under isochoric deformation conditions, the in-plane strains (s_x and s_y) and the

transverse strain are related by $(1 + s_x)(1 + s_y)(1 + s_z) = 1$. If the actuation-induced in-plane deformation is isotropic, $s_x = s_y = s_{xy}$ and

$$s_z = (1 + s_{xy})^{-2} - 1 \quad (4)$$

In the case of non-piezoelectric materials, such as polyurethane elastomers, the actuation strain along the thickness direction can be a consequence of either an electrostriction effect (*i.e.*, direct coupling between molecular polarization and the mechanical response of the material) or an electrostatic Maxwell stress or a combination of both. According to Zhang *et al.*,[48] the transverse strain due to electrostriction (s_e) is related to the polarizability (p) of an EAP through $|s_e| = qp^2$, where q is the electrostrictive coefficient. For a linear dielectric medium, $p = \varepsilon_o (\varepsilon - 1)E$ so that

$$|s_e| = q\varepsilon_o^2(\varepsilon - 1)^2E^2 \quad (5)$$

2.6.2.2 In-plane (lateral) and bending strains

The in-plane, or lateral, strain is the displacement generated by D-EAPs in the x- and/or y-directions as a result of transverse strain, as described in the previous section. Since the actuation performance of D-EAPs is normally assessed in a circular test configuration,[39,41] illustrated by the diagrams and images displayed in Fig. 2.6, the in-plane strain is commonly reported in terms of an areal strain, which is defined as $(A_z - A_{z,0})/A_{z,0}$, where A_z denotes the active area of actuation (or compression) in the x-y plane, and the subscripted 0 denotes pre-actuation. Recorded images such as those provided in Fig. 2.6 can be analyzed by standard image analysis methods[41] so that the area of actuation can be measured under a wide variety of experimental or material conditions. A similar approach is used to analyze linear in-plane strains during, for instance, blocking stress measurements.[39]

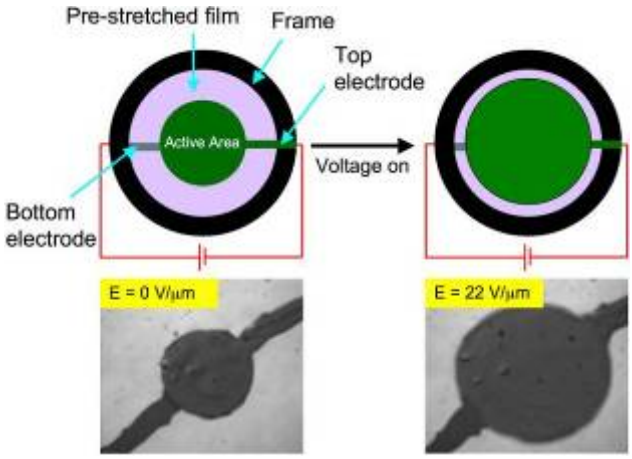

Figure 2.6 Circular experimental setup used to measure the electromechanical behavior of D-EAPs in the presence of an electric field and corresponding optical images. An elastomeric film is commonly subjected to a mechanical prestrain and subsequently fixed to a frame prior to coating the active area on both film surfaces with a compliant electrode. Actuation upon electrical stimulation results in an increase in the active area, which is digitally measured and quantified.

In many studies, in-plane actuation strains are relatively large, ranging from 10 to over 200%. On the high side, areal strains of 245% and 158% have been reported for ENPs[41] and acrylic D-EAPs,[39] respectively. Bending strains, on the other hand, arise from ionic EAPs, as well as some electrostrictive systems,[1-3] upon electrical stimulation. In this case, the bending strain of a linear actuator is measured as the angular displacement measured with respect to the long axis of the actuator. A generally important consideration regarding D-EAPs targeted for use in technologies such as MAVs and smart prosthetics that require actuation cycling is actuation hysteresis, commonly expressed in terms of a nonrecoverable strain.[2] Hysteresis is highly undesirable and occurs when the initial dimensions of an actuator change due to nonlinear viscoelastic effects upon repeated actuation. Whereas D-EAPs suffer the most from high actuation hysteresis due to the large strains achieved, recent studies[41] of ENPs, however, reveal a more modest level of hysteresis (< 5% in some cases) upon mechanical or actuation cycling.

2.7 Actuation performance

The energy or power generated upon electrical stimulation also constitutes crucial performance metrics of EAPs. In this section, key actuator parameters such as the strain energy density and coupling efficiency are introduced and discussed. The strain energy density for D-EAPs is defined[3,39] as the amount of work generated in one actuation cycle per unit volume of actuator, exclusive of overhead peripherals, such as electrolytes, power supplies, counter electrodes and packaging. It can be derived directly from experimentally measured quantities, such as the electrostatic stress and transverse strain discussed in previous sections. At small actuation strain levels typically encountered by ferroelectric EAPs (< 10% strain) or D-EAPs actuated under low electric fields, the stored elastic energy (E_S) is given by $-\sigma_M s_z/2$ on a unit volume basis. In terms of material properties, E_S can be rewritten as

$$E_S = Y s_z^2/2 \tag{6}$$

If large actuation strains are generated, Pelrine *et al.*[39] propose a description for the elastic energy density based on the assumptions of isochoric deformation and constant electrostatic stress (σ_M). Under these conditions, A_z relates to s_z by $x_0 y_0/(1 + s_z)$, and the corresponding elastic energy density (E_L) can be obtained by integrating the compressive force over the transverse displacement and putting the result on a unit volume basis. The closed-form analytical result is

$$E_L = -\sigma_M \ln(1 + s_z) \tag{7}$$

An equally useful performance parameter for comparing D-EAPs is the efficiency (η), which is given by the ratio of generated work to input energy.[3] As anticipated, theoretical efficiencies are never achieved in practice. According to Kornbluh *et al.*,[49] the overall efficiency (η_t) depends on the electrical and mechanical efficiencies of the D-EAP (η_e and η_m, respectively), as well as the efficiency associated with electric driver circuit (η_d), by $\eta_t = \eta_e \eta_m \eta_d$, where η_e and η_m relate directly to electrical and mechanical loss factors, respectively. The efficiency of the electric driver circuit, on the other hand, is given by the electromechanical coupling efficiency (K^2), which is the electrical energy converted into mechanical work per cycle relative to the electrical energy applied per cycle or, alternatively, the ratio of stored mechanical energy to input electrical energy.[3,39,41] Calculation of K^2 for D-EAPs is based on the electrostatic model, which presumes that permittivity of the actuator

does not change upon activation. For elastomeric materials under isochoric conditions, the change in electrical energy upon actuation is approximately equal to the work output, in which case K^2 can be conveniently written as[43]

$$K^2 = -2s_z - s_z^2 \quad (8)$$

Materials with a low K^2 value are not desirable as actuators because they require a large amount of electrical energy relative to the amount of work that can be harnessed.

2.8 Homogeneous dielectric elastomers

As mentioned earlier, a wide variety of elastomers derived from chemically cross-linked homopolymers have been investigated as D-EAPs. Specific examples include acrylics, silicones (including fluorinated silicones), polyurethanes, fluoroelastomers, ethylene-propylene rubber (EPR), polybutadiene (PB) and polyisoprene (PI, natural rubber). Relative to other EAPs, these network polymers must inherently possess low Y and high ε to maximize σ_M and s_z by Eqs. 1 and 3, respectively. Although the polyurethane, fluorosilicone and fluoroelastomer D-EAPs typically have a higher ε compared to the silicones and acrylics, the acrylics and silicone elastomers exhibit superior actuator performance relative to other D-EAPs, as well as EAPs in general. In fact, the maximum efficiency afforded by these materials, discussed in detail below, compares favorably with other types of electroactive materials, including inorganic ones.

2.8.1 Acrylic elastomers

This class of D-EAPs, commercially available as pressure-sensitive adhesives (*cf.* Table 2.2), constitutes one of the most extensively investigated D-EAPs to date due to its exceptional actuator efficacy.[39] Since the precise composition of these materials has not yet been reported, we presume here that they are homogeneous for the sake of classification. These elastomers, manufactured as double-sided adhesive tapes, are commonly pre-formed to film thicknesses of 0.5 and 1 mm, in which case they are routinely pre-strained prior to electrical stimulation.[42] An interesting feature of these acrylics is that their dielectric breakdown strength is reported[50] to increase upon pre-strain (which is typically applied biaxially). This material is mechanically robust and has been stretched to 36x its initial area

before breaking.[44] It is also reported[2] to be thermally stable from -10° to 80°C. While this acrylic elastomer is undoubtedly a low-modulus material, reported values of its elastic modulus vary considerably, ranging from 1-3 MPa according to Madden *et al.*[3] to much less than 1 MPa.[41] This variability may reflect material anisotropy or defects, as well as differences in the mode of testing (*i.e.*, tension *versus* compression), as well as the method (*i.e.*, direct tension/compression *versus* inflated diaphragm) by which the elastic modulus is measured. Unfortunately, important details such as these are not always and consistently documented in the literature. Mechanical measurements conducted in our laboratory yield a tensile modulus of 0.20 MPa and a compressive modulus of 0.27 MPa. This acrylic elastomer has been reported to exhibit an ultrahigh areal actuation strain of 158% and transverse strains up to *ca*. 60-70%, depending on the level of pre-strain applied in the in-plane direction, as indicated in Table 2.3. A blocking stress of 7.2 MPa and a corresponding elastic energy density of 3.4 MJ/m^3 constitute the highest actuation metrics reported[39] to date for D-EAPs. When such values are provided, however, care must be exercised in performing a comparative analysis among D-EAPs. Recall from Eq. 1 that the electrostatic (Maxwell) stress is directly proportional to E^2 and that E is inversely proportional to film thickness. While most reports of D-EAP actuation calculate E relative to the initial film thickness, others[39] use the instantaneous E arising from the true film thickness upon actuation. This difference will obviously change numerical values, but the benchmark actuation performance of the acrylic elastomers remains intact. In fact, these D-EAPs also possess the highest coupling efficiency (~90%) of all D-EAPs derived from homopolymers (*cf*. Table 2.3).

2.8.2 Silicone elastomers

Silicones, or polysiloxanes, consist of a silicon-oxygen backbone $(-SiR_1R_2-O-)_n$ with the side groups R_1 and R_2 covalently attached to the Si atoms. The flexibility associated with Si-O bonds propagates along the main chain, yielding molten macromolecules with an intrinsically high free volume and a low glass transition temperature. The most commonly used commercial silicones derive from polydimethylsiloxane, for which $R_1 = R_2 = CH_3$. These materials are readily processed into films by spin coating or solution casting, and, as with the acrylic elastomers, their actuation efficacy is dictated by the level of pre-strain

applied (*cf*. Table 2.3). In fact, Yang *et al.*[51] have demonstrated that the transverse strain achieved depends delicately on the geometry of the actuator.

Other important considerations governing actuation performance include (*i*) the chemistry and molecular weight of the polysiloxanes to be cross-linked, (*ii*) the chemistry (functionality) by which the macromolecules are cross-linked and (*iii*) the extent to which the macromolecules are cross-linked. [52] For a given silicone and cross-linking agent, only (*iii*) remains variable, but variation in cross-link density can strongly affect the elastic modulus and, hence, actuation performance. Therefore, caution must be exercised in maintaining systematic preparation conditions. Generally speaking, silicones exhibit marginally lower maximum electromechanical coupling efficiencies (63-79%) but greater thermal stability (from -65 to 240°C) than acrylic elastomers,[44] and they tend to be less sensitive to environmental degradation.[44] More importantly, though, they are more biocompatible than most carbon-based polymers[53] and are therefore ideally suited for actuation applications at the human-machine interface (*e.g.*, smart prosthetics).

2.9 Nanostructured dielectric elastomers

(Details of this section are presented in Chapter 3 and Chapter 4)

The D-EAPs described in the previous section derive from chemically cross-linked homopolymers and are therefore spatially homogeneous. More recent efforts[41,42] have begun to explore the use of nanostructured polymers as physically cross-linked (*i.e.*, thermally reversible) D-EAPs. The most ubiquitous class of nanostructured polymers consists of block copolymers, macromolecules that can undergo spontaneous molecular self-organization into a wide variety of periodic and aperiodic nanoscale morphologies under favorable environmental conditions.[54-56] These macromolecules are composed of long sequences of chemically dissimilar repeat units. If the sequences ("blocks") are sufficiently thermodynamically incompatible, they microphase-separate into discrete microdomains in the same fashion as surfactants.[57] In the case of linear bicomponent block copolymers with three blocks covalently linked together (generically referred to as an ABA triblock copolymer), the macromolecules can form a stable 3D network capable of behaving as an elastic solid.[58] An example of a linear multiblock copolymer with many "hard" (crystalline) and "soft" (rubbery) blocks is a segmented polyurethane, which has been observed[59] to exhibit both electrostatic and electrostrictive actuation, yielding a net actuation stress of 1.9

MPa (Table 2.3) and an electromechanical coupling efficiency of 21% upon electrical stimulation.

In this section, however, we focus exclusively on microphase-separated triblock copolymers that form micelle-stabilized networks in the presence of a nonvolatile, midblock-selective solvent. The copolymers used here are commercial poly[styrene-*b*-(ethylene-*co*-butylene)-*b*-styrene] (SEBS) triblock copolymers, wherein the endblocks are glassy and the midblock is rubbery at ambient temperature. These material systems have been previously referred[60,61] to as thermoplastic elastomer gels (TPEGs) to illustrate the nature of the SEBS copolymer (a thermoplastic elastomer, TPE) and the copolymer connectivity in the presence of solvent (gel). Note that this approach fundamentally differs from EAPs such as IPMCs in which a liquid is required to facilitate ion transport. The primary purpose of the extender solvent in TPEGs is to swell the rubbery EB midblock and reduce the elastic modulus, but enhance the elasticity and elongation at break, of the resultant molecular network. The micellar morphology is clearly visible in the TEM image and corresponding schematic depiction displayed in Fig. 2.7. We have recently demonstrated[41] that, in the presence of an aliphatic/alicyclic mineral oil, SEBS copolymers of comparable molecular composition but different molecular weight exhibit ultrahigh actuation displacements (~250% areal strain) at relatively low applied fields (22 V/μm) compared to, for instance, the acrylic elastomer. These apparent electromechanical responses are attributed to (*i*) the low modulus that can be achieved in a nearly ideal elastic matrix (with little viscous dissipation) and (*ii*) the presence of nanoscale-confined functionalities (phenyl rings) that likewise respond to the applied electric field. An important consideration with these physically cross-linked materials (wherein the glassy micelles serve as cross-link sites) is that their mechanical properties and actuation behavior can be tuned using several material-related attributes including, but not limited to, copolymer composition, copolymer molecular weight and solvent concentration.

Table 2.3 Common electrical and mechanical properties of homogeneous D-EAPs.[a]

Elastomer	Prestrain (x%, y%)	σ_M (MPa)	$\|s_z\|$ (%)	E_S or E_L (MJ/m^3)	K^2 (%)	Reference(s)
Acrylic	0, 0	0.2	7	0.01	14	42
	15, 15	0.1	29	0.02	50	39
	540, 75	2.4	68	1.36	90	39
	300, 300	7.2	61	3.40	85	39
Silicone-C	15, 15	0.6	25	0.09	44	39
	45, 45	3.0	39	0.75	63	39
	100, 0	0.8	39	0.20	63	39
Silicone-H	14, 14	0.1	41	0.03	65	39
	68, 68	0.3	48	0.10	73	39
	280, 0	0.4	54	0.16	79	39
Fluorosilicone	0, 0	0.1	28	0.02	48	43
Fluoroelastomer	0, 0	0.2	8[b]	0.01	15	43
Polyurethane	0, 0	1.9	11	0.10	21	43
Polybutadiene	0, 0	0.2	12	0.01	23	43
Polyisoprene	0, 0	0.1	11	0.01	21	43

[a] Values of the electromechanical coupling efficiency (K^2) are calculated from the transverse strain (s_z) by Eq. 8. [b] Estimated on the basis of the reported value of K^2.

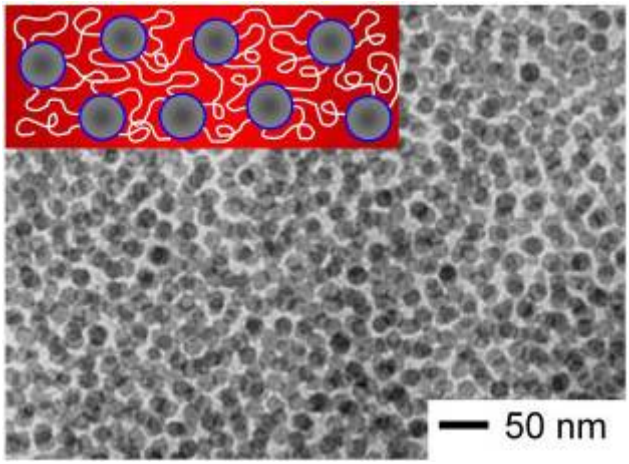

Figure 2.7 TEM image of an ENP composed of a microphase-separated SEBS triblock copolymer swollen with a midblock-selective oligomeric oil. The micellar morphology in this 10/90 w/w SEBS/oil system consists of swollen EB midblocks that form a molecular network stabilized by glassy S micelles, which appear electron-opaque (dark) due to selective staining with the vapor of RuO_4(aq). The copolymer network illustrated in the inset displays only bridged midblocks for the sake of clarity (the midblocks may also form loops and dangling ends).

The highest value of K^2 measured from these materials, collectively referred to as electroactive nanostructured polymers (ENPs) to distinguish their structure relative to conventional D-EAPs, is 92%, which exceeds that of the acrylic elastomers. Moreover, unlike the chemically cross-linked homogeneous elastomers discussed earlier, these highly elastic and reprocessable materials (*i*) undergo little actuation hysteresis (< 15%) upon cycling (*i.e.*, 100 cycles to 48-60% of the breakdown electric field)[41] and (*ii*) exhibit acceptable actuation without the need for mechanical pre-strain.[42]

2.10 Comparison of EAPs

Although a rigorously quantitative and global comparison of EAP actuation performance is not straightforward because the test performed for each type of actuator is different, property-specific comparisons have been reported by Huber *et al.*[7] and Wax and Sands,[62] as well as by institutions such as SRI International (U. S. A.) and Risø National Laboratory (Denmark).[1,2] Since one of the most important actuation metrics is voltage- or field-induced

displacement, in-plane actuation strain is presented as a function of voltage for various EAPs in Fig. 2.8a and as a function of electric field primarily for D-EAPs in Fig. 2.8b. For completeness, the transverse actuation strains corresponding to the D-EAPs in Fig. 2.8b are likewise provided in Fig. 2.8c. Figure 2.8a clearly shows that the ionic EAPs require the lowest applied voltages, whereas the electronic EAPs actuate at high voltages (> 1 kV). While this difference is broadly considered to be one of the practical limitations of electronic EAPs, Pelrine *et al.*[39] have suggested that compact voltage amplifiers could be designed to solve this problem. The requirement for high voltage may even be considered advantageous because less current is needed to produce a desired power level, thereby allowing efficient electrical energy transmission through thin wires and thus reducing concern associated with contact resistance. In all fairness, however, it must also be recognized that the voltage to be applied for actuation depends on specimen thickness, since the actuation performance of electronic EAPs depends on electric field.

This dependence is evident in Figs. 2.8b and 2.8c, which together confirm that the acrylic elastomer, some silicone elastomers and the copolymer-based ENPs discussed in the prior section exhibit the highest in-plane and transverse strains upon electrical stimulation (details of ENPs are presented in Chapters 3 and 4). These materials are attractive because of their desirable attributes such as light weight, mechanical resilience, rapid response and high energy density.

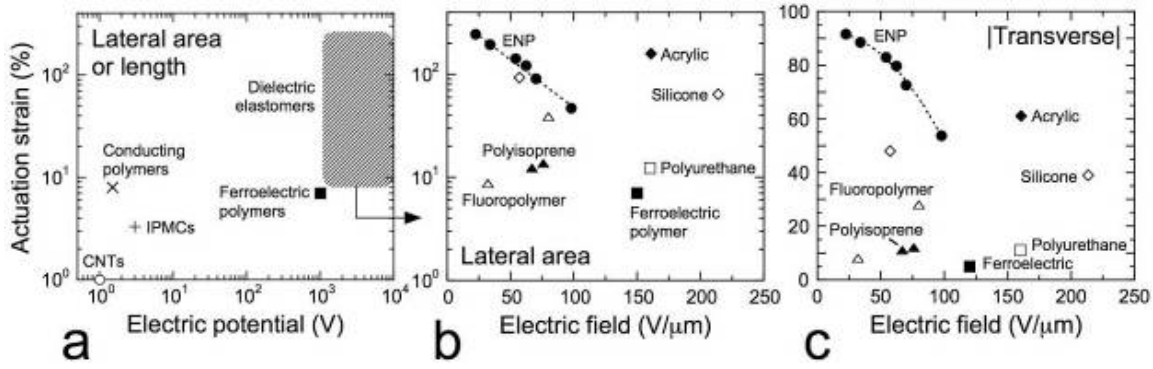

Figure 2.8 Comparison of the actuation strain levels achieved for (a) various EAPs as a function of electric potential and (b, c) D-EAPs and a ferroelectric polymer as a function of electric field. The actuation strains are labeled in each part and include (a) lateral area or length, (b) lateral area and (c) transverse. The dotted lines serve as guides for the eye.

Other important comparative metrics include the blocking stress and energy density, which are displayed as a function of actuation strain in Fig. 2.9. In this figure, the ionic CP and electrostrictive ferroelectric polymer (PVDF-TrFE) are seen to exhibit the highest blocking stresses (*ca.* 10 to more than 100 MPa) of the EAPs at relatively low strains, whereas the acrylic elastomer enjoys both a high blocking stress (between ~1 and 10 MPa) and a high actuation strain (> 100%). The straight lines with a slope of −1 are identified by discrete energy density values and connect actuator classes possessing comparable volumetric stroke work.[7] Included for comparison in Fig. 2.9 are the performance metrics for natural muscle, which is most closely emulated by the IPMC ionic EAP, as well as the dielectric silicone and ENP elastomers. Actuators located on the right side of this figure can provide a high stroke (large actuation displacement), thereby making them suitable candidates for (*i*) biomimetic applications including artificial muscle and microrobotics and (*ii*) microfluidic and haptic devices requiring lateral or transverse extension. It should be noted here that hydraulic actuators, which exhibit similar or slightly larger actuation strains than natural muscle with considerably higher blocking stresses (~10-100 MPa), have been used extensively in robotics (*cf*. Fig. 2.1).[1-3,62] However, the size and weight of the overhead peripherals (*i.e.*, pumps, piping and supports) required for such actuators preclude their use in small-scale and lightweight devices.

Other actuation metrics of EAPs, such as frequency response (or bandwidth) and specific power, have likewise been evaluated against those of more established actuator technologies to deduce the most appropriate and advantageous applications for EAPs. Another performance parameter of particular interest in this vein is the electromechanical coupling efficiency, which is included for several EAPs in Table 2.3. The ENPs and acrylic D-EAP constitute the most efficient EAPs to date, outperforming SMAs and comparing favorably relative to solenoids and, to a lesser extent, hydraulics. In addition to their displacement and energy conversion efficiency, actuators must respond quickly if they are of to be practical use. Sommer-Larsen[63] has assembled a comparison of conventional and EAP actuators and proposes that, on the basis of actuation time (*i.e.*, the time to full extension) and power density, actuators such as solenoids, piezoelectric and magnetostrictive drivers, in addition to electric motors, CPs and D-EAPs, are well-suited for use in robotic applications. The

response times of CPs and D-EAPs are on the order of milliseconds, in marked contrast to human muscle and SMAs, which require at least one and over two orders of magnitude more time to fully actuate.

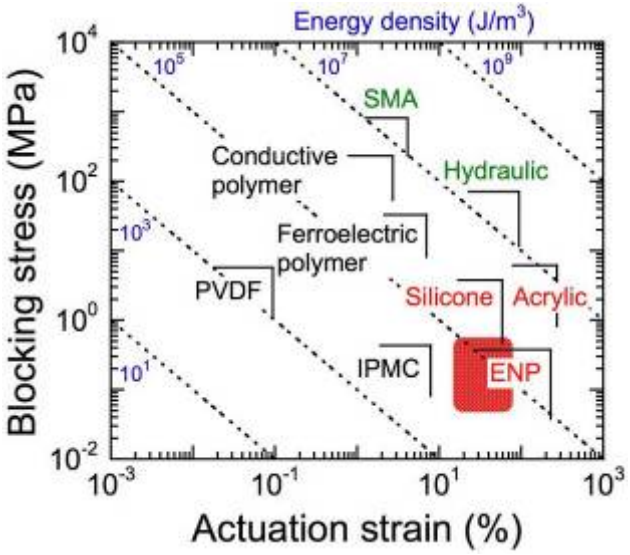

Figure 2.9 Dependence of blocking stress on actuation strain for various electroactive materials and systems: inorganic (green), ionic and ferroelectric EAPs (black) and D-EAPs (red). The dotted diagonal lines correspond to different energy densities (blue, labeled), and the red area signifies the characteristics of human muscle. (Modified from the SRI International document at http://ndeaa.jpl.nasa.gov/nasa-nde/lommas/eap/actuators-comp.pdf and used with permission).

2.11 Technological opportunities

As demonstrated earlier, D-EAPs are in many, but not all, ways superior to other classes of electroactive materials because of their tunable mechanical properties, robust and reliable performance, and net energy efficiency and power density. Because of their unique combination of attributes, D-EAPs have been used to design lightweight and compact actuators. Common actuator configurations containing D-EAPs are routinely described as tube, rolled, frame-supported and laminated.[2] Because of their light weight (elastomers typically have a density < 1 g/cm^3), D-EAP rolls are more efficient than solenoids and have been used in the development of snake-like robots, as well as steerable catheters and endoscopes.[2] Optical switches and microlenses designed around framed D-EAP actuators have also been recently proposed.[11] In this case, optical switching results from controllable

variation in optical density or refractive index as the actuator thickness changes with applied electrical field. Moreover, the high actuation strain levels and energy output of D-EAPs can be exploited to construct diaphragms capable of generating large out-of-plane deflection and correspondingly large volume displacements suitable for microfluidic pumps and valves, as well as loudspeakers and responsive haptic (*e.g.*, refreshable Braille) displays.[2,11,40] Other applications of D-EAPs include sensors, motors and even a heel-strike generator that operates in reverse fashion to produce electricity from compressive deformation. Recently, D-EAPs have been fabricated[64] into prototype fibers that can eventually be used in active textiles or in bundles to emulate natural muscle. As previously pointed out, D-EAPs constitute excellent artificial muscle candidates for biologically inspired robots, animatronics and responsive prosthetics, and prototype devices based on D-EAPs include a smart pill (*i.e.*, a tube-like structure that travels like an inchworm inside the gastrointestinal tract), multi-legged robots and bird-like MAVs.[2,11,40]

2.12 Summary

Electroactive polymers (EAPs) represent an emerging class of actuator materials that exhibit a tunable dimensional response to electrical stimulation. They can generate strains that are two orders of magnitude higher than rigid piezoelectric ceramics, and they exhibit superior performance than shape memory alloys in terms of mechanical resilience, response speed, cyclic hysteresis and light weight. Compared to conventional hydraulic or pneumatic actuators, EAPs can be used to design mechanical devices without traditional components such as gears and bearings once limitations associated with low actuation forces are overcome. These responsive materials can be divided into two classifications — ionic and electronic — on the basis of their actuation mechanism. Ionic EAPs function due to switchable ion transport, whereas electronic EAPs respond due to electrostatic or Coulomb forces that develop upon application of an electric field. Because of this difference, ionic EAPs typically require a solvent medium for electrolyte migration and low voltages to achieve actuation relative to electronic EAPs, which, on the other hand, exhibit higher actuation strains and greater overall reliability, durability and efficiency. Among the electronic EAPs reported thus far, homogeneous dielectric elastomers derived from acrylics and various silicones, as well as nanostructured dielectric elastomers generated from block

copolymers with and without an extender solvent (*i.e.*, ENPs and polyurethanes, respectively), have shown the most promising combination of mechanical and electrical actuation properties. Compared to other EAPs, the D-EAPs can produce very high actuation strains (> 200%) upon application of an external electric field due primarily to the development of an electrostatic (Maxwell) stress. Furthermore, D-EAPs possess fast response times, high energy densities and high electromechanical efficiencies. Although all D-EAPs require high electric fields to achieve maximum actuation (which undoubtedly poses a practical challenge), these materials nonetheless constitute viable and attractive alternatives for use in emerging microrobotic, aerospace, automotive, haptic, biomimetic and microfluidic technologies.

2.13 Acknowledgments

Support for this work has been provided by the U. S. Department of Commerce through the National Textiles Center.

2.14 Related websites

The following websites provide movie clips of electrical devices that could or already benefit from advances in EAP design and actuation performance:

http://eap.jpl.nasa.gov

http://www.artificialmuscle.com

http://www.sri.com/esd/automation/actuators.html

http://www.hansonrobotics.com

http://www.unm.edu/~amri

http://www.electropolymertechnology.com/web1.htm

2.15 Notes

This chapter was published in *Soft Matter* (in press), published under the authorship of Ravi Shankar,[§†] Tushar K. Ghosh[%] and Richard J. Spontak[†‡] ([§]Fiber and Polymer Science Program and Departments of [†]Materials Science & Engineering, [%]Textile & Apparel

Technology & Management and ‡Chemical & Biomolecular Engineering, North Carolina State University, Raleigh, NC 27695, USA).

2.16 References

1. J. L. Pons, *Emerging Actuator Technologies: A Micromechatronic Approach*, Wiley, NJ, 2005.
2. Y. Bar-Cohen (Ed.), *Electroactive Polymer (EAP) Actuators as Artificial Muscles: Reality, Potential, and Challenges*, SPIE Press, Bellingham, WA, 2004.
3. J. D. W. Madden, N. A. Vandesteeg, P. A. Anquetil, P. G. A. Madden, A. Takshi, R. Z. Pytel, S. R. Lafontaine, P. A. Wieringa and I. W. Hunter, *IEEE J. Ocean. Eng.*, 2004, **29**, 706-728.
4. R. H. Baughman, C. Cui, A. A. Zakhidov, Z. Iqbal, J. N. Barisci, G. M. Spinks, G. G. Wallace, A. Mazzoldi, D. De Rossi, A. G. Rinzler, O. Jaschinski, S. Roth and M. Kertesz, *Science*, 1999, **284**, 1340-1344.
5. I. R. Sinclair, *Sensors and Transducers*, Butterworth-Heinemann, Oxford, 2001.
6. M. Fremond and M. Miyazaki., *Shape Memory Alloys*, Springer, New York, 1996.
7. J. E. Huber, N. A. Fleck and M. F. Ashby, *Proc. R. Soc. London Ser. A*, 1997, **453**, 2185-2205.
8. Y. Bar-Cohen, *Expert Rev. Med. Devices*, 2005, **6**, 731-740.
9. Y. Bar-Cohen (Ed.), *Biomimetics Biology Inspired Technologies*, Taylor & Francis, Boca Raton, FL, 2005.
10. J.-H. Oh, D. Hanson, W.-S. Kim, Y. Han, J.-Y. Kim and W. Park, *Proc. 2006 IEEE/RSJ Int. Conf. Intel. Robot. Automat.*, Beijing, China, 2006, 1428-1433.

11. T. Mirfakhrai, J. D. W. Madden and R. H. Baughman, *Mater. Today*, 2007, **10**, 30-38.
12. V. H. Ebron, Z. W. Yang, D. J. Seyer, M. E. Kozlov, J. Y. Oh, H. Xie, J. Razal, L. J. Hall, J. P. Ferraris, A. G. MacDiarmid and R. H. Baughman, *Science*, 2006, **311**, 1580-1583.
13. A. Moulson and J. Herbert, *Electroceramics*, Chapman & Hall, London, 1995.
14. J. D. Nam, H. R. Choi, Y. S. Tak and K. J. Kim, *Sens. Actuators A*, 2003, **105**, 83-90.
15. M. Parthasarathy and D. J. Klingenberg, *Mater. Sci. Eng. R*, 1996, **17**, 57-103.
16. M. Doi, M. Matsumoto and Y. Hiroset, *Macromolecules*, 1992, **25**, 5504-5511.
17. S. Iijima, *Nature*, 1991, **354**, 56-58.
18. P. J. F. Harris, *Carbon Nanotubes and Related Structures: New Materials for the 21st Century*, Cambridge University Press, Cambridge, 1999.
19. R. H. Baughman, A. A. Zakhidov and W. A. de Heer, *Science*, 2002, **297**, 787-792.
20. S. Niyogi, M. A. Hamon, H. Hu, B. Zhao, P. Bhowmik, R. Sen, M. E. Itkis and R. C. Haddon, *Acc. Chem. Res.*, 2002, **35**, 1105-1113.
21. Y. Zhang, Y. Li, W. Kim, D. Wang and H. Dai, *Appl. Phys. A*, 2002, **74**, 325-328.
22. Y. L. Li, I. A. Kinloch and A. H. Windle, *Science*, 2004, **304**, 276-278.
23. R. H. Baughman, *Nat. Nanotech.*, 2006, **1**, 94-96.
24. E. Smela and O. Inganäs, *Science*, 1995, **268**, 1735-1738.
25. R. H. Baughman, *Synth. Met.*, 1996, **78**, 339-353.
26. L. Bay, K. West, P. Sommer-Larsen, S. Skaarup and M. Benslimane, *Adv. Mater.*, 2003, **15**, 310-313.
27. K. Kaneto, M. Kaneko, Y. Min and A. G. MacDiarmid, *Synth. Met.*, 1995, **71**, 2211-2212.

28. B. J. Akle, M. D. Bennett and D. J. Leo, *Sens. Actuators A*, 2006, **126**, 173-181.

29. S. Nemat-Nasser and Y. X. Wu, *J. Appl. Phys.*, 2003, **93**, 5255-5267.

30. B.-E. El Mohajir and N. Heymans, *Polymer*, 2001, **42**, 5661-5667.

31. C. Huang, R. Klein, F. Xia, H. Li, Q. M. Zhang, F. Bauer and Z.-Y. Cheng, *IEEE Trans.*, 2004, **11**, 299-311.

32. K. K. Tashiro, M. Takano, Y. Kobayashi, A. Chatani and H. Tadokoro, *Ferroelectrics*, 1984**, 57**, 297-326.

33. Q. M. Zhang, V. Bharti and X. Zhao, *Science*, 1998, **280**, 2101-2104.

34. F. Xia, H. Li, C. Huang, M. Y. M. Huang, H. Xu, F. Bauer, Z.-Y. Cheng and Q. M. Zhang, *SPIE Proc. Ser.*, 2003, **5051**, 133-142.

35. J. Su, J. S. Harrison, T. L. S. Clair, Y. Bar-Cohen and S. Leary, *Mater. Res. Soc. Symp. Proc.*, 1999, **600**, 131-136.

36. Q. M. Zhang, H. Li, M. Poh, F. Xia, Z.-Y. Cheng, H. Xu and C. Huang, *Nature*, 2002, **419**, 284-287.

37. V. Bobnar, A. Levstik, C. Huang and Q. M. Zhang, *Phys. Rev. Lett.*, 2004, **92**, Article No. 047604.

38. C. Huang, Q. M. Zhang and J. Su, *Appl. Phys. Lett.*, 2003, **82**, 3502-3504.

39. R. Pelrine, R. Kornbluh, Q. Pei and J. Joseph, *Science*, 2000, **287**, 836-839.

40. S. Ashley, *Sci. Am.*, October 2003, 53-59.

41. R. Shankar, T. K. Ghosh and R. J. Spontak, *Adv. Mater.* (in press).

42. R. Shankar, T. K. Ghosh and R. J. Spontak, *Macromol. Rapid Commun.* (in press).

43. R. Pelrine, R. Kornbluh, J. Joseph , R. Heydt, Q. Pei and S. Chiba, *Mater. Sci. Eng. C*, 2000, **11**, 89-100.

44. A. O'Halloran and F. O'Malley, in *Topics in Bio-Mechanical Engineering* (P. J. Prendergast and P. E. McHugh, Eds.) Trinity Centre for Bioengineering & the National Centre for Biomedical Engineering Science, Dublin & Galway, 2004, pp. 184-215.
45. G. Kofod, P. Sommer-Larsen, R. Kornbluh and R. Pelrine, *J. Intell. Mater. Syst. Struct.*, 2003, **14**, 787-793.
46. G. M. Spinks, T. E. Campbell and G. G. Wallace, *Smart Mater. Struct.*, 2005, **14**, 406-412.
47. G. Yang, W. Ren, B. K. Mukherjee and J. P. Szabo, *14th IEEE Int. Symp.*, 2004, 237-240.
48. Q. M. Zhang, J. Su, C. H. Kim, R. Ting and R. Capps, *J. Appl. Phys.*, 1997, **81**, 2770-2776.
49. R. Kornbluh, R. Pelrine, Q. Pei, S. Oh and J. Joseph, *SPIE Proc. Ser.*, 2000, **3987**, 51-64.
50. A. Mazzoldi, F. Carpi and D. D. Rossi, *Ann. Chim. Sci. Mater.*, 2004, **29**, 55-64.
51. G. Yang, G. Yao, W. Ren, G. Akhras, J. P. Szabo and B. K. Mukherjee, *SPIE Proc. Ser.*, 2005, **5759**, 134-143.
52. X. Zhang, C. Löwe, M. Wissler, B. Jähne and G. Kovacs, *Adv. Eng. Mater.*, 2005, **7**, 361-367.
53. D. Klee and H. Hocker, *Adv. Polym. Sci.*, 1999, **149**, 1-57.
54. I. W. Hamley, *The Physics of Block Copolymers*, Oxford University Press, New York, 1998.
55. I. W. Hamley (Ed.), *Developments in Block Copolymer Science and Technology*, Wiley, New York, 2004.

56. M. Lazzari, G. Liu and S. Lecommandoux (Eds.), *Block Copolymers in Nanoscience*, Wiley-VCH, Weinheim, 2007.

57. S. Jain and F. S. Bates, *Science*, 2003, **300**, 460-464.

58. G. Holden, N. R. Legge, R. Quirk and H. E. Schroeder, H. E. (Eds.), *Thermoplastic Elastomers*, 2nd ed., Hanser, Munich, 1996.

59. J. Su, Q. M. Zhang, C. H. Kim, R. Y. Ting and R. Capps, *J. Appl. Polym. Sci.*, 1997, **65**, 1363-1370.

60. J. H. Laurer, J. F. Mulling, S. A. Khan, R. J. Spontak and R. Bukovnik, *J. Polym. Sci. B: Polym. Phys.*, 1998, **36**, 2379-2391.

61. G. J. van Maanen, S. L. Seeley, M. D. Capracotta, S. A. White, R. R. Bukovnik, J. Hartmann, J. D. Martin and R. J. Spontak, *Langmuir*, 2005, **21**, 3106-3115.

62. S. G. Wax and R. R. Sands, *SPIE Proc. Ser.*, 1999, **3669**, 2-10.

63. P. Sommer-Larsen, "Artificial Muscles" technical report, Risø National Laboratory, posted at http://sitecoremedia.risoe.dk/research/artmus/Documents/MIC-ARTI.pdf, 1996.

64. S. Arora, T. Ghosh and J. Muth, *Sens. Actuators A* (in press).

65. W. Ma and L. E. Cross, *Appl. Phys. A*, 2004, **78**, 1201-1204.

66. X. Q. Zhang, M. Wissler, B. Jaehne, R. Broennimann and G. Kovacs, *SPIE Proc. Ser.*, 2004, **5385**, 78-86.

67. R. Pelrine, R. Kornbluh, Q. Pei, S. Stanford, S. Oh and J. Eckerle, *SPIE Proc. Ser.*, 2002, **4695**, 126-137.

CHAPTER 3

3 Thermoplastic Elastomer Gels –Reinventing the Wheel

3.1 Abstract

The ability of block copolymers to self assemble into different morphologies of nanometer length scale offers interesting properties. Triblock or multiblock copolymers in the presence of midblock selective solvent forms thermoplastic elastomer gels (TPEGs). This paper review the different types of TPEGs both styrenic and non-styrenic triblock copolymer based. In general, TPEGs are prepared with both saturated and unsaturated midblock containing triblocks. Properties of TPEGs are greatly influenced by chemical nature of the both midblock and endblocks.

3.2 Introduction

Two design strategies are commonly employed for material fabrication; the "top-down" approach is where bulk materials are modified using externally controlled tools, while the "bottom-up" approach simple building blocks self-organize into useful conformations[1]. Molecular self-assembly, being a "bottom-up" approach has greater adaptability than "top-down" methodologies. It enables to realize objects varying from nanometer to micrometer length scale that are difficult to achieve by conventional methods. Block copolymers (BCP), macromolecules composed of sequences or blocks of chemically dissimilar units connected by covalent bond, are a model system exhibiting self-organization. Schematic illustration of (A-B)n type block copolymer architecture is shown in Fig. 3.1[2]. They spontaneously "self-assemble" into wide variety of ordered nanoscale structures by microphase separation[3] which occur due to the phase separation of the homopolymer chains[4]. Size-coupled properties of such nanostructured polymeric systems are ubiquitous in wide variety of applications such as waveguides[5], sensing, nanotemplates[6-8], filtration[9, 10], and biomaterials.

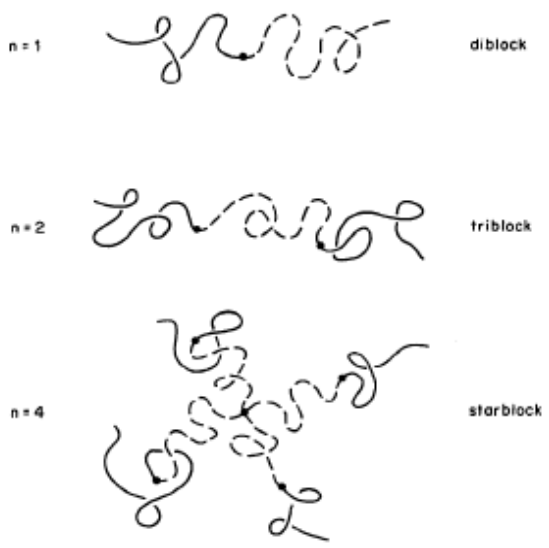

Figure 3.1 Schematic of $(A\text{-}B)_n$ block copolymers[2].

Nature and orientation of BCP nanostructured assemblies depend upon several factors such as molecular weight, composition, processing conditions, and block architecture[2, 3, 5, 11-17]. The morphological features of BCP are tunable either by addition of block-selective additives, such as homopolymer, solvents, cosurfactant (addition of second block copolymer)[18-21] or resins, or alternatively by tailoring of the blocks chemically. Extent of segregation in BCP is expressed in terms of thermodynamic incompatibility, χN[2, 16] (where χ is the Flory-Huggins interaction parameter, a temperature sensitive parameter and contains substantial enthalpic contribution and N denotes the number of repeat units along the copolymer backbone and dictate N-dependent translational and configurational entropy[22]). Figure 3.2 shows the phase diagram of a symmetric diblock copolymer melts in terms of χN and f (copolymer composition). When χN exceeds a critical value $(\chi N)_{ODT}$ (ODT is the order-disorder transition), BCP undergo a transition from a homogenous melt of chains to heterogeneous melt of ordered structure with a length scale of 5-500 nm[23].

Classical equilibrium morphologies observed in A-B diblock include body centered packed spheres, hexagonally packed cylinders (hex) and coalternating lamellar (lam). Complex and non-classical bicontinuous cubic gyroid (gyr) morphology is found for BCP between the lam and hex near the ODT. A metastable hexagonally-perforated lamella morphologies are also observed in this region[23, 25]. Extent of BCP segregation can be

summarized in phase diagram parameters based on χN and *f* into three regimes: weak (χN ~10) and strong (χN >100) segregation limits and intermediate (χN ~10-100) segregation region (WSL, SSL, and ISR, respectively), details of which can be found elsewhere[22, 26].

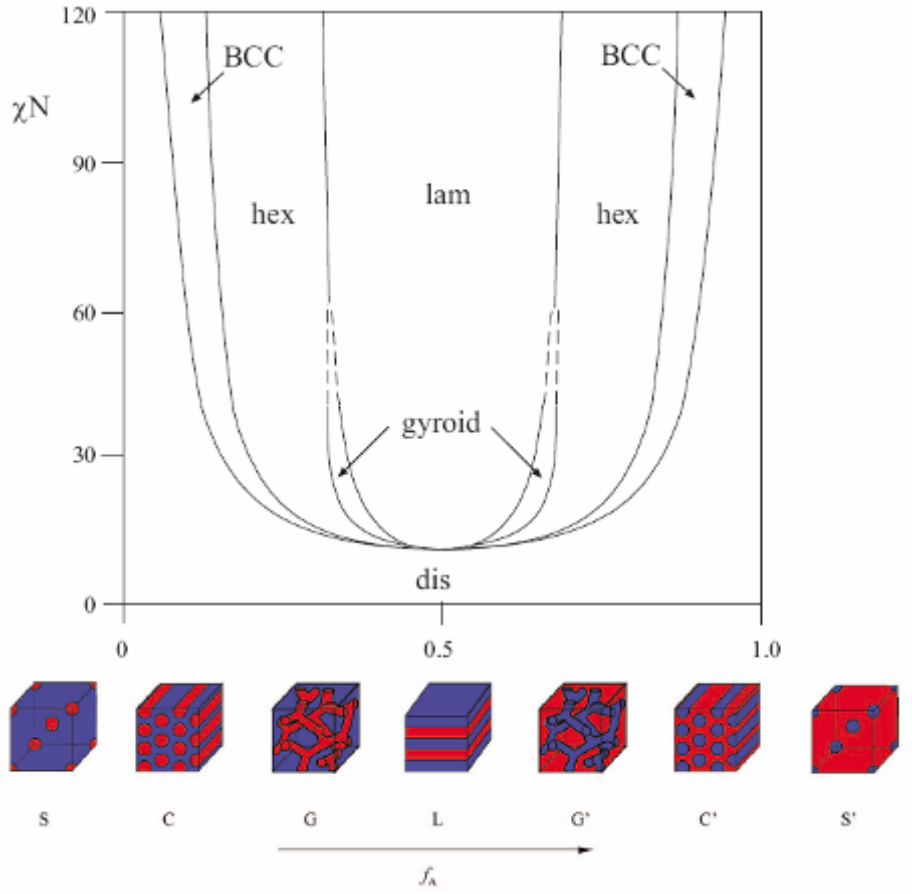

Figure 3.2 Phase behavior of symmetric diblock (A-B) copolymer based on self consistent mean field theory[23, 24].

3.3 Networks

Networks, under range of equilibrium and non-equilibrium conditions, are ubiquitous in several soft condensed matter systems such as gels (both chemical and physical), wormlike micelles, and dipolar liquids and colloids[27]. In recent years, polymer gels, like BCP, have attracted great technological and scientific interest. Polymer gels exhibit wetting properties of liquids and cohesive strength of solids and forms elastic cross-linked networks[28]. Network

formation in polymers depend either on covalent bonding or physical intermolecular interactions between macromolecules and are termed as covalent and 'entanglement networks' (EN), respectively[27, 29, 30]. Topological interaction of polymer chains in the melt or solution form EN when the concentration and molecular weight (MW) product exceeds a critical MW. This act as 'pseudogels' at time scale shorter than the lifetime of the topological entanglements[31]. However, covalently cross-linked networks are formed by various ways such as cross-linking of high molecular weight linear chains, by endlinking reactant chains with a branching unit[27, 31].

3.4 Gels

Gels are used since prehistoric times[32]; however, their definition is still matter of discussion. In 1926, Jordan Lloyd[33] defined gels as "The colloidal state which is easier to recognize than to define". In 1949, P. h. Hermans offered a more detailed definition as gels are coherent colloidal system having at least two components, possessing mechanical properties of solids where both the dispersed components and the dispersion medium are present continuously throughout the whole system[34]. Gels represent a state of matter in between solid and liquid exhibiting solid-like behavior when one of the components in solution forms a 3D network.

3.5 Gelation

Gelation involves the phase transition of a system from viscous liquid to a solid-like material. This transition is known as 'sol-gel' transformation and the point in the phase diagram at which first network molecule forms is known as "gel point"[35]. The Winter-Chambon criterion, which states that at gel point, the ratio of the loss and storage moduli is independent of frequency is often used to study polymer gels.[36-38]. The first quantitative description of molecular changes during gelation in polymerization was given by Flory[39, 40] and later elaborated by Stockmayer. Gelation transition is intriguing and it resembles the "bond-percolation" problem[41]. According to the Flory-Stockmayer model, gelation can be visualized by considering a rectangular grid with dots, as depicted in Fig. 3.3. Each dot represents a network forming molecule or polymer (monomer, dimmers, trimers,…),

characterized by probability P_b[42]. Gelation occurs when P_b reaches a critical or threshold value P_c ($P_b > P_c$), there exist a single dot or molecule which is infinite in spatial extent i.e., connected dots traverse the entire grid[41]. Flory Stockmayer model is recognized as "bond-percolation" problem[41, 43].

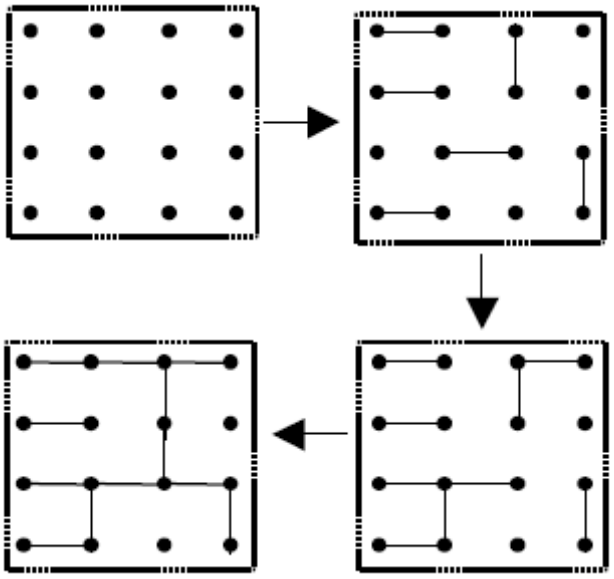

Figure 3.3 Schematic illustration of percolation theory of network formation.[42]

3.6 Classification of Gels

Gels are classified based on either their constituent phases, polymers or structurally. Table 3.1 shows the classifications of gels based on their constituents properties[30]. Flory[44] classified gels on the basis of structure into four categories, catalogued in Table 3.2. Figure 3.4 displays the schematic of gels based on Flory's classifications[32]. Alternatively, depending on the nature of the bond which forms the network, gels are classified either "chemical" or "physical".

3.6.1 Chemical gels

Network formation in chemical gels takes place either by chemically cross-linking or by covalent linkages. These gels form irreversible networks because tends to degrade on exposure to high temperature and large deformation[42]. Chemical gels have infinite MW;

therefore, have infinite relaxation times and an equilibrium modulus. Figure 3.5 illustrates the schematic of physical and chemical crosslinkings[30].

Table 3.1Gels classifications*

Basis	Type	Examples-Solvent	Materials
Constituent phases and solvents	Solid-liquid	Hydrogel-water[45, 46]	poly(ethylene glycol-b-propylene glycol-b-ethylene glycol) (Poloxamer), poly(ethylene glycol) / poly(D,L-lactic acid-co-glycolic acid) block copolymers
		Organogel-organic[47, 48]	Dibenzylidene sorbitol, 12-hydroxystearate, 2-amino-2-phenylethanol
		Alcogel-alcohol[49]	Phenol-Furfural
	Solid-gas	Xerogel-air[50-52]	Gelatin, tetraethoxysilane (TEOS) xerogel
		Aerogel-air[53-56]	Silica, alumina, carbon aerogels
Constituent polymers	Natural gel	Protein and polysaccharide gels[30, 57]	Pectin, agarose, agar, Fibrin clots
	Synthetic gel	Organic polymer and inorganic gels{[58-60]	Collagen based, TiO_2 based
	Hybrid gel	Polysaccharide/protein and synthetic polymer, Polymer andinorganic material[61, 62]	polysaccharide-silica, TEOS and poly(ethylene glycol)

*Modified table from reference[30]

Table 3.2Flory's structural classification of gels

Flory Category	Statement	Example	Property
I	well-ordered lamellar structures, contain gel mesophases	Soap gels and phospholipids, liquid crystalline materials	Long range order
II	covalent polymeric networks	Vulcanized rubber, elastic structure protein elastin, vinyl-divinyl copolymers	Completely disordered
III	Polymer network formed through physical aggregation	Biopolymer gels gelatin, PVC,PVA	Predominantly disordered but with ordered regions
IV	Particulate	V_2O_5 gels, globular and fibrillar protein gels	Disordered structure

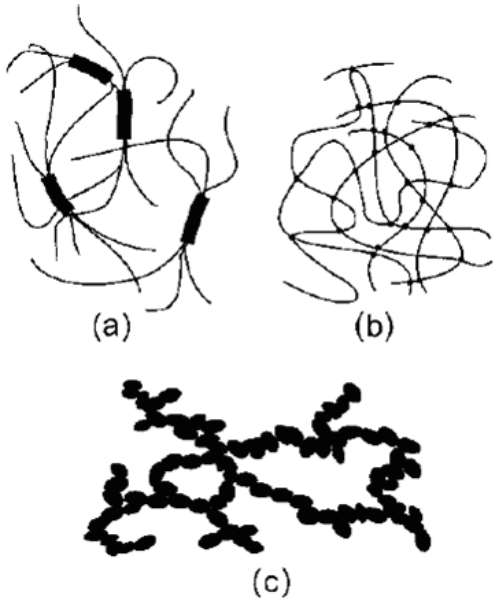

Figure 3.4 Schematic representations of gels (a) Flory III type, (b) Flory II, (C) Flory IV.[32]

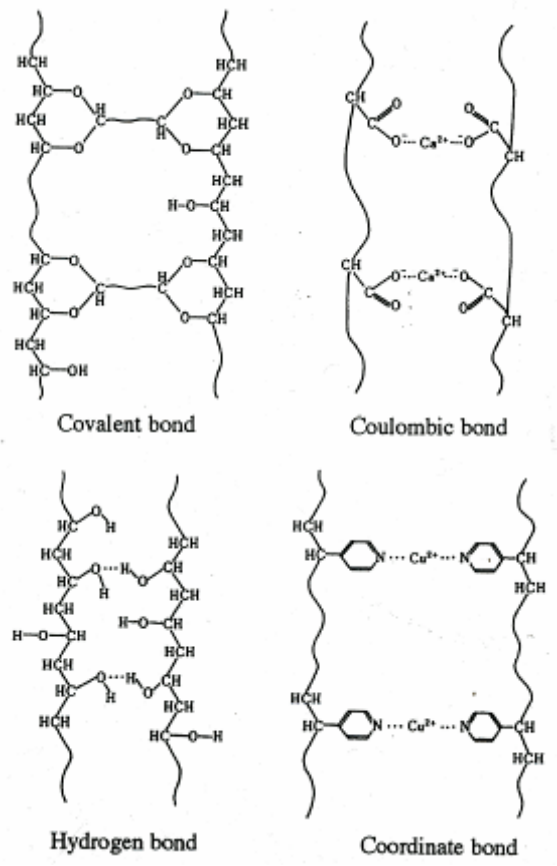

Figure 3.5 Schematic illustrating chemical and physical crosslinking.[30]

3.6.2 Physical Gels

These gels are formed by weak forces (i.e., non-covalent forces) such as hydrogen bonds, Van der Waals forces, electrostatic interactions, or hydrophobic and ionic interactions that favor association between certain points on different polymeric chains. These gels also termed as thermoreversible gels because interactions taking place between connecting domains are of the order of kT (k, Boltzmann constant and T, temperature). Hence, the network can collapse upon heating and reform upon cooling[31, 42]. According to Flory's classification, physical gels belong to the third type[44]. If the solvent molecules are organic, then physical gels are referred as "organogels", details of which can be found elsewhere[48, 63-65]. Entangled networks, characteristics of physical gels, at very low frequency in the 'terminal zone' flow as high viscosity liquids, however this behavior is absent in cross-linked networks (i.e., chemical gels). Chemical gels swell in appropriate solvents but do not

dissolve; however, physical gels dissolve to form more dilute polymer solution. Length of the disordered chains between junctions of the physical gels is shorter and inflexible than the regions of random coils in chemical gels[32]. Network formed in chemical gels are considered as homogenous (self-similar) in the sense of free of ordered regions such as micelles or structured aggregates, present in physical gels[27, 44].

The Percolation model considered responsible for gel formation is a continuous transition unrelated to the thermodynamic properties of the systems[66]. It is successfully applied for chemical gels[67, 68], but debated for physical systems[69, 70]. Guenet emphasized that thermoreversible gelation is not always percolation phenomenon[71]. Zilman and Safran, using men field approach, predict that percolation transition partially overlaps with the first-order transition, and is continuous[66].

3.7 Micellization and Phase Behavior

Morphology and thermodynamics of microphase separation in diblock (AB) and linear multiblock (ABA) BCP is published in detail in recent reviews[26, 72]. In case of diblock copolymer (AB), A and B blocks are fixed at junction site, and therefore adopt a tail conformation. However, in case of linear multiblock copolymer (ABA), endblocks (A) acquire either looped conformation (both the endblocks reside in the same interface) or bridged conformation (both the endblocks reside in adjacent interfaces). In presence of a solvent which is poor for one block (block A) and compatible/selective for the other block (B block), BCP tends to associate and form aggregates called micelles[48, 73-79]. Micellization occurs in dilute solution that is selective for one of the blocks, above a concentration known as the critical micelles concentration (CMC)[26] (see Figure 3.6[26]) and corresponds to a concentration at which sufficient number of micelles are formed to be detected by current characterization tools[80].

The soluble blocks (B block), due to their affinity towards the continuous medium form the “corona” of the micelles, and the insoluble blocks (A block), in order to reduce their enthalpy, form the “core” of the micelles, as displayed in Fig. 3.6[26]. CMC shows strong dependence of thermodynamic incompatibility (χN)[81, 82]. As the concentration of BCP increases further in the solution, beyond a critical gel concentration (CGC) a gel phase appear, as shown in Fig. 3.6.

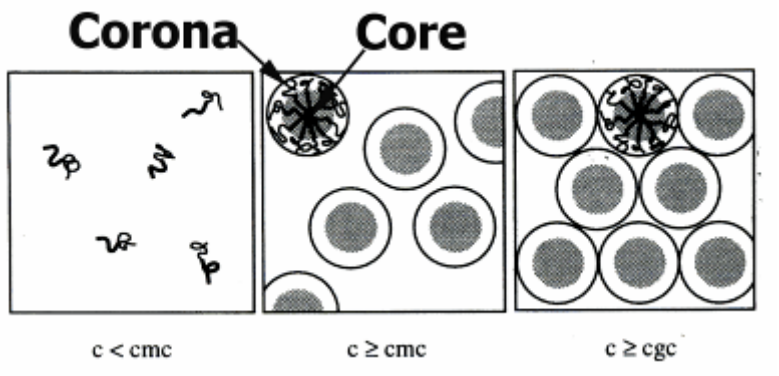

Figure 3.6 Schematic representation of critical micelles concentration (CMC) and critical gel concentration (CGC) in BCP solution.[26]

Both diblock and triblock copolymers forms micelles with selective solvents, however triblock copolymers adopt more topologies. Balsara et al. schematically showed the possible structures formed by diblock and triblock copolymers in selective solvents, as displayed in Fig. 3.7[83]. Figure 3.7 (a) reveals the case of diblock (AB) and triblock (BAB) copolymers where solvent is selective to end blocks. The micelle core is made up of A block surrounded by corona of solvated B blocks whose one end is "tethered" with core-corona interface, while the other end is free. Preferential dissolution of midblock in BAB triblock is shown in Fig. 5 (b-d). Fig. 7 (b) shows flower like micelles due to the formation of loops by solvated endblocks, which causes an additional entropic penalty. If this penalty is too large, endblocks extend into the solution as free ends (Fig. 7 (c)). This entropic penalty is also overcome by formation of branched structures of the triblock copolymers (BAB) where endblocks (B blocks) connect the different cores (A block), as illustrated in Fig. 7 (d).

In the semidilute and concentrated solutions, microdomain formation of diblock and triblock copolymers are different. In case of diblock (AB) copolymers, molecules are coupled through the entanglements of the solvated B blocks in the corona of the close-packed micelles, known as microlattice[85, 86, 86], as elucidated from Fig. 8 (a). In case of triblock copolymers at high copolymer dilution, midblock adopts conformation such as loops (both endblock resides in the micelles), bridges (each endblocks resides in different micelles), and dangling ends (one endblock resides within the matrix) (see Fig. 8 (b)),

gelation could occur by bridging of the micelles[87, 88] along with entanglements[81] which results in a 3-D network formation, known as physical gel[89-94] or mesogels[95-101].

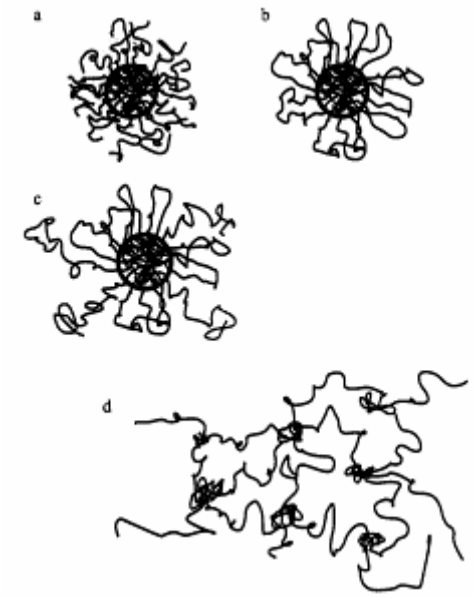

Figure 3.7 Possible micelles and aggregates formed by diblock and triblock copolymers in selective solvents. (a) Solvent is selective towards end blocks or B block in case of AB and BAB block copolymers. (b) For high loop/bridge ratio, Flower like micelles in case of BAB triblock copolymer where solvent is selective towards A block. (c) A block selective BAB triblock with some free B block extending into solution. (d) A block selective BAB triblock, branched structure formation where strands of B block extending into the cores of different micelles.[83, 84]

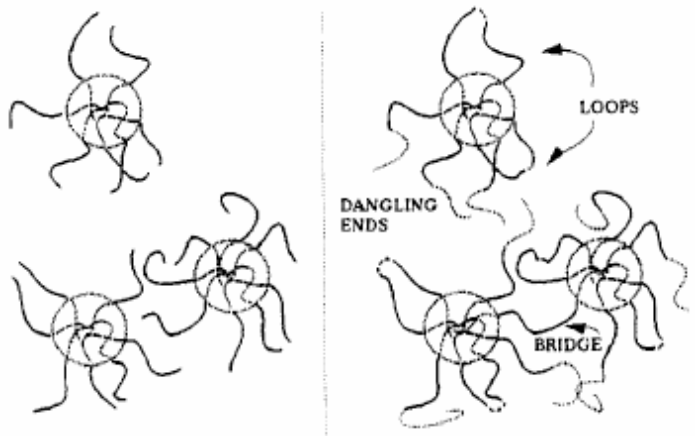

Figure 3.8 Chain topologies of (a) diblock and (b) ABA triblock copolymers in selective solvents.[81]

Low molar mass non volatile solvent selective thermoplastic elastomer multiblock copolymers with rubbery midblock and glass/semicrystalline endblocks are designated as thermoplastic elastomer gels (TEPG)[89, 94, 102-109]. Table 3.3 shows a comparison between diblock and triblock copolymer gels.

Table 3.3 Diblock vs Triblock copolymers gels

Property	Diblock copolymer (AB) gel	Triblock copolymer (ABA) gel	Reference
Topology	Dangling ends	Bridges, loops, and dangling ends	[83]
Gelation	Gelation occurs by extensive entanglement of the coronal chains	Gelation occur by bridging and entanglement	[81, 85, 86]
Aggregation number	For same MW, higher aggregation number	Lower than diblock at same MW	[84]
Elastic modulus	Lower than triblock copolymer gel	Higher than diblock copolymer gel	[81]
Rheological response at very low shear stain rate ($T<T_g^{core}$)	Behaves as fluid	Behaves as elastic solid	[81]
Free Energy of micelles	$F_{core}+F_{corona}F_{int}$	$F_{core}+F_{corona}F_{int}+F_{loop}$	[83, 84]

3.8 Types of TPEG

Microphase separated molecular networks of multiblock copolymer such as ABA, BAB, and ABAB, ABABA, and ABC swollen by midblock selective solvents forms TPEG (where A or C is crystalline or semi-crystalline end blocks and B is the rubbery midblocks). Commonly investigated TPEGs are based on triblock copolymers (ABA)[86, 102, 105, 110, 111]. These TPEGs can be classified based on their endblocks into three broad categories.

a) Symmetric styrenic triblock (ABA) copolymers
b) Non-symmetric styrenic triblock (ABC) and multiblock copolymers
c) Symmetric non-styrenic triblock copolymers

3.8.1 Symmetric Styrenic Triblock (ABA) Copolymers based TPEG

Over the past decade, numerous experimental studies aimed to establish fundamental relationships between morphology and property development in styrenic triblock copolymer gels[89, 94, 109, 112, 113]. Both commercial[89, 94, 109, 114] and synthesized[96, 115] styrenic based triblock copolymers have been used for studying effect of molecular weight, copolymer compositions, and process parameters such as temperature and shear on properties of these gels[89, 94, 109]. Based on the bonding state of the midblock, these triblocks can be subdivided as hydrogenated and non-hydrogenated triblocks.

3.8.1.1 Non-Hydrogenated TPEG

These TPEGs consist of polybutadiene and polyisoprene midblocks and have one double bond per monomer unit and are commercially available as styrene-isoprene-styrene (SIS) and styrene-butadiene-styrene (SBS)[12, 116, 117]. Synthesis of these triblocks can be found elsewhere[116]. Structure-property relationships of oil-extended unsaturated triblocks have been studied extensively by researchers[93, 117-125]. Bordeianu and co-workers established the relationship between the mechanical properties of SBS diluted with two types of mineral oils[118-121]. Figure 3. 9 shows the stress-strain plot of SBS triblock copolymers diluted with mineral oil. This figure shows that at low strains, yielding and drawing (plastic-to-rubber transition) occur, which is followed by hardening effect at medium strains and finally an inflection point at larger strain beginning from an oil concentration 50%, as shown by an arrow[119].

They found that oil with more aromatic hydrocarbons exhibited larger stress values at any given elongation and oil level[118]. They used small angle X-ray scattering (SAXS) to determine the morphology of the SBS copolymer dilute with paraffinic mineral oil,

polybutadiene (PB) (lithene PM), and aromatic mineral oil[118, 120]. Figure 3.10 reveals the long period (L), determined from SAXS, as a function of volume fraction of oil in the polymer. It shows that L first increases with increasing oil fraction and reaches to a maxima at 33 vol% for paraffinic oil and lithene and 43 vol% for aromatic oil followed by sudden drop. The authors believed that this is an indication of morphological transition of polystyrene (PS) domains from cylinders to spheres[118, 120]. Linear viscoelastic properties of SBS with midblock selective either oil[117] or n-tetradecane[126] was studied by dynamic rheology.

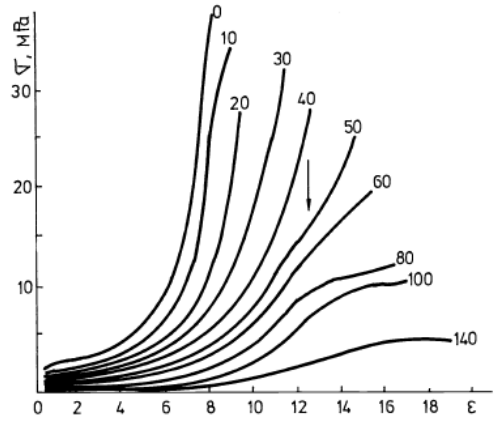

Figure 3.9 Stress-strain plot of SBS copolymers diluted with mineral oil varying from 0 to 140 wt%.[119]

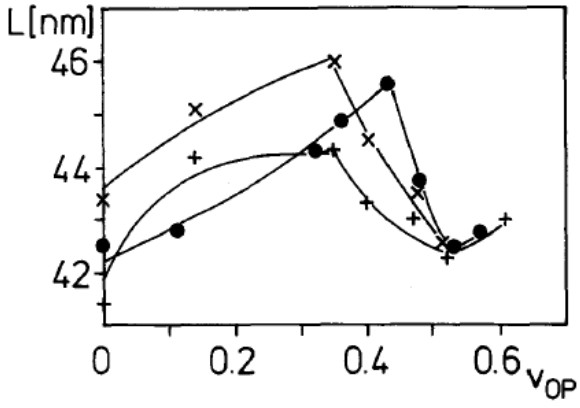

Figure 3.10 Long period (L) of SBS copolymers diluted with (+) low molecular weight PB (lithane PM), (x) paraffinic oil, and (●) aromatic oil.[121]

Watanabe et al. developed a transition map which classified the temperature response of SBS, diluted with n-tetradecane[126], as displayed in Fig. 3.11. They found that rubbery-to-plastic transition temperature (48-53^{0}C) did not show pronounced dependency on SBS concentration; however plastic-to-viscous transition (103-119^{0}C) showed a strong concentration dependence.

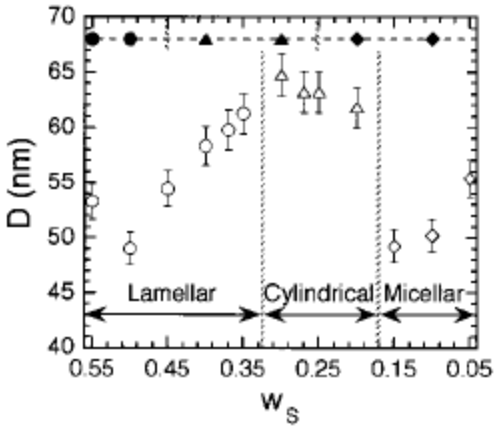

Figure 3.11 Experimental morphology diagram for SIS (filled symbol) and SEPS (open symbol) triblocks, diluted with mineral oil, displaying composition ranges over which different morphology lamellar (● and ○), cylindrical (▲ and Δ), and micellar (◆ and ◊) have been observed.[109].

Similar to SBS TPEG, morphology[96, 109], rheology[109, 123], and tensile deformation under both static[127] and dynamic[96] loading of SIS TPEG has been studied extensively. Based on SAXS measurements, Spontak and co-workers developed an experimental morphology diagram for SIS/oil blends displayed in Fig. 3.11[109].

This figure reveals that unsaturated (I) midblock of the SIS copolymer is less incompatible with S endblock compared to saturated (EB) midblock of SEPS copolymer, therefore exhibits shorter lamellar regime. Linear viscoelastic response of SIS copolymers dissolved in I selective n-tetradecane (C14) was studied by Sato et al[123]. They found that SIS/C14 exhibited composition fluctuation in the vicinity of T_{ODT}. For the isothermally equilibrated state, the power law behavior was observed at high frequency (ω) (in the narrow range of ω) and slow relaxation mode was found at low ω that indicates that self-similarity in the get structure lost at larger length scale. Prasman and Thomas examined the large strain (i.e., 300% uniaxial) deformation behavior of SIS/oil blends via in-situ SAXS

measurements[127]. They demonstrated that soft rubber matrix deformed in an affine manner, while glassy S domain remained spherical. They found that there was no stress relaxation during deformation and microstructure was completely reversible upon unloading.

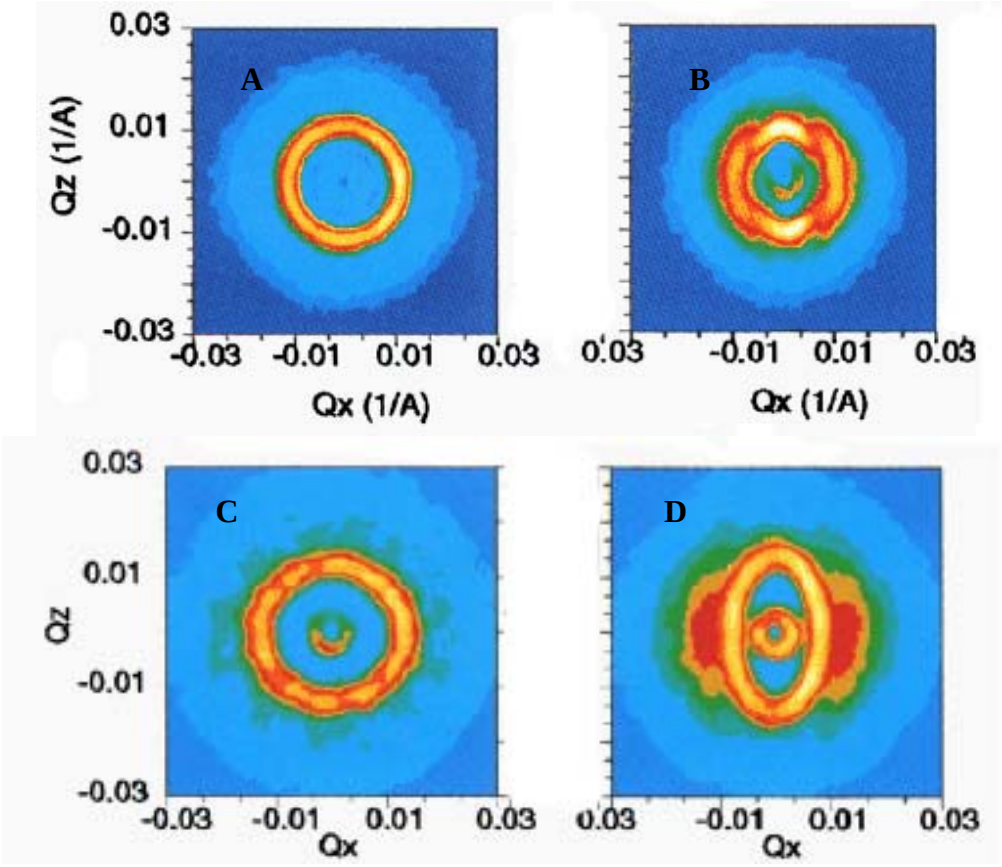

Figure 3.12 SANS pattern of 12% SEPS (A and B) and SEBS (C and D) TPEGs. A and C original undeformed states. B and D after 100% deformation.[128]

3.8.1.2 Hydrogenated TPEG

Non-hydrogenated linear triblocks are more susceptible to the chemical attack due to the presence of unsaturated bonds in their backbone, which limits their thermal and oxidative stability[12]. In addition, butadiene in SBS tends to crosslink and I in SIS go through chain scission on ageing[129]. In order to overcome these limitations, hydrogenation of unsaturated midblocks of these triblocks is carried out. Different hydrogenated styrenic triblocks available to date are poly[styrene-*b*-(ethylene-co-butylene)-*b*-styrene] (SEBS), poly[styrene-

b-(ethylene-co-propylene)-*b*-styrene] (SEPS), and poly[styrene-*b*-ethylene-*b*-(ethylene-co-butylene)-*b*-styrene] (SEEPS). The most readily available commercial styrenic triblock copolymer is SEBS, manufactured by Kraton and Kuraray and available in different molecular weights, due to which this triblock is most extensively studied TPEG. Several researchers using different techniques such as TEM, SAXS, and SANS under different conditions have looked at morphology of these TPEGs[89, 94, 106, 108, 109, 128, 130]. Reynders et al. used small-angle neutron scattering (SANS) to study the effect of stretching on microstructure of the SEPS and SEBS gels[128]. They observed that 12 wt% SEBS copolymer gel with 35% S exhibited affine deformation upon stretching to 100% like SBS gels, explained in the previous section[127] (Fig. 12 A & B), and chemically cross-linked networks[131]. However, improvement in the angular as well as spatial order was observed when similar composition of SEPS gels was stretched to 100% (Fig. 3.12 C & D) which indicated the formation of relatively well-defined layers of regularly spaced S domains. Reynders and co-workers in another publication reported that S domains of SEPS/SEBS TPEG distorted at large deformation (>200%)[132]. In-situ studies of microdomain network deformation and its dependence on macroscopic extension rate was also investigated by Reynders and co-workers[133] for the SEBS TPEGs. Figure 3.13 shows that at low deformation rates (Fig. 3.13a), the deformation of the microstructure deviates from ideal behavior (solid line in this figure). However, at large deformation rate (Fig. 3.13b); this figure indicates that deformation pattern follows affine behavior. Apart from tensile deformation, Mortensen et al. investigated in-situ microstructure deformation under shear using rheology[134]. Shear induced bcc texture development are shown in Fig. 3.14 which reveals γ-ω phase diagram. At low strain/frequency no shear alignment was observed. For small γ (10 - 40%) and ω ($1 – 10s^{-1}$), a two dimensional powder was found with pronounced {100}/<011> sliding plane configuration.

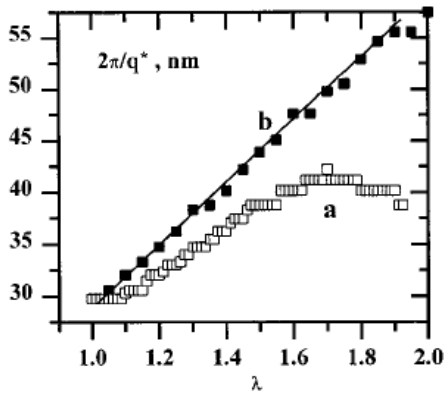

Figure 3.13 The position of structure factor maxima q^* plotted as a function of the deformation ratio λ. Solid line indicates the affine deformation. Extension rates were (a) 4E-4 s^{-1} and (b) 1E-2 s^{-1}.[133]

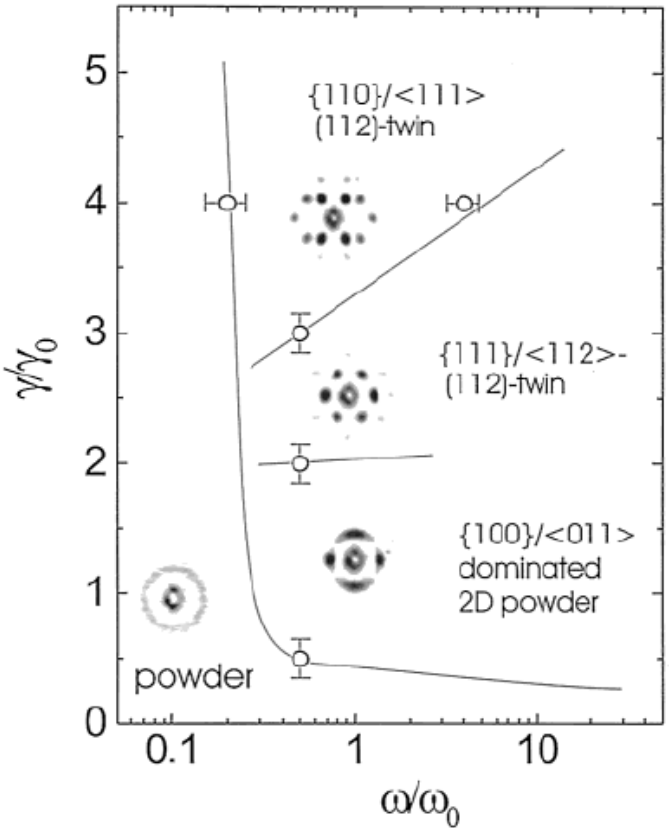

Figure 3.14 Phase diagram displaying texture development for normalized shear amplitude and angular frequency where normalized frequency (ω_0) and shear amplitude (γ_0) are 2 s^{-1} and 20%, respectively.[134]

A twin-domain oriented ({111}/<-1-12>) morphology was observed at intermediate strain levels. A {110}/<-111> twin bcc texture was developed at largest strain. The stress relaxation response of SEBS TPEGs was determined under compressive deformation by Quintana et al[114, 135136]. They found the large relaxation rates for the SEBS gels which indicative of high mobility of these physical networks over the time of measurement. They believed that a dynamic equilibrium existed in the SEBS gels where some junctions were broken and new ones were formed continuously. Figure 3.15A shows that rate of relaxation (m) is slightly dependent on λ. They also showed that relaxation rates (m) were relatively independent of the copolymer concentration. Relaxation rates were high for lower copolymer[114] (as shown in Fig. 3.15B) and oil molar masses[136]. This figure shows the variation of m with temperature and m is independent of temperature for temperature substantially lower than the gelation temperature.

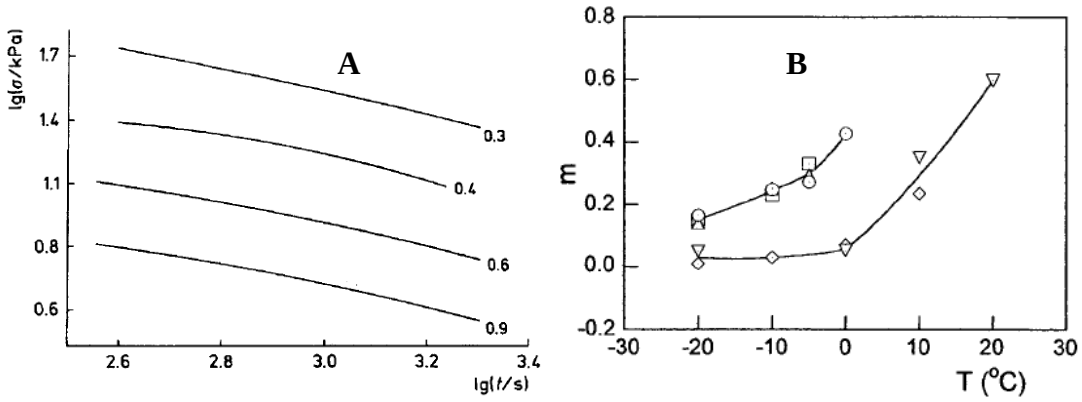

Figure 3.15 Compressive stress relaxation plots on a double logarithmic scale for SEBS gels at 25^{0}C and 15 wt% copolymer at different deformation (λ).[135] (B) Stress relaxation rate [m = -d(log σ)/d(log t)] as a function of temperature for SEBS (87.3 Kg/mol with 32 % S) at 8.5 (□), 11.2 (Δ), and 17.5 wt% (○) and SEBS (260 Kg/mol with 30 % S) at 4.9 (◊) and 6.8 wt% (▽) at deformation 0.7.[114]

Relaxation rates show an abrupt increase when the temperature is reached to a certain point, which implies that near the gelation temperature with the increase of temperature the lifetime of gel junction, decreases. Spontak and co-workers studied in detail this class of styrenic TPEG[25, 42, 89, 89, 94, 96, 106, 109] for structure-property correlations. They did extensive TEM to show the microstructure of the styrenic triblock copolymer gels. Figure 3.16 demonstrates the morphology of SEBS TPEG as a function of copolymer fraction[89, 94]. They

found that shape and size of the styrenic micelles are not strongly dependent on either the wt% copolymer or processing history (quenching vs. slow cooling). They observed that as the copolymer fraction increases, inder-domain distance (D) and linear viscoelastic strain (γ_{LVE}) decreases, however, time to rupture, dynamic tensile and shear storage moduli, and order-disorder temperature (ODT) increases[94, 96, 106]. In addition, they found that γ_{LVE} decreases with increase of both temperature and copolymer fraction[94]. They found a power law relationship between moduli, both dynamic storage modulus and stress-relaxation modulus, and copolymer concentration (C in g/cm^3) which scaled as C^{β} ($\beta \approx 2.43$) for the SEBS/oil blends and concluded that measured moduli was contribution of entangled midblock loops and dangling ends along with bridged midblocks[89].

King et al. monitored the change in the time dependent oil content upon swelling of the SIS and SEPS triblocks[96]. Due to the greater chemical similarity of EP than I with mineral oil, they found that maximum oil uptake in the SEPS/oil and SIS/oil blends were 154% and 34% mass increase, respectively. For the SEPS/oil blend, Laurer et al. observed a linear increment in D with increasing oil fraction; however SIS/oil series revealed that D was not sensitive to oil content[109]. Figure 3.11 shows that hydrogenation of midblock I substantially shifts the threshold over which lamellar morphology is observed. This figure also suggests the greater compatibility of hydrogenated midblock (EP) than non-hydrogenated midblock (I) with the oil. The broader lamellar morphology stability in SEPS/oil blend was attributed to greater incompatibility of EP and S that eclipses the compatibility between EP and oil.

3.8.2 Non-Symmetric Styrenic Triblock (ABC) and Multiblock Copolymers

Commonly investigated non-symmetric styrenic triblock copolymer is polystyrene-polybutadiene-poly(methyl methacrylate) (SBM). To the best of our knowledge, only Yamaguchi et al. investigated SBM gels[103]. They showed that SBM had an advantage over ABA (such as SBS) triblock because in the case of SBM, B midblocks formed bridges between two dissimilar endblocks such as S and M end blocks[103], unlike ABA triblock. Figure 3.17 shows the presence of twinned hexagonal structure in the SBM/oil gels. Yamaguchi et al. studied the morphology of these gels by first staining with RuO2 which stained only M block, as displays in Fig 3.17a. This figure reveals the presence of 6-fold

symmetry where cylinders of M are hexagonally arranged which were cut perpendicularly to their long axis. TEM in Fig 3.17b shows OsO4 stained gels where S blocks appear gray and M blocks appear white. This micrograph has families of cylinders namely large cylinders made of M endblocks and small cylinders comprised of S endblocks. When a portion in the Fig. 3.17b was blown up in Fig 3.17c, it elucidated the presence of both types of cylinders, hence Yamagchi et al, concluded the presence of twinned hexagonal structure of S and M, as shown in Fig 3.17d.

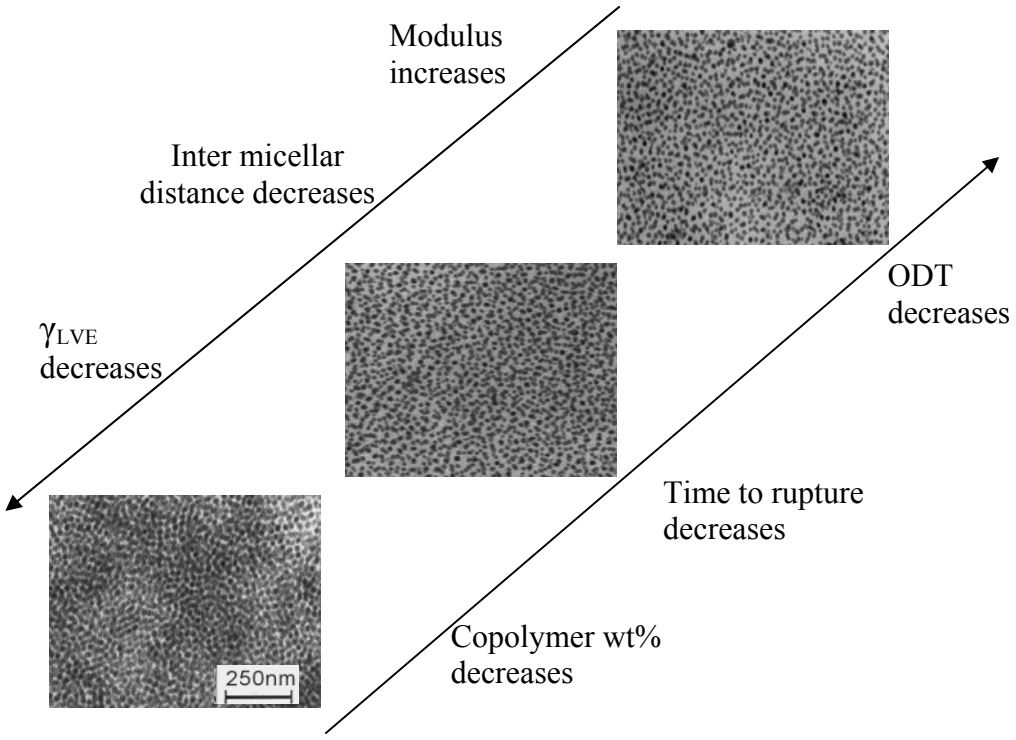

Figure 3.16 TEM micrograph of SEBS TPEG with 30, 20, 10 wt% copolymer quenched from 180 to 0^0C.[89]

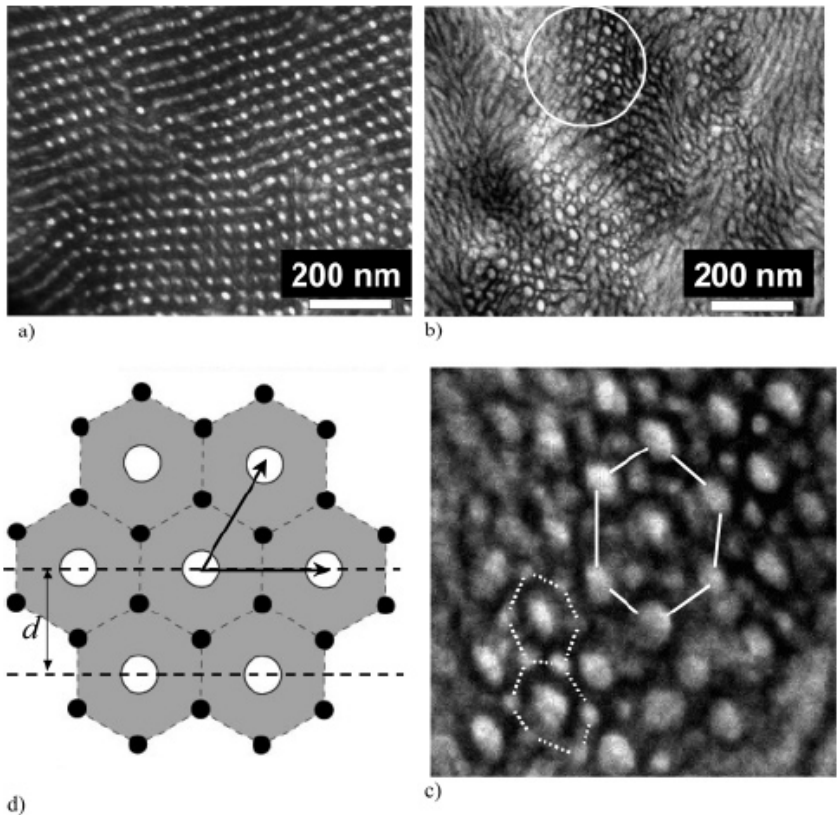

Figure 3.17 TEM micrograph of an annealed SBM/oil blend of (50/50 g/g). (a) RuO_2 stained gels showing hexagonally array of cylinders of M endblocks. (b) OsO_4 stained gels showing both S and M cylinders. (c) Circle in the (b) zoomed here showing PMMA hexagon in the centre and dotted lines showing hexagon of S. (d) schematic illustration of proposed twinned hexagonal structure.[103]

Apart from these gels, a few reports are also available on $(AB)_n$ ($n \geq 2$) multiblock copolymer gels[137, 138]. Lal and co-workers examined the SBSBS pentablock copolymer in n-heptane[137], a strongly selective solvent for PB blocks and in 1,4-dioxane[138], which is a slightly selective solvent for PS and a Θ solvent for PB. For the SBSBS and n-heptane case, they observed that gels were formed by association of the multiple domains (domain of the insoluble blocks, PS) and not by bridging of the miceller domains (PB)[137]. The petablock/n-heptane blend exhibited strong microsynerisis and did not form flower-like micelles unlike the similarly reported SBS triblock gels. On the other hand, SBSBS/1,4-dioxane blends displayed bridging of the insoluble PB block by the soluble middle-block PS chains and formed large aggregates which were randomly distributed crosslinks on length scale greater than the domain size[138].

3.8.3 Symmetric Non-Styrenic Triblock Copolymers

Triblocks examined in this category include poly(methyl methacrylate)-b-poly(n-butyl acrylate)-b-poly(methyl methacrylate) [PMMA-PnBA-PMMA][139], poly(methyl methacrylate)-b-poly(tert-butyl acrylate)-b-poly(methyl methacrylate) [PMMA-PtBuA-PMMA][140, 141], syndiotactic poly(methyl methacrylate)-b-polybutadiene-b-syndiotactic poly(methyl methacrylate) [sPMMA-PB-sPMMA][142-144], and sPMMA-PEB-sPMMA[93]. Acrylic gels have been examined for their mechanical and rheological properties based on either synthesized[141, 145] or commercially[139, 141, 146] available acrylic triblock copolymers. Shull and co-workers studied [PMMA-PtBuA-PMMA]/alcohols (including ethanol, 1-butanol, 2-ethylhexanol, and 1-octanol) blends and observed two transition temperatures: the critical micelle temperature near 60 ^{0}C, below which PMMA endblocks aggregated to form gel network, and glass transition temperature, varied from 35 to 50 ^{0}C, of the aggregated PMMA endblocks, as illustrated in Fig.18, although both transition temperatures unveiled block length and concentration dependence[141]. They observed that tacticity of the PMMA block did not play an important role in either micellization or the glass transition process. Recently, they studied the effect of endblock length, endblock fraction, and gel concentration on the [PMMA-PnBA-PMMA]/2-ehylhenanol gel properties[139]. They found that aggregation number increased with increasing gel concentration and PMMA block length; however, inter-micellar spacing was relatively insensitive to concentration changes. Relaxation time of these gels revealed an increment of 10^6 when PMMA block length increased from 9K to 25K with a polymer fraction of 0.15[139].

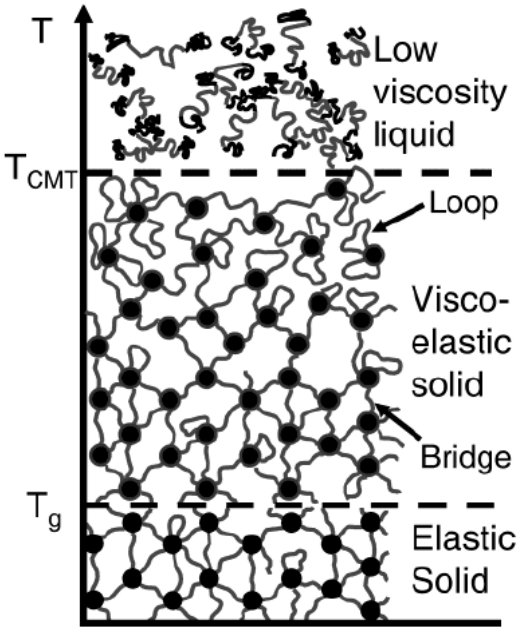

Figure 3.18 Schematic illustration of temperature dependent structure of PMMA triblock copolymer gels in alcohols.[141]

Jérôme and co-workers studied the sPMMA-PB-sPMMA triblock copolymers (MBM type) of different molecular weights and chemical compositions with o-xylene, a PB block selective solvent[93, 143, 144, 147]. These are particular class of physical gels where interactions are stronger than in most of the physical gels. MBM based thermoreversible gels are formed by intra- and intra associations of the sPMMA domains[147]. Based on scaling theory $G`(\omega) \sim G``(\omega) \sim \omega^{\Delta}$, they found scaling exponent (Δ) was independent of molecular weight and composition of MBM copolymers[143]. In another report, they examined the gelation behavior of both hydrogenated (PBD) and non-hydrogenated (PEB) midblock (X) containing MXM gels[93]. They found that gelation time of a hydrogenated block copolymer under the same experimental conditions was much longer (twice) compared to non-hydrogenated copolymer. However, scaling exponent (Δ) of MXM gels was independent of chemical nature of the midblock.

3.9 Nanocomposites

In order to overcome the shortcoming of TPEGs, several strategies have been suggested in the literature, which include the formation of nanocomposites[102, 105, 110, 144, 148, 149].

Nanocomposites are formed by (i) addition of amorphous/semicrystalline homopolymer to the micellar core[102, 110, 144], (ii) addition of cosurfactant (chemically identical diblock)[115, 149, 150], (iii) addition of inorganic fillers such as silica and nanoclay[105, 148], and (iv) addition of both carbon nanotubes and nanoclay[105]. TPEGs based nanocomposites are classified here as organic/inorganic that corresponds to organic triblock copolymers and inorganic fillers; and organic/organic which relates to organic triblock copolymers and organic fillers.

3.9.1 Organic/Inorganic

To improve the inherent low modulus and low maximum operating temperature of TPEGs, these gels were reinforced with (nano scale) inorganic fillers such as nanoclay and silica particles[105, 148, 151]. Spontak and co-workers investigate the effect of nanoscale inorganic additives such as silica nanoparticles, silicate nanoclays, and carbon nanotubes on the property and morphology development of SEBS gels[105, 151]. They found that most pronounced increment in the storage modulus for the nanoclay having hydrophobic treated surface, attributed to the formation of secondary load bearing nanoclays networks at higher loading levels. However, it was reported that thermomechanical properties of SEBS/mineral oil TPEGs did not change much due to the addition of inorganic fillers such as fumed silica and carbon nanotubes. Contrary, Theunissen et al. found that viscoelastic transition from rubber to plastic fluid and from a plastic fluid to a viscoelastic liquid are shifted to higher temperature upon silica addition to SEBS based TPEGs[148]. They proposed that silica served as a reinforcing agent of the rubbery matrix of SEBS TPEGs which was attributed to the hydrophobic-hydrophilic interactions between silica particles and polystyrene endblocks.

3.9.2 Organic/Organic

Apart from the aforementioned methodologies to alter the mechanical properties of TPEGs, perusal of the literature suggests that by addition of either endblocks (S or PMMA) selective homopolymer)[102, 110, 144] (to swell micellar cores or diblock copolymers[115, 149, 150] (to alter the extent to which midblock connects neighboring micelles) properties can be altered. Here authors have categorized them as organic/organic nanocomposites due to the organic

nature of the additive. Further, we have classified them in two subcategories: homopolymer and cosurfactant, based on the type of polymer additive.

3.9.2.1 Homopolymer

TPEGs micellar cores have been modified by incorporation of homopolymer which mixed either exothermically[102] (negative χ) or athermally[150] (zero χ) with the endblocks. Jackson et al. used poly[2,6-dimethyl-phenylene oxide] (PPO), as S selective, to modify the SEBS and mineral oil TPEGs[102]. They observed an increase in micellar size and disordering temperature, while decrease in extension ratio (λ) with the increase of PPO. The observed decrease in λ with PPO was attributed to the reduction in the bridged EB block fraction due to the increase in micellar diameter. However, it was observed that presence of PPO had little impact on the tensile strength of these ternary blends at room temperature. Walker et al. observed pronounced increment of G' in SEBS gel through addition of a high molecular weight semicrystalline homo polystyrene (shS)[110]. This large increment in G' was accredited to the formation of nanoscale shS filaments and sheets, dispersed uniformly within the micelles-stabilized gel matrix, of varying thickness, length, and shape. Comparisons of shS and silica modified gels revealed that the shS is far more superior to inert filler. Quintana et al. also found an increase in the sol-gel transition temperature, the elastic storage modulus, and the equilibrium swelling ratio with the increase in polystyrene percentage[111]. In another class of triblock copolymers, the stereocomplexation of sPMMA-PBD-sPMMA with isotactic PMMA (iPMMA) and its effect on the gel's morphology, thermal and mechanical properties were studied[140, 144]. Yu and Jérôme observed two types of gelation mechanism in sPMMA-PBD-sPMMA and iPMMA blend i.e., the self aggregation of sPMMA outer blocks and the stereocomplexation of sPMMA blocks with iPMMA[144]. It was observed that stereocomplexation accelerated the gelation process and decreased from 4200s to 180s for MBM/iPMMA (15/1). However, addition of sPMMA to MBM triblock copolymers in o-xylene delayed the gelation process. Shull and co-workers found that addition of low molecular weight iPMMA significantly strengthened the sPMMA-PBD-sPMMA gels.

3.9.2.2 Cosurfactant

Bidisperse gels were prepared by mixing diblock copolymer (AB) to ABA triblock in the presence of a midblock selective solvent[115, 149, 150]. Register and co-worker observed that addition of SI diblock to SIS triblock copolymers in squalane eliminated the macrophase separation and produced optically clear gels of very low modulus[149]. They found that an increment in the modulus as the diblocks are added at a constant triblock content which was ascribed to entanglements due to diblocks and reduction in the intermiceller spacing. Spontak et al. also observed a similar trend in the storage modulus upon addition of SI diblock in the SIS triblock copolymer in the presence of mineral oil[115]. They explained results based on the tail-induced volume exclusion, accredited to the presence of AB molecules, within the micellar coronas that improved network development by increasing the population of bridged B midblock (I). In another study, Karime and co-workers examined the blend of SEBS and SEP in the presence of n-octane[150]. They found that hybrid gels of SEBS and SEP exhibited lower stress relaxation rate than the pure SEBS gels.

3.10 Conclusions

The self-assembly of triblock copolymers in presence of midblock selective solvents is a promising way to create physically gels network on the nanometer scale. In the present overview, an attempt has been made to gain a deeper understanding of the TPEGs. These gels have properties which make them useful in applications such as vibration dampening, insulation and recently, electroactive polymers. Improvement of these properties by modifying the chemistry of the blocks, or introducing additives such as another polymer or nanofiller needs to be studied in greater detail.

3.11 Notes

This chapter will be submitted to *Macromolecular Rapid Communication* for publication. It will be published under the authorship of Ravi Shankar,[§†] Arjun S. Krishnan, [‡] Tushar K. Ghosh[%] and Richard J. Spontak[†‡] ([§]Fiber and Polymer Science Program and Departments of [†]Materials Science & Engineering, [%]Textile & Apparel Technology & Management and [‡]Chemical & Biomolecular Engineering, North Carolina State University, Raleigh, NC 27695, USA).

3.12 References

(1) Shenhar, R.; Norsten, T. B.; Rotello, V. M. *Adv Mater* **2005**, *17*, 657-669.

(2) Bates, F. S.; Fredrickson, G. H. *Annu. Rev. Phy. Chem.* **1990**, *41*, 525-557.

(3) Adhikari, R.; Michler, G. H. *Progress in Polymer Science* **2004**, *29*, 949-986.

(4) Bates, F. S.; Fredrickson, G. H. In *Block Copolymer Thermodynamics: Theory abd Experiment;* Holden, G., Legge, N. R., Quirk, R. P. and Schroder, H. E., Eds.; Thermoplastic Elastomers; Hanser: Munich, **1998**; Vol. 2, pp 336-364.

(5) Park, C.; Yoon, J.; Thomas, E. L. *Polymer* **2003**, *44*, 6725-6760.

(6) Simon, P. F. W.; Ulrich, R.; Spiess, H. W.; Wiesner, U. *Chemistry of Materials* **2001**, *13*, 3464-3486.

(7) Zhao, D. Y.; Feng, J. L.; Huo, Q. S.; Melosh, N.; Fredrickson, G. H.; Chmelka, B. F.; Stucky, G. D. *Science* **1998**, *279*, 548-552.

(8) Templin, M.; Franck, A.; DuChesne, A.; Leist, H.; Zhang, Y. M.; Ulrich, R.; Schadler, V.; Wiesner, U. *Science* **1997**, *278*, 1795-1798.

(9) Hedrick, J. L.; Miller, R. D.; Hawker, C. J.; Carter, K. R.; Volksen, W.; Yoon, D. Y.; Trollsas, M. *Adv Mater* **1998**, *10*, 1049-+.

(10) Pai, R. A.; Humayun, R.; Schulberg, M. T.; Sengupta, A.; Sun, J.; Watkins, J. J. *Science* **2004**, *303*, 507-510.

(11) krishnamoorthy, S.; Hinderling, C.; Heinzelmann, H. *Mater. Today* **2006**, *9*, 40-47.

(12) Walker, B. M.; Rader, C. P., Eds.; In *Handbook of Thermoplastic Elastomers Second Edition;* Van Nostrand Reinhold Company Inc.: New York, **1988**, pp 430.

(13) Fukahori, Y.; Mashita, N. *Polym. Adv. Technol.* **2000**, *11*, 472-480.

(14) Quintana, J. R.; Diaz, E.; Katime, I. *Macromolecules* **1997**, *30*, 3507-3512.

(15) Ishizu, K.; Tsubaki, K.; Mori, A.; Uchida, S. *Progress in Polymer Science* **2003**, *28*, 27-54.

(16) Leibler, L. *Macromolecules* **1980**, *13*, 1602-1617.

(17) Bates, F. S.; Fredrickson, G. H. *Phys. Today* **1999,** *52*, 32.

(18) Hashimoto, T.; Koizumi, S.; Hasegawa, H. *Macromolecules* **1994**, *27*, 1562-1570.

(19) Koneripalli, N.; Levicky, R.; Bates, F. S.; Matsen, M. W.; Satija, S. K.; Ankner, J.; Kaiser, H. *Macromolecules* **1998**, *31*, 3498-3508.

(20) Spontak, R. J.; Fung, J. C.; Braunfeld, M. B.; Sedat, J. W.; Agard, D. A.; Kane, L.; Smith, S. D.; Satkowski, M. M.; Ashraf, A.; Hajduk, D. A.; Gruner, S. M. *Macromolecules* **1996**, *29*, 4494-4507.

(21) Sakurai, S.; Irie, H.; Umeda, H.; Nomura, S.; Lee, H. H.; Kim, J. K. *Macromolecules* **1998**, *31*, 336-343.

(22) Fredrickson, G. H.; Bates, F. S. *Annual Review of Materials Science* **1996**, *26*, 501-550.

(23) Hamley, I. W. *Journal of Physics: Condensed Matter* **2001**, *13*, R643-R671.

(24) Li, M.; Ober, C. K. *Materials Today* **2006**, *9*, 30-39.

(25) Spontak, R. J.; Patel, N. P. In *Phase Behavior of Block Copolymer Blends;* Hamley, I. W., Ed.; Developments in Block Copolymer Science and Technology; Wiley: New York, 2004; pp 159-212.

(26) Hamley, I. W. In *The Physics of Block Copolymers;* Oxford University Press: New York, 1998; .

(27) Stepto, R. F. T., Ed.; In *Polymer Networks Principle of their Formation. Structure and Properties;* Thomson Science: London, UK, 1998; Vol. First Edition, pp 343.

(28) Addad, J. P. C., Ed.; In *Physical Properties of Polymer Gels;* John Wiley: New York, 1996; , pp 311.

(29) Kleppinger, R.; Mischenko, N.; Reynaers, H. L.; Koch, M. H. J. *Journal of Polymer Science Part B: Polymer Physics* **1999**, *37*, 1833-1840.

(30) Osada, Y.; Gong, J. P. In *Gels(overview);* Salamone, J. C., Ed.; Polymeric Materials Encyclopedia; CRC Press: Florida, USA, 1996; Vol. 4, pp 2742-2749.

(31) Nijenhuis, K. t. *Adv. Polym. Sci.* **1997**, *130*, 1-267.

(32) Osada, Y.; Khokhlov, A. R., Eds.; In *Polymer Gels and Networks;* Marcel Dekker: New York, 2002; , pp 381.

(33) Jordan Llyod, D. In *Colloid Chemistry I;* Alexander, J., Ed.; Colloid Chemistry I; Chemical Catalog Co., Inc.: New York, 1926; Vol. 1, pp 1-767.

(34) Hermans, P. H. In *Colloid Science II;* Kruyt, H. R., Ed.; Colloid Science II; Elsevier Publishing Inc.: Amsterdam, 1949; Vol. II, pp 483-651.

(35) Young, R. J. In *Introduction to Polymers;* Chapman and Hall: New York, 1981; , pp 331.

(36) Chambon, F.; Petrovic, Z. S.; MacKnight, W. J.; Winter, H. H. *Macromolecule* **1986**, *19*, 2146-2149.

(37) Winter, H. H.; Chambon, F. *J. Rheol.* **1986**, *30*, 367-382.

(38) Winter, H. H. *Polymer Engineering & Science* **1987**, *27*, 1698-1702.

(39) Flory, P. J. In *Principles of Polymer Chemistry;* Cornell University Press: Ithaca, 1953; , pp 663.

(40) Flory, P. J. *J. Am. Chem. Soc.* **1941**, *63*, 3083-3090.

(41) Coniglio, A.; Stanley, H. E.; Klein, W. *Phys. Rev. Lett.* **1979**, *42*, 518-522.

(42) Wilder, E. A.; Hall, C. K.; Khan, S. A.; Spontak, R. J. *Recent Res. Dev. Mater. Sci.* **2002**, *3*, 93-115.

(43) Shankar, R.; Ghosh, T. K.; Spontak, R. J. *Mater. Sci. Eng. R* **Submitted 2006**.

(44) Flory, P. J. *Faraday Discuss. Chem. Soc.* **1974**, *57*, 7-18.

(45) Kang, G. D.; Cheon, S. H.; Khang, G.; Song, S. C. *European Journal of Pharmaceutics and Biopharmaceutics* **2006**, *63*, 340-346.

(46) Jeong, B.; Kim, S. W.; Bae, Y. H. *Adv. Drug Delivery Rev.* **2002**, *54*, 37-51.

(47) Fages, F. *Top Curr. Chem.* **2005**, *256*, 1-273.

(48) Abdallah, D. J.; Weiss, R. G. *Adv Mater* **2000**, *12*, 1237-1247.

(49) Dingcai Wu; Ruowen Fu ER - *Journal of Porous Materials* **2005**, *V12*, 311-316.

(50) Abdelghani, A.; Cherif, K.; Jaffrezic-Renault, N.; Matejec, V. *Materials Science & Engineering C, Biomimetic and Supramolecular Systems* **2006**, *26*, 542-5.

(51) Hao, Y.; Wagner, J. B.; Su, D. S.; Jin, G.; Guo, X. *Nanotechnology* **2006**, *17*, 2870-2874.

(52) Chan, Z.; Miao, F.; Xiao, Z.; Juan, H.; Hongbing, Z. *Mater Lett* **2007**, *61*, 644-647.

(53) Chien-Tsung Wang; Chun-Lung Wu *Thin Solid Films* **2006**, *496*, 658-64.

(54) Fesmire, J. E. *Cryogenics* **2006**, *46*, 111-17.

(55) Burchell, M. J.; Graham, G.; Kearsley, A. *Annu. Rev. Earth Planet. Sci.* **2006**, *34*, 385-418.

(56) Arachchige, I. U.; Brock, S. L. *J. Am. Chem. Soc.* **2006**, *128*, 7964-7971.

(57) Osada, Y.; Gong, J. P.; Tanaka, Y. In *Polymer Gels;* Takemoto, K., Ottenbrite, R. M. and Kamachi, M., Eds.; Functional Monomers and Polymers; Marcel Dekker Inc.: New York, 1997; pp 497-529.

(58) Sharma, D. K.; Verma, S.; Sharma, P.; Tomar, R. *Journal of the Indian Chemical Society* **2006**, *83*, 405-408.

(59) Brown, B. R.; Hughes, M. E.; Russo, C. *Physical Review E* **2004**, *70*, 031917.

(60) Tomar, R.; Sharma, D.; Saxena, A.; Sharma, P. *Journal of the Indian Chemical Society* **2002**, *79*, 520-521.

(61) Wang, G. H.; Zhang, L. M. *J Phys Chem B* **2006**, *110*, 24864-24868.

(62) Joseph, J.; Son, K. M.; Vittal, R.; Lee, W.; Kim, K. J. *Semiconductor Science and Technology* **2006**, *21*, 697-701.

(63) Duncan, D. C.; Whitten, D. G. *Langmuir* **2000**, *16*, 6445-6452.

(64) Bauer, T.; Thomann, R.; Mulhaupt, R. *Macromolecules* **1998**, *31*, 7651-7658.

(65) Terech, P.; Weiss, R. G. *Chem. Rev.* **1997**, *97*, 3133-3160.

(66) Zilman, A. G.; Safran, S. A. *Phys Rev E.* **2002**, *66*, 051107.

(67) Schosseler, F.; Daoud, M.; Leibler, L. *Journal De Physique* **1990**, *51*, 2373-2385.

(68) Colby, R. H.; Rubinstein, M.; Gillmor, J. R.; Mourey, T. H. *Macromolecules* **1992**, *25*, 7180-7187.

(69) Axelos, M. A. V.; Kolb, M. *Phys. Rev. Lett.* **1990**, *64*, 1457-1460.

(70) Li, L.; Aoki, Y. *Macromolecules* **1997**, *30*, 7835-7841.

(71) Guenet, J. -. *J. Rheol.* **2000**, *44*, 947-960.

(72) Sakurai, S. *Trends Polym. Sci.* **1997**, *5*, 210-212.

(73) McConnell, G. A.; Gast, A. P.; Huang, J. S.; Smith, S. D. *Phys. Rev. Lett.* **1993**, *71*, 2102-2105.

(74) Halperin, A. *Macromolecules* **1987**, *20*, 2943-2946.

(75) Lairez, D.; Adam, M.; Carton, J. -.; Raspaud, E. *Macromolecules* **1997**, *30*, 6798-6809.

(76) Sakurai, S.; Hashimoto, T.; Fetters, L. J. *Macromolecules* **1996**, *29*, 740-747.

(77) Semenov, A. N.; Joanny, J. -.; Khokhlov, A. R. *Macromolecules* **1995**, *28*, 1066-1075.

(78) Hanley, K. J.; Lodge, T. P. *Journal of Polymer Science Part B: Polymer Physics* **1998**, *36*, 3101-3113.

(79) Hamley, I. W.; Fairclough, J. P. A.; Ryan, A. J.; Ryu, C. Y.; Lodge, T. P.; Gleeson, A. J.; Pedersen, J. S. *Macromolecules* **1998**, *31*, 1188-1196.

(80) Elias, H. -. *J Macromol. Sci. Chemistry* **1973**, *7*, 601.

(81) Nguyen-Misra, M.; Mattice, W. L. *Macromolecules* **1995**, *28*, 1444-1457.

(82) Leibler, L.; Orland, H.; Wheeler, J. C. *J. Chem. Phys.* **1983**, *79*, 3550-3557.

(83) Balsara, N. P.; Tirrell, M.; Lodge, T. P. *Macromolecules* **1991**, *24*, 1975-1986.

(84) Hadjichristidis, N.; Pispas, S.; Floudas, G. A. In *Block Copolymers Synthetic Stratgies, Physical Properties, and Applications;* John Wiley & Sons, Inc.: New Jersey, 2003; , pp 419.

(85) Watanabe, H.; Kotaka, T. *Polym. J.* **1982**, *14*, 739-747.

(86) Hashimoto, T.; Shibayama, M.; Kawai, H.; Watanabe, H.; Kotaka, T. *Macromolecules* **1983**, *16*, 361-371.

(87) Mortensen, K.; Pedersen, J. S. *Macromolecules* **1993**, *26*, 805-812.

(88) Brown, W.; Schillen, K.; Hvidt, S. *J. Phys. Chem.* **1992**, *96*, 6038-6044.

(89) Laurer, J. H.; Mulling, J. F.; Khan, S. A.; Spontak, R. J.; Bukovnik, R. *J. Polym. Sci. B: Polym. Phys.* **1998**, *36*, 2379-2391.

(90) Raspaud, E.; Lairez, D.; Adam, M.; Carton, J. -. *Macromolecules* **1996**, *29*, 1269-1277.

(91) Soenen, H.; Berghmans, H.; Winter, H. H.; Overbergh, N. *Polymer* **1997**, *38*, 5653-5660.

(92) Yu, J. M.; Jerome, R.; Overbergh, N.; Hammond, P. *Macromolecular Chemistry and Physics* **1997**, *198*, 3719-3735.

(93) Yu, J. M.; Blacher, S.; Brouers, F.; L'Homme, G. L.; Jerome, R. *Macromolecules* **1997**, *30*, 4619-4625.

(94) Laurer, J. H.; Mulling, J. F.; Khan, S. A.; Spontak, R. J.; Lin, J. S.; Bukovnik, R. *Journal of Polymer Science Part B-Polymer Physics* **1998**, *36*, 2513-2523.

(95) Halperin, A.; Zhulina, E. B. *Europhys. Lett.* **1991**, *16*, 337-341.

(96) King, M. R.; White, S. A.; Smith, S. D.; Spontak, R. J. *Langmuir* **1999**, *15*, 7886-7889.

(97) Halperin, A. *J. Adhesion* **1996**, *58*, 1-13.

(98) Zolzer, U.; Eicke, H. F. *Journal De Physique Ii* **1992**, *2*, 2207-2219.

(99) Chen, C. -.; MacKintosh, F. C.; Williams, D. R. M. *Langmuir* **1995**, *11*, 2471-2475.

(100) Zhulina, E. B. *Macromolecules* **1993**, *26*, 6273-6283.

(101) Zhulina, E. B.; Halperin, A. *Macromolecules* **1992**, *25*, 5730-5741.

(102) Jackson, N. R.; Wilder, E. A.; White, S. A.; Bukovnik, R.; Spontak, R. J. *Journal of Polymer Science Part B-Polymer Physics* **1999**, *37*, 1863-1872.

(103) Yamaguchi, D.; Cloitre, M.; Panine, P.; Leibler, L. *Macromolecules* **2005**, *38*, 7798-7806.

(104) Sudarsan, A. P.; Wang, J.; Ugaz, V. M. *Anal. Chem.* **2005**, *77*, 5167-5173.

(105) van Maanen, G. J.; Seeley, S. L.; Capracotta, M. D.; White, S. A.; Bukovnik, R. R.; Hartmann, J.; Martin, J. D.; Spontak, R. J. *Langmuir* **2005**, *21*, 3106-3115.

(106) Laurer, J. H.; Bukovnik, R.; Spontak, R. J. *Macromolecules* **1996**, *29*, 5760-5762.

(107) Julthongpiput, D.; Ahn, H. -.; Sidorenko, A.; Kim, D. -.; Tsukruk, V. V. *Tribol. Int.* **2002**, *35*, 829-836.

(108) Mischenko, N.; Reynders, K.; Mortensen, K.; Scherrenberg, R.; Fontaine, F.; Graulus, R.; Reynaers, H. *Macromolecules* **1994**, *27*, 2345-2347.

(109) Laurer, J. H.; Khan, S. A.; Spontak, R. J.; Satkowski, M. M.; Grothaus, J. T.; Smith, S. D.; Lin, J. S. *Langmuir* **1999**, *15*, 7947-7955.

(110) Walker, T. A.; Semler, J. J.; Leonard, D. N.; van Maanen, G. J.; Bukovnik, R. R.; Spontak, R. J. *Langmuir* **2002**, *18*, 8266-8270.

(111) Quintana, J. R.; Diaz, E.; Katime, I. *Langmuir* **1998**, *14*, 1586-1589.

(112) Nunalee, F. N.; Shull, K. R. *Langmuir* **2006**, *22*, 431-439.

(113) Kleppinger, R.; van Es, M.; Mischenko, N.; Koch, M. H. J.; Reynaers, H. *Macromolecules* **1998**, *31*, 5805-5809.

(114) Quintana, J. R.; Hernaez, E.; Katime, I. *J. Phys. Chem. B* **2001**, *105*, 2966-2970.

(115) Spontak, R. J.; Wilder, E. A.; Smith, S. D. *Langmuir* **2001**, *17*, 2294-2297.

(116) Holden, G.; Kricheldorf, H. R.; Roderic, P. Q., Eds.; In *Thermoplastic Elastomers;* Hanser Gardner Publications, Inc.: Cincinnati, OH, USA, 2004; , pp 540.

(117) Navarro, F. J.; Martínez-Boza, F. J.; Partal, P.; Gallegos, C.; Muñoz, M. E.; Areizaga, J.; Areizaga, J.; Santamaría, A. *Polym. Eng. Sci.* **2001**, *41*, 2216-2225.

(118) Polizzi, S.; Stribeck, N.; Zachmann, H. G.; Bordeianu, R. *Polymer Composites* **1988**, *9*, 434-442.

(119) Ceauescu, E.; Bordeianu, R.; Ghioca, P.; Buzdugan, E.; Stancu, R.; Cerchez, I. *Pure Appl. Chem.* **1984**, *56*, 319-328.

(120) Stribeck, N.; BÃ¶secke, P.; Polizzi, S. *Colloid & Polymer Science* **1989**, *267*, 687-701.

(121) Polizzi, S.; Stribeck, N.; Zachmann, H. G.; Bordeianu, R. *Colloid & Polymer Science* **1989**, *267*, 281-291.

(122) Sulaiman, N.; Farid, A. S.; O'Brien, M. G. *Plastics Rubber and Composites Processing and Applications* **1998**, *27*, 356-361.

(123) Sato, T.; Watanabe, H.; Osaki, K. *Macromolecules* **2000**, *33*, 1686-1691.

(124) Barral, M.; Santamaría, A.; Peña, J. J.; Muñoz, M. E. *Macromol Mater. Eng.* **2003**, *288*, 951-956.

(125) Barral, M. S.; Lizaso, I.; Muñoz, M. E.; Santamarí-a, A. *Rheol. Acta* **2001**, *40*, 193-195.

(126) Watanabe, H.; Kuwahara, S.; Kotaka, T. *J. Rheol.* **1984**, *28*, 393-409.

(127) Prasman, E.; Thomas, E. L. *J. Polym. Sci. B: Polym. Phys.* **1998**, *36*, 1625-1636.

(128) Reynders, K.; Mischenko, N.; Mortensen, K.; Overbergh, N.; Reynaers, H. *Macromolecules* **1995**, *28*, 8699-8701.

(129) De, S. K.; Bhowmick, A. K., Eds.; In *Thermoplastic elastomer from rubber-plastic blends;* Ellis Horwood: New York, 1990; , pp 268.

(130) Kleppinger, R.; van Es, M.; Mischenko, N.; Koch, M. H. J.; Reynaers, H. *Macromolecules* **1998**, *31*, 5805-5809.

(131) Straube, E.; Urban, V.; Pyckhout-Hintzen, W.; Richter, D. *Macromolecules* **1994**, *27*, 7681-7688.

(132) Mischenko, N.; Reynders, K.; Koch, M. H. J.; Mortensen, K.; Pedersen, J. S.; Fontaine, F.; Graulus, R.; Reynaers, H. *Macromolecules* **1995**, *28*, 2054-2062.

(133) Kleppinger, R.; van Es, M.; Mischenko, N.; Koch, M. H. J.; Reynaers, H. *Macromolecules* **1998**, *31*, 5805-5809.

(134) Mortensen, K.; Theunissen, E.; Kleppinger, R.; Almdal, K.; Reynaers, H. *Macromolecules* **2002**, *35*, 7773-7781.

(135) Quintana, J. R.; Diaz, E.; Katime, I. *Macromolecular Chemistry and Physics* **1996,** *197*, 3017-3026.

(136) Quintana, *Polymer* **1998,** *39*, 3029.

(137) Nie, H.; Li, M.; Bansil, R.; Koňák, Č; Helmstedt, M.; Lal, J. *Polymer* **2004,** *45*, 8791-8799.

(138) Bansil, R.; Nie, H.; Koňák, Č; Helmstedt, M.; Lal, J. *Journal of polymer science. Part B, Polymer physics* **2002,** *40*, 2807-2816.

(139) Seitz, M. E.; Burghardt, W. R.; Faber, K. T.; Shull, K. R. *Macromolecules* **2007,** *40*, 1218-1226.

(140) Flanigan, C. M.; Crosby, A. J.; Shull, K. R. *Macromolecules* **1999,** *32*, 7251-7262.

(141) Drzal, P. L.; Shull, K. R. *Macromolecules* **2003,** *36*, 2000-2008.

(142) Yu, J. M.; Jerome, R.; Teyssie, P. *Polymer , 38*, 347-354.

(143) Yu, J. M.; Dubois, P.; Jerome, R.; Teyssie, P.; Blacher, S.; Brouers, F.; L'Homme, G. *Macromolecules* **1996,** *29*, 5384-5391.

(144) Yu, J. M.; Jerome, R. *Macromolecules* **1996,** *29*, 8371-8378.

(145) Mowery, C. L.; Crosby, A. J.; Ahn, D.; Shull, K. R. *Langmuir* **1997,** *13*, 6101-6107.

(146) Inomata, K.; Nakanishi, D.; Banno, A.; Nakanishi, E.; Abe, Y.; Kurihara, R.; Fujimoto, K.; Nose, T. *Polymer* **2003,** *44*, 5303-5310.

(147) Yu, J. M.; Jerome, R.; Teyssie, P. *Polymer* **1997,** *38*, 347-354.

(148) Theunissen, E.; Overbergh, N.; Reynaers, H.; Antoun, S.; Jerome, R.; Mortensen, K. *Polymer* **2004,** *45*, 1857-1865.

(149) Vega, D. A.; Sebastian, J. M.; Loo, Y. -.; Register, R. A. *Journal of Polymer Science Part B: Polymer Physics* **2001,** *39*, 2183-2197.

(150) Quintana, J. R.; Hernaez, E.; Katime, I. *Polymer* **2002**, *43*, 3217-3222.

(151) van Maanen, G. J.; Seeley, S. L.; Hartmann, J.; Bukovnik, R.; Spontak, R. J. *Macromol. Rapid Commun.* **submitted**.

CHAPTER 4

4 Electroactive Nanostructured Polymers as Tunable Actuators

4.1 Abstract

Lightweight and conformable electroactive actuators stimulated by acceptably low electric fields are required for emergent technologies such as microrobotics, flat-panel speakers, micro air vehicles and responsive prosthetics. High actuation areal strains (>50%) are currently afforded by dielectric elastomers at relatively high electric fields (>50 V/μm). In this work, we demonstrate that incorporation of a low-volatility, aliphatic-rich solvent into a nanostructured poly[styrene-*b*-(ethylene-*co*-butylene)-*b*-styrene] triblock copolymer yields physically cross-linked micellar networks that exhibit excellent displacement under an external electric field. Such property development reflects solvent-induced reductions in matrix viscosity and nanostructural order, as well as field-enhanced polarization of the styrenic units, which together result in ultrahigh areal actuation strains (>200%) at significantly reduced electric fields (<40 V/μm) with remarkably low cyclic hysteresis. Use of nanostructured polymers whose properties can be broadly tailored by varying copolymer characteristics or blend composition represents an innovative and tunable avenue to reduced-field actuation for advanced engineering, biomimetic and biomedical applications.

4.2 Introduction

Polymeric electroactive materials are capable of mechanical actuation induced by an external electric field and thus afford tremendous promise in emerging technologies ranging from micro air vehicles and flat-panel speakers[1] to active video displays, microrobotics and responsive prosthetics.[2] Some of the key characteristics required in the development of actuator materials include high strain and strain energy density, high fatigue resistance and reliability.[3] Several classes of materials including single-crystal piezoelectric ceramics[4] and single-wall carbon nanotubes[5] have been considered as suitable candidates for actuators, but these rigid materials afford relatively low displacement and poor electromechanical coupling in the presence of an electric field.[6] While shape memory alloys can generate high forces

and displacements, they generally suffer from slow response times, large mechanical hysteresis and short cycle life.[7] Electroactive polymers (EAPs) are attractive due to their low cost, light weight, facile processability,[8] favorable power-to-mass ratio and, perhaps most importantly, their potential to emulate biological muscle in terms of resilience, toughness and vibration dampening.[9] Examples of EAPs investigated thus far include electrically conductive polymers,[10,11] electrostrictive polymers,[12] ferroelectric polymers,[3,8] dielectric elastomers[1] and acidic hydrogels.[13] Of these, dielectric elastomers exhibit the largest actuation strain upon exposure to an electric field, efficiently coupling input electrical energy and output mechanical energy.[14]

The electromechanical response of dielectric EAPs is attributed to the development of a "Maxwell stress" upon application of an external electrical field.[15] This Maxwell stress arises in response to electrostatic attraction between two conductive surfaces in contact with the opposing surfaces of a dielectric elastomer film, and generates a dominant uniaxial stress (σ_M) given by

$$\sigma_M = \varepsilon_0 \varepsilon E^2 \quad (1)$$

where ε_0 is the permittivity of free space, ε corresponds to the dielectric constant of the EAP, and E denotes the applied electric field.[1] Since the Maxwell stress acts normal to the film surface, it serves to compress the film along its thickness (z) and stretch the film laterally (along x and y). Repulsive like charges accumulate along both film surfaces and further increase the extent to which the film stretches laterally, as schematically depicted in Fig. 4.1A. Three dielectric media that show technological promise derive from homopolymers and include an acrylic adhesive,[1,16] polyurethane[17] and silicone elastomers.[1,18] The VHB 4910 acrylic adhesive manufactured by 3M Co. (Minneapolis, MN) exhibits the largest actuation strain in this class of materials.

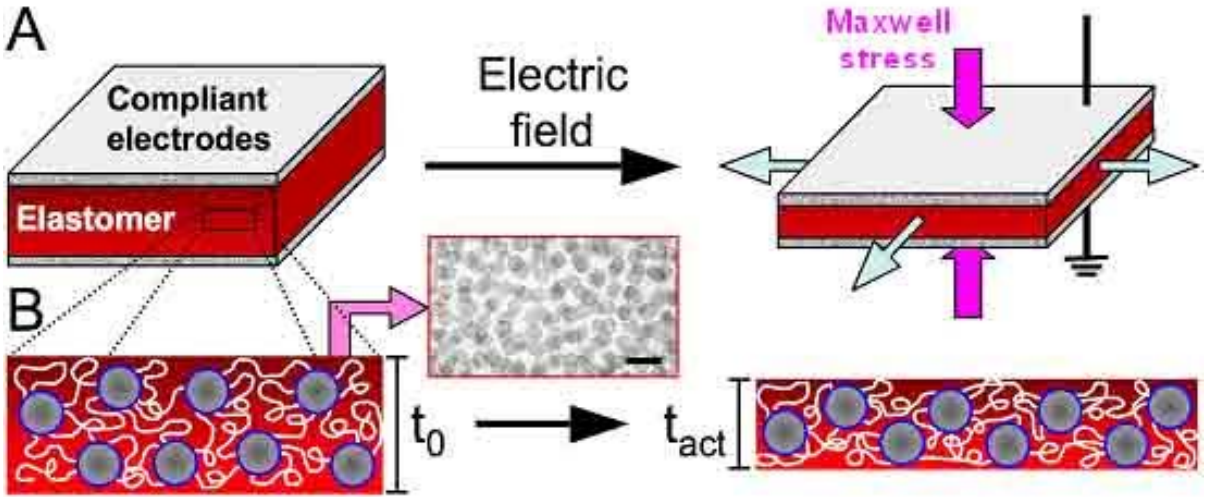

Figure 4.1 In (A), the operational principle of a conventional elastomeric EAP before and after actuation. Development of a Maxwell stress (labeled) between oppositely charged compliant electrodes squeezes the elastomer, thereby causing lateral displacement of the specimen. The morphology of a midblock-swollen triblock copolymer that self-organizes into glassy micelles connected by a midblock network before and after actuation is schematically depicted in (B). A TEM image (scale marker = 50 nm) of a solvated copolymer system containing 10 wt% SEBS161, with the S-rich micelles selectively stained by the vapor of RuO_4(aq), is included to confirm the existence of the micellar morphology in the inset of (B).

Independent experimental[19-21] and theoretical[22] studies designed to elucidate the electric field-induced response of another class of macromolecules, microphase-separated block copolymers, have been conducted in an ongoing effort to control nanostructural orientation for various emerging nanotechnologies such as optical waveguides.[23] Linear block copolymers consist of two or more chemically dissimilar homopolymers covalently linked together to form a single macromolecule. If the blocks are sufficiently incompatible, these copolymers spontaneously self-organize into a wide variety of (a)periodic nanostructures such as spherical or cylindrical micelles, bicontinuous networks or lamellar bilayers alone[24,25] or in the presence of other organic species (e.g., low-molar-mass solvents or other macromolecules).[26-29] Russell and co-workers have established that, due to polarizability differences between the constituent blocks, the lamellar[19] and cylindrical[21] morphologies of poly(styrene-*b*-methyl methacrylate) block copolymer thin films can be (re)aligned in a dc electric field. Nanostructural alignment in a block copolymer thin film is

likewise achieved by annealing the film in solvent vapor, which serves to alter viscosity, interfacial tension and surface segregation.[30] Both strategies have been successfully implemented[31] to align the morphologies of bulk poly(styrene-*b*-isoprene) (SI) diblock copolymers cast from a neutral, volatile solvent.

Solvated block copolymers are likewise of considerable importance in various technologies ranging from personal care products and pharmaceuticals to shock-absorbing media for fiber optics, novel adhesives and sporting goods.[26] One of the most ubiquitous and economically attractive block copolymer solutions of commercial relevance consists of a thermoplastic elastomer such as a poly[styrene-*b*-(ethylene-*co*-butylene)-*b*-styrene] (SEBS) triblock copolymer (with glassy S endblocks and a rubbery EB midblock) and a low-volatility solvent that selectively swells the EB midblock (i.e., an aliphatic-rich oil). At relatively high solvent concentrations, thermoplastic elastomer systems such as this behave as physical networks wherein glassy S micelles serve as thermally reversible cross-links.[32] This nanostructure is illustrated in Fig. 4.1B, and the inset displays a transmission electron microscopy (TEM) image of the S micelles. Organic molecules possessing π-extended functionalities such as the phenyl rings located on the S repeat units of the SEBS copolymer are known to exhibit nonlinear optical properties[33] and, unlike the EB units and the solvent, are expected to be polarizable in an electric field. Such polarizability contrast, confirmed in the electric field-driven alignment of SI diblock copolymers,[31] suggests that styrenic thermoplastic elastomer networks with solvent-reduced matrix viscosity and nanostructural order could exhibit tunable electromechanical behavior. We explore this possibility with two SEBS copolymers (31-33 wt% S) hereafter referred to as SEBS161 and SEBS217, where the numerical designation denotes the number-average molecular weight of the copolymer in kDa. The solvent employed here is a white mineral oil, and network concentrations range from 5 to 30 wt% SEBS in 5 wt% increments.

4.3 Result and Discussion

A sequence of digital images acquired from the active area of the network composed of 5 wt% SEBS217 copolymer upon exposure to electric fields varying in strength is shown in Fig. 4.2A and illustrates that the active region increases, while the film thickness correspondingly decreases, with increasing electric field, thereby confirming that the

copolymer network exhibits an electromechanical response due to the development of a Maxwell stress. To reflect their supramolecular network design, we refer to these EAPs as electroactive nanostructured polymers (ENPs). Analysis of images such as those displayed in Fig. 4.2A by the Matrox Inspector software package yields areal actuation strain values, which are provided as a function of applied electric field for ENPs containing the SEBS161 and SEBS217 copolymers at various concentrations in Figs. 4.2B and 2C, respectively.

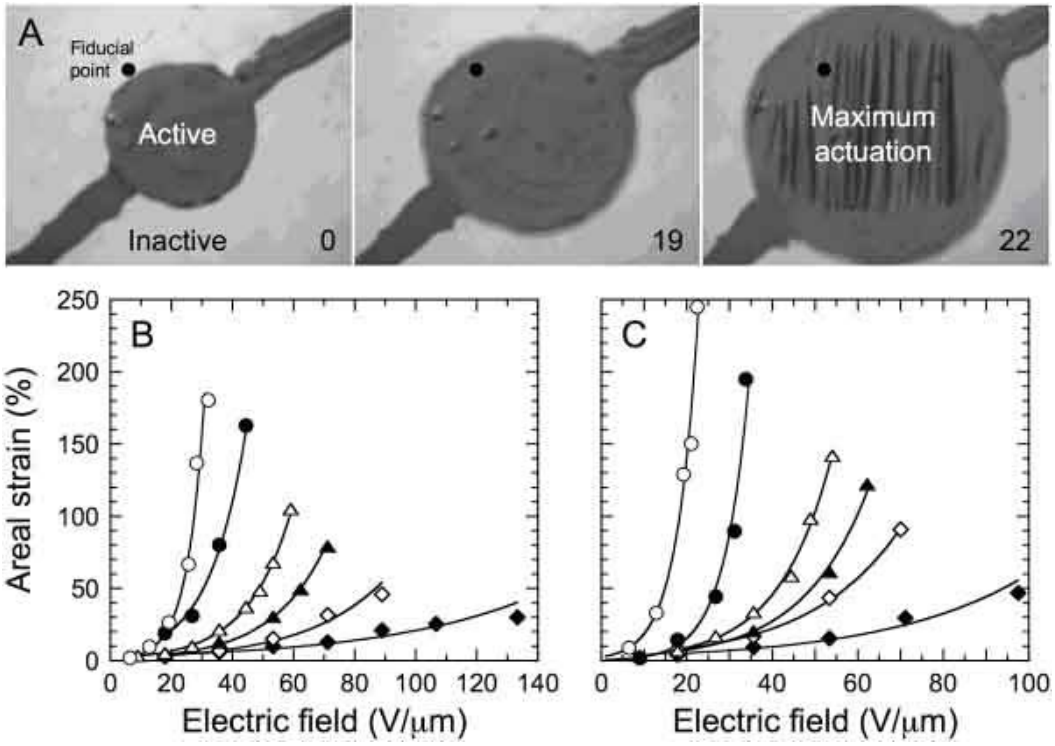

Figure 4.2 In (A), a series of digital images showing the effect of electric field (listed values in V/□m) on areal activation in the ENP containing 5 wt% SEBS217. The dependence of areal actuation on electric field is provided in (B) and (C) for ENP systems composed of the SEBS161 and SEBS217 copolymers, respectively, at various concentrations (in wt%): 5 (○), 10 (●), 15 (△), 20 (▲), 25 (◇) and 30 (◆). The solid lines represent exponential fits to the data.

Several important features are evident from these results. The first is that the areal actuation strain increases with increasing electric field, which is consistent with observations reported[18] for other dielectric EAPs. Another noteworthy feature is that the maximum areal actuation strain, measured at an electric field within <1% of the breakdown field (where

failure occurs), increases with decreasing copolymer content and increasing copolymer molecular weight. Conversely, the breakdown field is found to decrease sharply with decreasing copolymer concentration and, to a lesser extent, increasing molecular weight. The latter results indicate that the breakdown field increases with increasing size and number density of S-rich micelles and, therefore, with decreasing intermicellar distance. While the results presented in Fig. 4.2 correspond to single cycle, we hasten to point out that actuation cycling up to 100 cycles shows negligible hysteresis, as measured in terms of non-recoverable (areal) strain (~2.0% for the SEBS217 systems and 3.4-14% for the SEBS161 systems, depending on copolymer concentration) at applied fields ranging from 48 to 60% of the concentration-dependent breakdown fields. These conditions are representative of typical EAP applications.

Taken together, these results demonstrate that the field-induced strain of the ENPs can be greatly enhanced by decreasing the viscosity (or, alternatively, modulus) of the matrix component and the extent of nanostructural order, while increasing the population of polarizable phenyl rings (i.e., increasing the mass of the S block). The former simply requires higher solvent loading insofar as network behavior is retained,[32] and the latter can be achieved by increasing the copolymer molecular weight. Comparison of the SEBS161 and SEBS217 copolymers reveals a difference of ~43% in the number of phenyl rings. Since the phenyl rings are largely immobilized due to nanoscale confinement within the glassy S-rich micelles that stabilize the ENP networks, they are not expected to individually respond to the applied electric field, although limited molecular reorientation may occur if the micelles are slightly plasticized due to low solvent inclusion. These networked micelles are presumed to cooperatively respond to the electric field and thus displace laterally upon actuation, as illustrated in Fig. 4.1B. Such supramolecular response, which is consistent with our observed non-hysteretic actuation cycling, has been previously reported[34] for comparable systems subjected only to high-strain tensile deformation with no applied electric field. Time-resolved synchrotron x-ray scattering further confirms that macroscopic deformation of these materials translates into either affine or nonaffine network deformation, depending on extension rate.[35] In similar fashion, Böker *et al.*[31] have likewise shown that the microphase-ordered nanostructural elements of concentrated block copolymer solutions align in the presence of an electric field. The dependence of the maximum areal actuation strain on

electric field determined for ENPs in this study is provided in Fig. 4.3A and demonstrates that, unlike other dielectric EAPs, these ENPs exhibit a broad range of composition-tunable electromechanical behavior. An increase in copolymer molecular weight (i.e., the population of polarizable phenyl rings within each micelle and correspondingly the length of the swollen EB midblock) or, conversely, a reduction in copolymer concentration significantly improves actuation strain at low electric field in both ENP series. To establish a relationship between the field-induced actuation and mechanical behavior of these materials, we now turn our attention to the results of uniaxial tensile tests, of which a limited but representative number are provided in Fig. 4.3B. Widely ranging mechanical behavior can be systematically produced by varying copolymer molecular weight and ENP composition. The property range displayed in this figure can be extended further by either increasing the copolymer concentration beyond 30 wt% or using SEBS copolymers of comparable composition with a molecular weight less than 161 kDa or greater than 217 kDa. Similar tunability is observed for the tensile modulus (provided in the inset). Included for comparison in Fig. 4.3B are data obtained from the VHB 4910 acrylic.

The very high strains (2000–4000%) and strain energies at failure measured for some of these ENPs attest to the superior potential of solvated triblock copolymers as actuator materials. Since the maximum actuation strain and energy density (which constitutes a measure of an actuator to perform work) are inversely related to modulus, the highest maximum areal actuation strain levels and, thus, the highest energy densities are achieved with the lowest-modulus materials, namely, the ENPs containing 5-10 wt% SEBS217 copolymer.

Although the precise supramolecular response of the copolymer micelles to electrical actuation is not yet known, the superior actuation-induced strains provided by the present materials (with measured dielectric constant, ε, values ranging from 1.8 to 2.2) relative to other EAPs, such as the VHB 4910 acrylic (with ε reported[9] as 4.8), is primarily attributed at present to the low modulus achieved in ENP elastomers at high solvent concentrations. To ensure proper perspective, collective results of this study are compared with discrete values for dielectric EAPs discussed elsewhere[1,9,14] in Table 4.1.

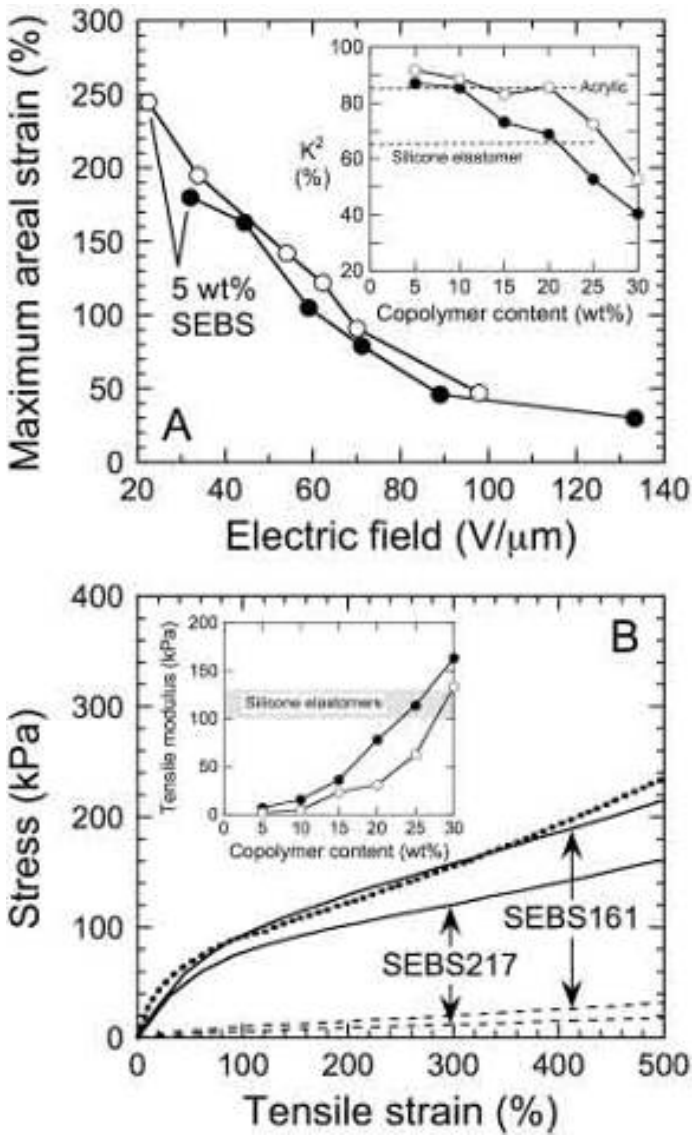

Figure 4.3 In (A), the maximum areal actuation strain measured for ENPs varying in SEBS161 (●) or SEBS217 (○) copolymer concentration as a function of near-breakdown electric field at 300% biaxial prestrain. The dependence of the electromechanical coupling factor (K^2) on copolymer concentration is provided in the inset, with K^2 values for other dielectric EAPs (dashed lines) labeled for comparison. The solid lines connect the data in (A). The low-strain tensile behavior (displaying engineering stress) of select ENPs at different copolymer concentrations (in wt%) — 30 (solid lines) and 10 (dashed lines) — at ambient temperature is presented in (B). Results obtained from the VHB 4910 acrylic (heavy dotted line) are included for comparison. The dependence of tensile modulus on copolymer concentration and molecular weight, using the same symbols as in (A), is shown in the inset of (B). The solid lines connect the data. In all cases, the extension rate is 127 mm/min.

This comparison, which excludes hybrid materials containing polarizable inorganic particles,[36,37] illustrates that, although the ENP materials possess low-to-moderate energy densities (especially relative to ferroelectric polymers[38]), they nonetheless show exceptional electroactive behavior with composition-tunable properties. Relative to the VHB 4910 acrylic, for instance, the lowest-modulus ENPs reported here exhibit a 14-55% increase in maximum areal actuation strain at markedly lower breakdown electric fields (22-32 V/μm *vs.* 161 V/μm). The increase in maximum areal strain is more pronounced with regard to the HS3 silicone elastomer (94-163%). Although Table 4.1 further reveals that the moduli measured from the two ENP series examined here are less than the moduli of the other EAPs, higher moduli are achievable at higher copolymer concentrations and lower copolymer molecular weights than those investigated here.

Another important issue in the design of electroactive materials is mechanical hysteresis, since the target technologies requiring such materials impose cyclic deformation. As mentioned earlier, the VHB 4910 acrylic suffers from progressive hysteresis during cyclic deformation due to viscoelastic losses.[1] After 100 cycles to 400% strain at a fixed uniaxial extension rate of 500 mm/min, this EAP undergoes 38% non-recoverable strain due to permanent deformation. For comparison, we have performed strain-cycling tests under identical conditions to assess the mechanical hysteresis of the ENPs. While the ENPs generally exhibit relatively low non-recoverable strain upon cycling (<18%, with only the ENP containing 5 wt% SEBS161 prematurely failing after 65 cycles), hysteresis is negligible (~1%) in the most dilute SEBS217 system, which behaves as a model elastomer. The high elastic resilience of these ENPs suggests that these materials could enjoy long cycle lives as soft and reliable actuators. Another measure of EAP performance is the electromechanical coupling factor (K^2), defined as the ratio of stored mechanical energy to input electrical energy and related to the thickness strain due to actuation (s_z) by[14]

$$K^2 = -2s_z - s_z^2 \qquad (2)$$

where $s_z = t_{act}/t_0 - 1$, and the film thicknesses before (t_0) and after (t_{act}) actuation are depicted in Fig. 4.1B. Measured values of K^2 are included in the inset of Fig. 4.3A and confirm that, even without optimization to minimize defects that can influence dielectric behavior, ENP efficacy extends over a broad range that includes the VHB 4910 acrylic and HS3 silicone elastomer.

Table 4.1Actuation Behavior of ENPs Varying in Composition and Other Dielectric EAPs[a]

System	Polymer fraction (wt%)	Lateral prestrain (x%,y%)	Tensile modulus (kPa)	Maximum areal strain (%)	Maximum thickness strain (%)	Breakdown electric field (V/μm)	Energy density[b] (kJ/m^3)
VHB 4910 Acrylic	100	300,300[c]	1000-3000[d] 200[e]	158[c]	61[c]	161[f]	3400[c]
HS3 Silicone Elastomer	100	68,68[c]	130[f]	93[c]	48[c]	57[f]	98[c]
CF19-2186 Silicone Elastomer	100	45,45[c]	100[g]	64[c]	39[c]	214[f]	750[c]
ENPs[e]							
SEBS216	15-30	300,300	7-163	180-30	64-22	32-133	137-140
SEBS217	15-30	300,300	2-133	245-47	71-31	22-98	119-130

[a] Electric fields reported here are expressed relative to the pre-actuation film thickness after biaxial pre-straining (t_0 in Fig. 4.1B), unless otherwise specified. Applied voltages used in conjunction with the ENPs are calculated by multiplying the electric field by t_0 (0.16 or 0.11 mm for ENPs with 5 or 10-30 wt% copolymer, respectively). [b] Energy density values are based on the actual film thickness upon actuation (t_{act} in Fig. 4.1B).
[c] Reported in ref. 1. [d] Reported in ref. 9, but believed to correspond to the compressive, not tensile, modulus.
[e] Measured in this work. [f] Values reported in ref. 1 are determined from t_{act}. For an equitable comparison with respect to t_0, the electric field values measured in ref. 1 are multiplied by $(1 + s_z)$. [g] Reported in ref. 14.

Since the ENPs reported here can be produced from a wide variety of starting materials including different block copolymers[39] and low-volatility selective solvents varying in chemical constitution, molecular weight and physical properties, the general strategy described here, based on molecular self-assembly, constitutes a breakthrough to dielectric elastomers exhibiting ultrahigh displacement at relatively low electric fields. Direct comparison of the maximum areal actuation strains measured for the ENPs with other

dielectric polymers is displayed in Fig. 4.4. Included in Fig. 4.4 are linear actuation strains reported for a ferroelectric polymer[9] and ceramic.[4] Thickness strains corresponding to the electroactive systems portrayed in Fig. 4.4 exhibit similar trends. Although dielectric elastomers generally require much higher actuation voltages compared to other electroactive materials such as carbon nanotubes,[5] ionic polymer-metal composites[40] and conductive polymers,[41] they can achieve considerably greater (in some cases by more than two orders of magnitude) and wider ranging actuation displacements. In contrast to the other materials shown in Fig. 4.4, the range over which ENPs exhibit electrical actuation is remarkably broad due to composition tunability and shifted to substantially higher displacements at reduced electric fields. On the basis of their tunable actuation performance and robust mechanical properties (e.g., low-hysteretic, high-strain cycling and very high failure strains), these materials deserve further consideration as candidates for high-strain electromechanical applications such as microrobotics, biomedical devices (e.g., steerable catheters) and active Braille or haptic interfaces, as well as physical models[42] for biological organisms that exhibit tremendous muscular resilience (e.g., octopi and jellies). Further property improvement is expected through the use of existing design rules to controllably alter the copolymer nanostructure.

4.4 Experimental

Each triblock copolymer network was prepared by mixing the aliphatic/alicyclic white mineral oil (Witco Hydrobrite 380, Crompton Corp., Petrolia, PA) and a SEBS copolymer (GLS Corporation, McHenry, IL) at a predetermined concentration, along with 1 wt% antioxidant, for 30 min in a Ross LDM double-planetary mixer under vacuum at 180 °C. Portions of the resultant materials were compression-molded at 180 °C and then slowly cooled to ambient temperature,[32] yielding films 1.8-2.5 mm thick. Since the actuation response of elastomeric materials is strongly influenced by their mechanical properties, quasi-static uniaxial tensile tests were performed to discern the stress-strain behavior of the copolymer systems under investigation as functions of copolymer molecular weight and concentration. The films were then evaluated for electric field-induced actuation under 300% biaxial prestrain in the circular test configuration to permit direct comparison with existing EAPs.[1] Prestrain was necessary to reduce film thickness and, thus, the electrical potential

required for actuation. A circular active area in each prestrained test specimen (identified in Fig. 4.2A) was created by applying compliant electrodes (Ag grease from Chemtronics Circuit Works, Kennesaw, GA) on both sides of the film. Dielectric constants were measured on an Agilent dielectric test fixture 16451B with HP4284A LCR meter operated over a frequency range of 20 Hz to 1 MHz at 25°C. Actuation response characteristics were evaluated using a manual voltage trigger, followed by frame-by-frame analysis of captured real-time video images. In the actuation cycling tests, the voltage across a specimen was ramped from zero to an applied voltage in 10 s, and no noticeable lag was observed between voltage ramping and full specimen actuation. Afterward, the specimen was held at voltage for 10 s before the voltage was returned to zero for 10 s to permit discharge. This process was repeated for 100 cycles, and photographs obtained initially and after 100 cycles showed no evidence of specimen deterioration.

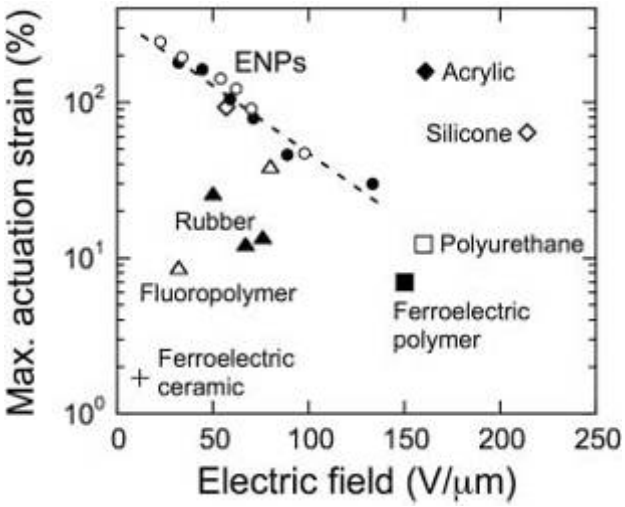

Figure 4.4Maximum actuation strain presented as a function of electric field for several promising classes of dielectric organic materials: an acrylic,[1] two silicone elastomers[1] (see Table 4.1), a ferroelectric polymer,[9] a single-crystal ferroelectric ceramic,[4] and the ranges of the two series of ENPs under investigation in this work (SEBS161, green; SEBS217, blue). Values shown for polyurethane, as well as natural and synthetic rubber, are calculated from actuation measurements reported in refs. 43 and 44. Data displayed here for dielectric elastomers refer to areal strains, whereas linear strains are included for the two classes of ferroelectric materials.

4.5 Acknowledgments

This work was supported by the U. S. Department of Commerce through the National Textiles Center. We thank Professors J. Genzer and O. D. Velev for reading this work and providing helpful comments.

4.6 Supplementary Information

Strain cycling of the two ENP series reveals that these elastomeric materials undergo little mechanical hysteresis, which constitutes an important consideration in the design of polymeric actuators. Illustrative data of systems at the concentration extremes examined in this study are provided in Fig. 4.5. Strain thicknesses measured upon electrical actuation of the EAPs shown in Fig. 4 in the text are provided as a function of electric field in Fig. 4.6.

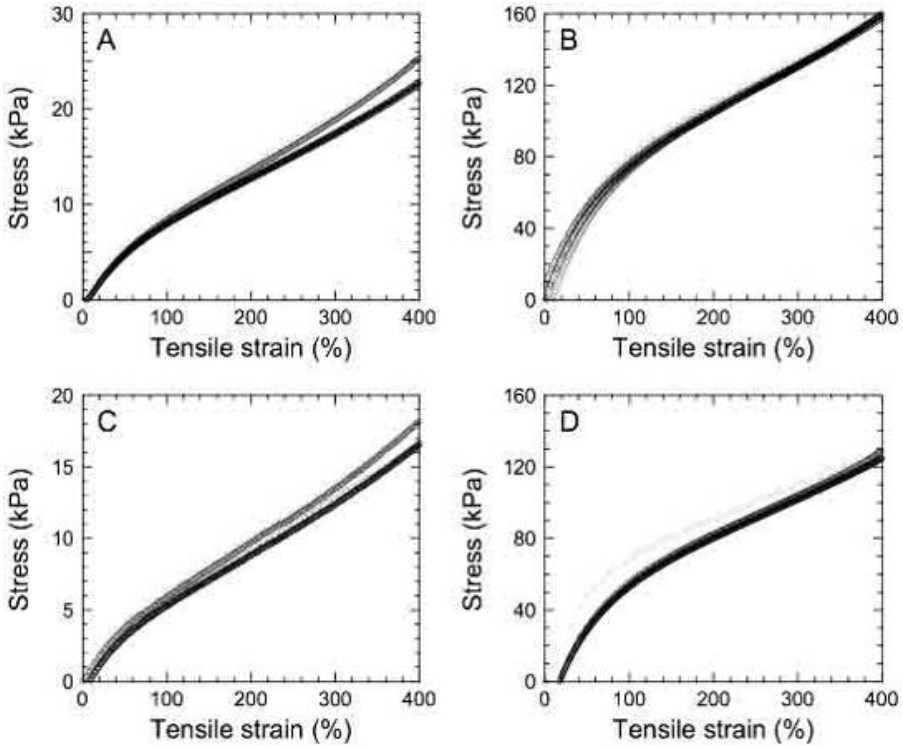

Figure 4.5Low-strain tensile data acquired after 1, 50 and 100 cycles from the SEBS161 (A,B) and SEBS217 (C,D) series at concentrations of 10 (A,C) and 30 (B,D) wt% copolymer. All tests were performed at a constant uniaxial extension rate of 500 mm/min at ambient temperature.

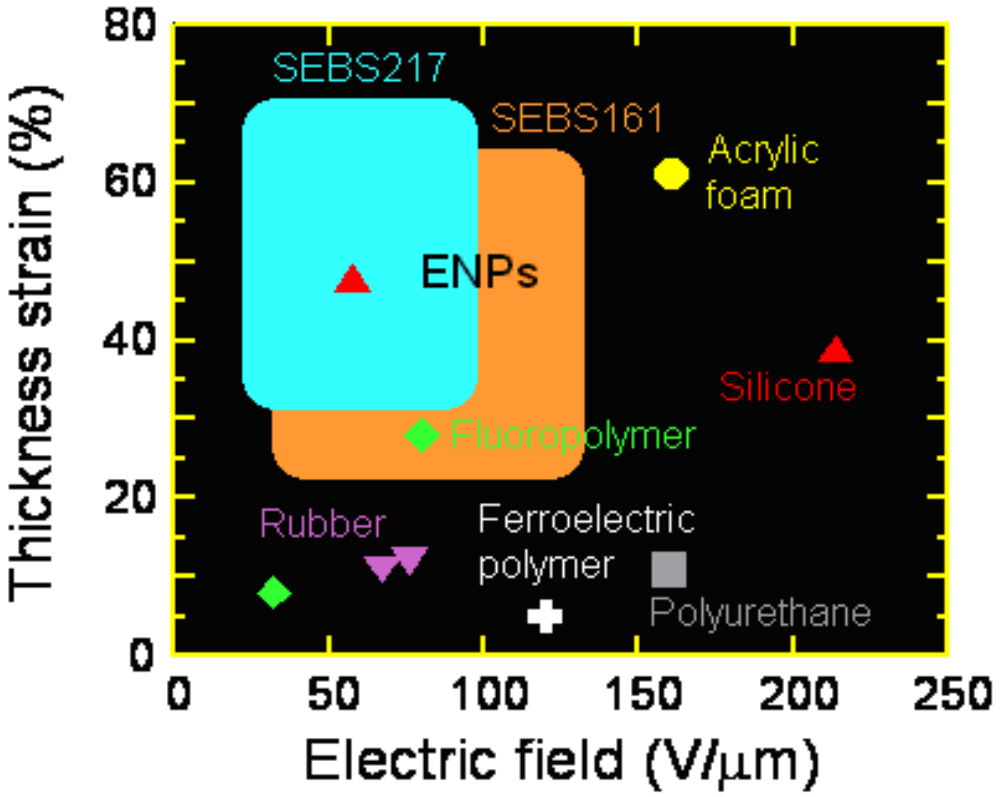

Figure 4.6 Thickness strain due to electrical actuation (s_z) presented as a function of electric field for the dielectric and ferroelectric organic materials displayed in Fig. 4.4 in the text. The cited reference sources are the same as those listed in the caption of Fig. 4.4 with the exception of the ferroelectric polymer.[45] On the basis of its definition, the thickness strain is an inherently negative quantity. The negative sign is routinely omitted in literature reports, and so we adopt this convention here.

4.7 Notes

This chapter was published in *Advanced Materials* (in press), published under the authorship of Ravi Shankar,[§†] Tushar K. Ghosh[%] and Richard J. Spontak[†‡] ([§]Fiber and Polymer Science Program and Departments of [†]Materials Science & Engineering, [%]Textile & Apparel Technology & Management and [‡]Chemical & Biomolecular Engineering, North Carolina State University, Raleigh, NC 27695, USA).

4.8 References

[1] R. Pelrine, R. Kornbluh, Q. Pei, J. Joseph, *Science* **2000,** *287*, 836.

[2] A. Cho, *Science* **2000**, *287*, 783.

[3] Q. M. Zhang, V. Bharti, X. Zhao, *Science* **1998**, *280*, 2101.

[4] S. -E. Park, T. R. Shrout, *J. Appl. Phys.* **1997**, *82*, 1804.

[5] R. H. Baughman, C. X. Cui, A. A. Zakhidov, Z. Iqbal, J. N. Barisci, G. M. Spinks, G. G. Wallace, A. Mazzoldi, D. De Rossi, A. G. Rinzler, O. Jaschinski, S. Roth, M. Kertesz, *Science* **1999**, *284*, 1340.

[6] G. Gu, M. Schmid, P. W. Chiu, A. Minett, J. Fraysse, G. T. Kim, S. Roth, M. Kozlov, E. Munoz, R. H. Baughman, *Nature Mater*. **2003**, *2*, 316.

[7] H. Funakubo (ed.), *Shape Memory Alloys*, Gordon and Breach, New York, 1987.

[8] Q. M. Zhang, H. F. Li, M. Poh, F. Xia, Z. Y. Cheng, H. S. Xu, C. Huang, *Nature* **2002**, *419*, 284.

[9] J. D. W. Madden, N. A. Vandesteeg, P. A. Anquetil, P. G. A. Madden, A. Takshi, R. Z. Pytel, S. R. Lafontaine, P. A. Wieringa, I. W. Hunter, *IEEE J. Oceanic Eng.* **2004**, *29*, 706.

[10] R. H. Baughman, *Science* **2005**, *308*, 63.

[11] Y. Berdichevsky, Y. H. Lo, *Adv. Mater.* **2006**, *18*, 122.

[12] T. Yamwong, A. M. Voice, G. R. Davies, *J. Appl. Phys.* **2002**, *91*, 1472.

[13] L. Yao, S. Krause, *Macromolecules* **2003**, *36*, 2055.

[14] R. Kornbluh, R. Pelrine, J. Joseph, R. Heydt, Q. Pei, S. Chiba, *Proc. SPIE* **1999**, *3669*, 149.

[15] R. Pelrine, R. Kornbluh, G. Kofod, *Adv. Mater.* **2000**, *12*, 1223.

[16] W. Ma, L. E. Cross, *Appl. Phys. A* **2004**, *78*, 1201.

[17] Y. Bar-Cohen (ed.), *Electroactive Polymer (EAP) Actuators as Artificial Muscles: Reality, Potential, and Challenges,* 2nd ed., SPIE Press, Bellingham, WA, 2004.

[18] G. Kofod, P. Sommer-Larsen, *Sens. Actuator A* **2005**, *122*, 273.

[19] T. L. Morkved, M. Lu, A. M. Urbas, E. E. Ehrichs, H. M. Jaeger, P. Mansky, T. P. Russell, *Science* **1996**, *273*, 931.

[20] A. Böker, H. Elbs, H. Hansel, A. Knoll, S. Ludwigs, H. Zettl, V. Urban, V. Abetz, A. H. E. Muller, G. Krausch, *Phys. Rev. Lett.* **2002**, *89*, 135502.

[21] T. Xu, A. V. Zvelindovsky, G. J. A. Sevink, K. S. Lyakhova, H. Jinnai, T. P. Russell, *Macromolecules* **2005**, *38*, 10788.

[22] K. Amundson, E. Helfand, X. N. Quan, S. D. Hudson, S. D. Smith, *Macromolecules* **1994**, *27*, 6559.

[23] C. Park, J. Yoon, E. L. Thomas, *Polymer* **2003**, *44*, 6725.

[24] I. W. Hamley, *The Physics of Block Copolymers*, Oxford University Press, New York, 1998.

[25] F. S. Bates, G. H. Fredrickson, *Phys. Today* **1999**, *52*, 32.

[26] P. Alexandridis, B. Lindman (eds.), *Amphiphilic Block Copolymers: Self-Assembly and Applications*, Elsevier Science, Amsterdam, 2000.

[27] D. E. Discher, A. Eisenberg, *Science* **2002**, *297*, 967.

[28] S. Jain, F. S. Bates, *Science* **2003**, *300*, 460.

[29] R. J. Spontak, N. P. Patel, in *Developments in Block Copolymer Science and Technology* (I. W. Hamley, ed.), Wiley, New York, 2004, pp. 159-212.

[30] K. A. Cavicchi, K. J. Berthiaume, T. P. Russell, *Polymer* **2005**, *46*, 11635.

[31] A. Böker, H. Elbs, H. Hansel, A. Knoll, S. Ludwigs, H. Zettl, A. V. Zvelindovsky, G. J. A. Sevink, V. Urban, V. Abetz, A. H. E. Muller, G. Krausch, *Macromolecules* **2003**, *36*, 8078.

[32] J. H. Laurer, J. F. Mulling, S. A. Khan, R. J. Spontak, R. Bukovnik, *J. Polym. Sci. B: Polym. Phys.* **1998**, *36*, 2379.

[33] L. -T. Cheng, W. Tam, S. R. Marder, A. E. Stiegman, G. Rikken, C. W. Spangler, *J. Phys. Chem.* **1991**, *95*, 10643.

[34] E. Prasman, E. L. Thomas, *J. Polym. Sci. B: Polym. Phys.* **1998**, *36*, 1625.

[35] R. Kleppinger, M. van Es, N. Mischenko, M. H. J. Koch, H. Reynaers, *Macromolecules* **1998**, *31*, 5805.

[36] J. P. Szabo, J. A. Hiltz, C. G. Cameron, R. S. Underhill, J. Massey, B. White, J.Leidner *Proc. SPIE* **2003**, 5051, 180.

[37] Cameron, C. G., *R. S. Underhill, M. Rawji, J. P. Szabo Proc. SPIE* **2004,** 5385, 51.

X Zhang, C Lowe, M Wissler, B Jahne, G Kovacs, Adv. Eng. Mater., 2005, 7, 361.

[38] B. J. Chu, X. Zhou, K. L. Ren, B. Neese, M. R. Lin, Q. Wang, F. Bauer, Q. M. Zhang, *Science* **2006**, *313*, 334.

[39] J. H. Laurer, S. A. Khan, R. J. Spontak, M. M. Satkowski, J. T. Grothaus, S. D. Smith, J. S. Lin, *Langmuir* **1999**, *15*, 7947.

[40] S. Nemat-Nasser, Y. X. Wu, *J. Appl. Phys.* **2003**, *93*, 5255.

[41] L. Bay, K. West, P. Sommer-Larsen, S. Skaarup, M. A. Benslimane, *Adv. Mater.* **2003**, *15*, 310.

[42] Y. Bar-Cohen (ed.), *Biomimetics: Biologically Inspired Technologies*, CRC Press/Taylor & Francis, Boca Raton, FL, 2005.

[43] R. Pelrine, R. Kornbluh, J. Joseph, R. Heydt, Q. B. Pei, S. Chiba, *Mater. Sci. Eng. C* **2000**, *11*, 89.

[44] H. R. Choi, K. M. Jung, J. C. Koo, J. D. Nam, Y. K. Lee, M. S. Cho, *Key Eng. Mater.* **2005**, *297-300*, 622.

[45] Klein, R. J., Xia, F., Zhang, Q. M., & Bauer, F.,. *J. Appl. Phys.* **2005**, 97, 094105.

CHAPTER 5

5 Electromechanical Response of Nanostructured Polymer Systems with No Mechanical Pre-strain

5.1 Abstract

Electroactive polymers have recently become a subject of increasing fundamental and technological interest due to their intrinsic ability to transform electrical energy into useable mechanical work, as well as their potential utility in the development of □icrorobotics, sensors, microfluidic pumps and haptic interfaces. While most studies of dielectric elastomers, in particular, are restricted to a small family of acrylic, siloxanes and polyurethane homopolymers, our previous work has established that nanostructured block copolymer systems afford attractive alternatives with composition-tunable electromechanical properties. A persistent challenge plaguing dielectric elastomers is the need for pre-strained films. In this work, we report that a dielectric elastomer derived from a poly[styrene-*b*-(ethylene-*co*-butylene)-*b*-styrene] triblock copolymer swollen in a midblock-selective solvent shows promise as an actuator with no pre-strain.

5.2 Introduction

Fabrication of actuator materials for biomimetic applications, especially those involving active prosthetics and microrobotics, has long been a goal of functional materials research. Materials developed for the purpose of converting electrical energy to mechanical work are generally referred to as electroactive or electroresponsive, and include piezoelectric ceramics,[1,2] carbon nanotubes[3,4] and shape-memory alloys.[5] Rigid actuators such as these, while generally requiring low voltages to operate, tend to suffer from performance restrictions such as limited mechanical displacement, hysteretic actuation cycling and slow response times. Organic actuators, on the other hand, are broadly classified[6,7] as electroactive polymers (EAPs) and are likewise capable of mechanical deformation upon electrical stimulation on the basis of several different operational principles.[6,7] Due to their light weight, facile processability, robust properties and reliable performance, EAPs have begun to attract substantial attention as next-generation responsive materials. Two important

classes of EAPs include ferroelectric (co)polymers[8-10] and dielectric elastomers,[7,11,12] but only the latter are considered further in the present work due to the large actuation strains (>200%), high energy densities (>3 MJ/m^3) and high electromechanical coupling efficiencies (>90%) achievable.[11] We have, for instance, recently reported[13] that a nanostructured EAP can exhibit an areal actuation strain of 245% and an associated electromechanical coupling efficiency of 92% under relatively low electric fields (22 V/μm) relative to conventional (homopolymer-based) dielectric elastomers.

The operative mechanism of dielectric elastomers, or electroelastomers, is that the electrostatic force of attraction between two conductive and oppositely charged compliant electrodes on opposing sides of a dielectric elastomer film induces a primarily compressive (Maxwell) stress (σ_M). The magnitude of this stress, schematically depicted in Fig. 5.1, is determined from[11,14]

$$\sigma_M = \varepsilon_0 \varepsilon E^2 \quad (1)$$

where ε_0 and ε are the permittivity of free space and of the dielectric elastomer, respectively, and E denotes the applied electric field given by the applied voltage (V) imposed across the thickness of the film (L). Films are commonly subjected to large uniaxial or biaxial pre-strain *(e.g.*, 300% x 300%) prior to actuation to enhance performance by reducing L (and increasing E).[11] Common actuator configurations (*e.g.*, tube, rolled, bow and frame) must support the requisite pre-strain despite added weight and space.[15,16] Thus, pre-straining the elastomer promotes a net reduction in performance parameters such as the elastic energy density (by 10-100x)[17] and variation in actuator performance due to time-dependent stress relaxation.[18] Cyclic stress concentration of the elastomer along a rigid support may further limit actuator life. It is therefore desirable to develop actuators without mechanical pre-strain or with support-free pre-strain. The latter has been achieved by Ha *et al.*,[12] who designed acrylic actuators with pre-strain retained by a second elastomer. Here, we describe a route to dielectric elastomers with no (0%) pre-strain by using electroactive nanostructured polymers (ENPs) with composition-tunable properties. Electrical actuation results reported here correspond to ENP films without mechanical pre-strain.

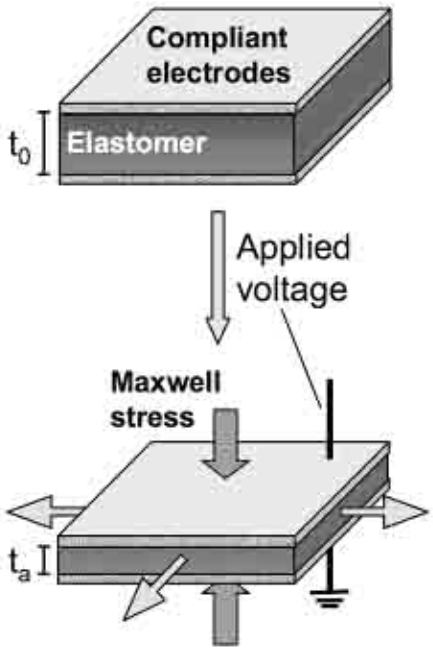

Figure 5.1Schematic illustration of a dielectric elastomer before and after application of an external electrical potential across the film. The development of a Maxwell stress compresses the film from t_0 to t_a, which depends on the magnitude of the electric field [E in Equation (1)], as well as on several material properties (e.g., ε and compressive modulus).

5.3 Experimental

The materials used to produce the ENPs under investigation included three poly[styrene-*b*-(ethylene-*co*-butylene)-*b*-styrene] (SEBS) triblock copolymers differing in molecular weight but having comparable compositions (30-33 wt% S). These Kraton copolymers were obtained from GLS Corp. (McHenry, IL) and are hereafter designated as SEBS*M*, where *M* (75, 161 and 217) denotes the copolymer molecular weight in kg/mol. An EB-selective aliphatic/alicyclic white mineral oil (MO, Witco Hydrobrite 380) was obtained from Crompton Corp. (Petrolia, PA) and used as-received. Each ENP was prepared by mixing a copolymer at a predetermined concentration with the MO and 1 wt% antioxidant at 180 °C in a Ross LDM double-planetary mixer under vacuum for 30 min. Due to the apparent critical gel concentration (the copolymer fraction at which a molecular network, or gel, stabilized by glassy S-rich micelles forms[19-21]), the SEBS75 concentrations ranged from 25 to 50 wt% in 5 wt% increments. For comparison, the concentration of ENPs containing either SEBS161 or SEBS217 was 30 wt%. Once these physical copolymer gels were generated, they were

compression-molded at 180 °C and then slowly cooled to ambient temperature,[19] yielding elastomeric films measuring 0.5-0.6 mm thick.

Electrical actuation of the resultant films was assessed at 0% pre-strain. A small circular active area in each specimen was created by applying compliant electrodes composed of Ag grease (Chemtronics Circuit Works, Kennesaw, GA) on both sides of the film. Actuation under ambient conditions was induced using a manual voltage trigger, and the applied voltage was ramped from zero to a target voltage in 10 s with no discernible lag between voltage ramping and specimen actuation. The specimen was subsequently held at voltage for 10 s before the voltage was returned to zero for 10 s to permit discharge. Real-time video sequences were acquired during actuation, and image analysis was performed frame-by-frame with the Matrox Inspector software package to measure the areal actuation.[13,22] Dielectric constants of the films were measured on an Agilent dielectric test fixture 16451B with HP4284A LCR meter operated over a frequency range of 20 Hz to 1 MHz at 25°C. Since the electromechanical response of dielectric elastomers is described as a Maxwell stress (*cf*. Fig. 5.1) and is thus dictated by the mechanical properties of the elastomers in compression, quasi-static uniaxial compression tests were likewise conducted at ambient temperature to discern the stress-strain behavior of the ENPs under investigation as functions of copolymer molecular weight and concentration.

5.4 Results and Discussion

Our previous study[13] of SEBS-based ENPs is based on growing evidence that the nanostructures of microphase-separated block copolymers in thin[23,24] and bulk[25] films can reorient in response to an applied electric field, and addresses SEBS161/MO and SEBS217/MO films varying in copolymer concentration and biaxially pre-strained by 300%. Under these conditions, physically cross-linked networks are stabilized by micelles consisting of glassy S cores and MO-swollen EB coronas.[26,27] As Figure 5.2a illustrates, the pre-strained ENPs exhibit excellent and composition-tunable actuation displacement, which is expressed here in terms of areal strain. This is a commonly accepted method by which to report[11,28] the isotropic electromechanical behavior of dielectric elastomers. Although such displacement is principally attributed to the development of a Maxwell stress during actuation, the response of these copolymer-based ENPs to an applied electric field may also

reflect differences in polarizability between the S endblocks and the MO-swollen EB midblock. When the SEBS161- and SEBS217-based ENPs are pre-strained, two important trends become evident in Fig. 5.2a: the maximum areal strain increases with (*i*) increasing copolymer molecular weight and (*ii*) decreasing copolymer concentration. As is seen in this figure, the former is likewise true in the absence of pre-strain. In both cases, the distance between physical cross-links (i.e., the intermiceller distance) increases. Included in the inset is the actuation strain as a function of mechanical pre-strain for the SEBS217/MO ENP with 5 wt.-% copolymer, depicting the commonly seen dependence of actuation strain on biaxial pre-strain up to ≈300%. Beyond this pre-strain level, however, the measured actuation strain decreases, suggesting the existence of an optimal pre-strain level that has not been previously reported. It is noteworthy that the dielectric strength of the ENP described in the inset of Figure 5.2(a) increases monotonically with increasing pre-strain up to ≈300% and then remains nearly constant thereafter (data not shown). An increase in pre-strain typically increases the dielectric strength, but decreases ε.[29] Thus, the initial increase in actuation strain with increasing pre-strain observed in the inset of Figure 5.2(a) is attributed to an increase in dielectric strength. At higher pre-strain levels (beyond 300%), the reduction in e becomes dominant while the dielectric strength remains constant, thereby resulting in lower actuation strain.

Figure 5.2(a) likewise establishes that copolymer molecular weight has relatively little influence on actuation strain in the absence of pre-strain, whereas Figure 5.2(b) reveals that the corresponding elastic energy density (US), which describes the ability of an actuator to perform mechanical work, increases substantially with decreasing copolymer molecular weight at 0% pre-strain conditions. For a linear dielectric medium exhibiting only elastic deformation (typically < 20% strain)[11], U_S is given by[8]

$$U_S = Y s_z^2/2 \qquad (2)$$

where Y represents the compressive modulus, and s_z is the thickness, or transverse, strain defined by $t_{act}/t_0 - 1$ (t_a denotes the film thicknesses after actuation, as depicted in Figure 5.1). Values of sz are normally determined from the measured areal strains by assuming isochoric deformation with isotropic lateral displacement. According to Eq. 2, U_S is proportional to Y, which is expected to increase with decreasing copolymer molecular weight due to shortening of the rubbery EB midblock and a accompanying reduction in intermicellar

distance. At a concentration of 30 wt% copolymer in MO, measured values of Y (in MPa) are 2.0 for SEBS75, 1.3 for SEBS161 and 1.1 for SEBS217. The increase in U_S with decreasing molecular weight under near constant-composition conditions in Fig. 5.2b is therefore consistent with the relationship between U_S and Y established by Eq. 2.

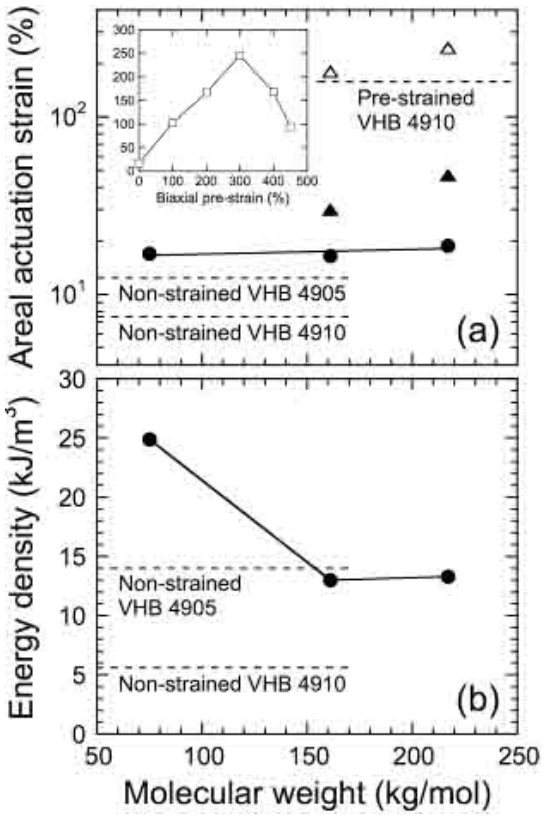

Figure 5.2 (a) Maximum areal actuation strain measured just below the breakdown field presented as a function of SEBS molecular weight for three different ENP systems: 5 wt.-% copolymer biaxially pre-strained to 300% (□), 30 wt.-% copolymer biaxially pre-strained to 300% (▲), and 30 wt.-% copolymer with no pre-strain (●). Values of VHB acrylics under the same conditions (labeled, dashed lines) are included for comparison. The solid line serves as a guide for the eye, and the inset shows the dependence of the maximum areal actuation strain on the extent of biaxial pre-strain for the SEBS217/MO ENP with 5 wt.-% copolymer (the solid line connects the data). (b) Corresponding elastic energy density (US) values of the ENPs with no pre-strain(●) and nonstrained VHB acrylics (dashed lines). The solid line serves to connect the data

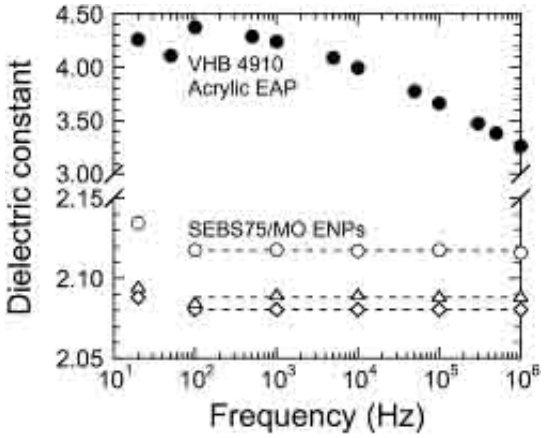

Figure 5.3 The frequency dependence of the real component of the complex dielectric constant (e0) measured for the VHB acrylic (●) and three SEBS75/MO ENPs varying in concentration (in wt.-% copolymer): 25 (◊), 35 (Δ), and 45 (○). The dashed lines signify the range over which e0 does not vary with frequency

In this section, the concentration dependence of electrical actuation for SEBS75/MO ENPs under 0% pre-strain is explored and compared with analogous SEBS161/MO and SEBS217/MO ENPs at 30 wt% copolymer, as well as a commercially available acrylic EAP (VHB by 3M Co.) at two different film thicknesses (0.5 mm for VHB 4905 and 1.0 mm for VHB 4910), under identical actuation conditions. Since development of a Maxwell stress is sensitive to ε of the test specimen, measurements of the real component of the complex dielectric constant (ε') are provided in Fig. 5.3 as a function of frequency for three SEBS75/MO ENPs varying in SEBS75 concentration. An increase in copolymer concentration promotes a marginal increase in ε' from *ca*. 2.08 to just under 2.12. Another interesting observation is that the three ENPs exhibit similar behavior: ε' initially decreases at low frequency and then remains invariant with increasing frequency. These results indicate that the dielectric properties of the ENPs are composition-tunable and that these ENPs are stable over at least 4 orders of magnitude in frequency (which makes them attractive for high-frequency applications involving, for instance, flapping[30]). In marked contrast, values of ε' measured from the VHB 4910 acrylic over the same frequency range (included in Fig. 5.3) are higher than those determined for the ENPs under investigation, but are frequency-sensitive,[29] monotonically decreasing with increasing frequency.

Figure 5.4 is a compilation of various electromechanical properties of the SEBS75/oil

ENPs displayed as a function of copolymer concentration at ambient temperature. Included for comparison and correspondingly labeled in each part of the figure are data collected from the SEBS161/MO, SEBS217/MO and VHB dielectric elastomers. The dependence of Y on SEBS75 concentration in Fig. 5.4a confirms that (*i*) Y increases almost linearly with increasing copolymer content and (*ii*) these ENPs are generally stiffer than their high molecular weight counterparts (SEBS161 and SEBS217) at the highest copolymer concentration examined (30 wt%). Values of Y measured from the two VHB acrylic specimens (2.3 MPa) are in quantitative agreement with the value previously reported by Madden *et al*.[31] Figure 5.4b reveals that the maximum areal and thickness strains achieved upon actuation are relatively independent of copolymer concentration from 25 to 35 wt% SEBS75 and then decrease at higher copolymer concentrations, due presumably to an increase in material stiffness and/or a change in copolymer morphology.[27,32] Note that the maximum strain values displayed in Fig. 5.4b for the SEBS75/MO ENPs at low copolymer concentrations are comparable to those measured from the SEBS161/MO and SEBS217/MO ENPs, but are higher than those determined for the VHB acrylic elastomers. Values of the breakdown electric field, which governs the net dielectric strength of EAPs, vary from 29 to 41 V/μm for the SEBS75/MO ENPs, whereas corresponding breakdown fields for the SEBS161/MO, SEBS217/MO, VHB 4905 and VHB 4910 systems are 27, 29, 34 and 17 V/μm, respectively.

A curious observation is that an apparent maximum in breakdown field exists at 35 wt% SEBS75 in the SEBS75/MO series. While no definitive reason is as of yet available to explain this property characteristic, it may reflect either a change in morphology or an abrupt change in midblock conformation[33-36] (from bridged to looped) or both. Whatever the reason for its origin, this signature feature is again evident in the dependence of U_S on copolymer concentration, which is shown in Fig. 5.4c. Recall from Eq. 2 that U_S depends explicitly on both Y and the thickness strain (s_z) provided in Figs. 5.4a and 4b, respectively. At 30 wt% copolymer under zero prestrained condition, the SEBS75/MO ENP exhibits an energy density that is ~90% larger than that measured from the SEBS161/MO and SEBS217/MO systems, confirming that U_S increases with increasing Y under near constant-composition conditions. At 35 wt% copolymer, the value of U_S from the SEBS75/MO ENP (26.3 kJ/m^3) is ~88% higher than that of the VHB 4905 acrylic EAP and about 4.7x higher

than that of the VHB 4910 material despite comparable Y values (2.1 MPa for the ENP versus 2.3 MPa for the EAPs).

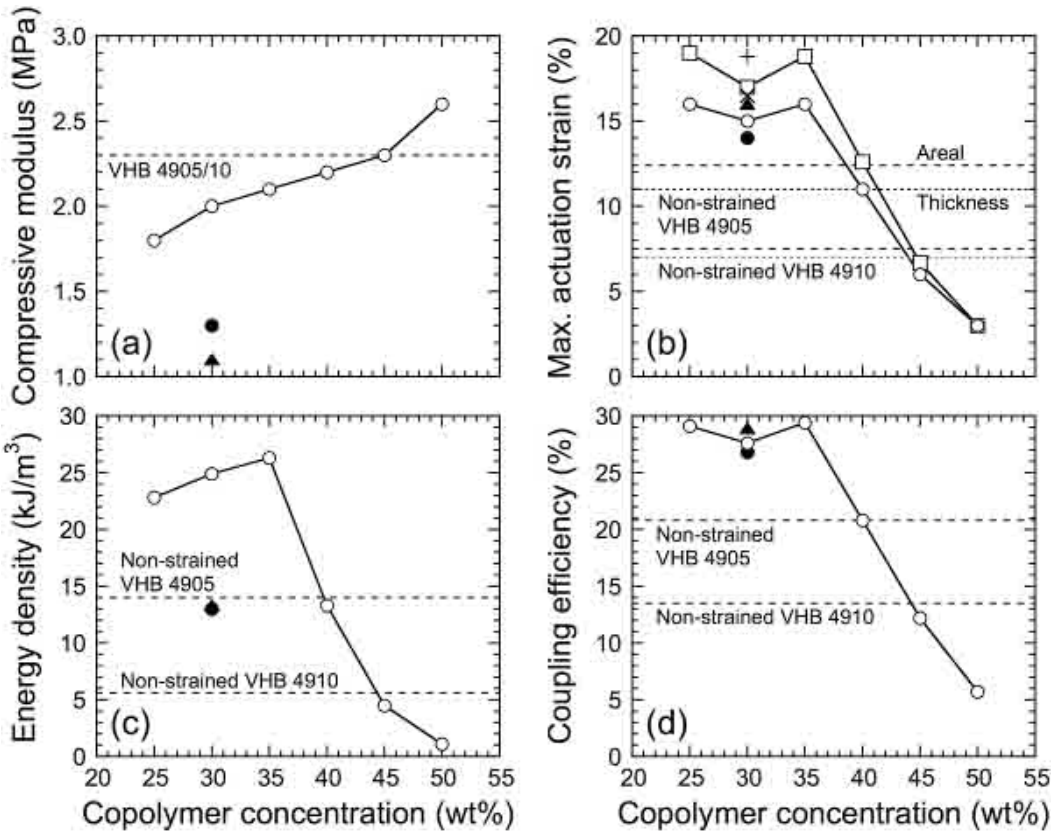

Figure 5.4 The dependence of (a) compressive modulus (Y), (b) maximum areal and thickness actuation strain, (c) elastic energy density (U_S), and (d) electromechanical coupling efficiency (K^2) on copolymer concentration for ENPs with no mechanical pre-strain and containing the following copolymers: SEBS75 (○,□), SEBS161 (●,×), and SEBS217 (▲,+). Note that the secondary symbols are only used to denote areal actuation strains in (b). The dashed (and dotted, as labeled) lines identify values measured for the VHB acrylic EAPs in the absence of pre-strain. The solid line in each part serves to connect data displayed for the SEBS75/MO ENP series.

This difference in U_S between the present ENPs and the acrylic EAPs indicates that factors other than just Y must be carefully considered in the ground-up design[37,38] of multicomponent, possibly nanostructured, electroresponsive polymeric materials. A more in-depth analysis of some of these factors is currently underway. One should recognize in all fairness, however, that the value of U_S for the VHB 4910 acrylic is reported[11] to increase to ~3.4 MJ/m^3, a jump of over two orders of magnitude, when it is biaxially pre-strained by

300%. This change in actuation performance clearly demonstrates the general importance of pre-straining EAPs and the need to identify viable means by which to achieve such high energy densities without resorting to mechanically supported pre-strain. The last actuation performance metric discussed here is the electromechanical coupling efficiency (K^2), which is defined as the ratio of stored mechanical energy to input electrical energy by[11]

$$K^2 = -2s_z - s_z^2 \tag{3}$$

We have previously reported[13] that values of K^2 for the SEBS161/MO and SEBS217/MO ENPs with 5 wt% copolymer can reach 87 and 92%, respectively, under 300% biaxial pre-strain. Under similar conditions, K^2 = 85% for the VHB 4910 acrylic.[11] At 30 wt% copolymer, the efficiencies of the ENPs drop to 40 and 53%, respectively. Without pre-strain, however, K^2 decreases further to 28±1% for both ENPs, which is comparable to the K^2 values measured from the SEBS75/MO ENPs at low copolymer concentrations (*cf*. Fig. 5.4d). Corresponding values of K^2 determined for the VHB acrylics without pre-strain are much lower (by 29 and 54% for VHB 4905 and 4910, respectively) relative to the SEBS75/MO ENP with 35 wt% copolymer.

5.5 Conclusions

Nanostructured electroactive polymers afford an attractive and highly tunable alternative to conventional homopolymer-based dielectric elastomers. Such actuators currently require mechanical pre-strain to increase the effective electric field and thus improve the magnitude of the Maxwell stress generated and the net electromechanical response. Mechanical pre-strain is accompanied by several drawbacks related to both material and system performance, and ongoing efforts are underway to mitigate this requirement. We have demonstrated in this study that ENPs composed of a relatively low-molecular-weight SEBS75 triblock copolymer swollen in the presence of a primarily aliphatic mineral oil are energy-efficient materials that are capable of converting a large fraction of input energy into useful mechanical work more effectively than either (*i*) ENPs containing high-molecular-weight copolymers of comparable composition or (*ii*) EAPs based on acrylic dielectric elastomers (which have become the benchmark standard in this research field) in the absence of mechanical pre-strain. If substantial pre-strain is tolerable, however, the ENPs derived from higher molecular weight copolymers (SEBS161 and SEBS217) exhibit vastly superior actuation and mechanical

properties. Unlike conventional EAPs derived from homopolymers without added inorganic fillers (to improve ε), the ENPs under investigation here provide much broader application versatility due to their remarkable property tunability.

5.6 Acknowledgments

This work was supported by the U. S. Department of Commerce through the National Textiles Center.

5.7 Notes

This chapter was published in *Macromolecular Rapid Communication, (*2007, 28, 1142-1147**)**, published under the authorship of Ravi Shankar,[§†] Tushar K. Ghosh[%] and Richard J. Spontak[†‡] ([§]Fiber and Polymer Science Program and Departments of [†]Materials Science & Engineering, [%]Textile & Apparel Technology & Management and [‡]Chemical & Biomolecular Engineering, North Carolina State University, Raleigh, NC 27695, USA).

5.8 References

[1] S. Zhang, C. A. Randall, T. R. Shrout, *Jpn. J. Appl. Phys. , Part 2* 2003, **42**, L1152.

[2] S.-E. Park, T. R. Shrout, *J. Appl. Phys.* 1997, **82**, 1804.

[3] R. H. Baughman, *Science* 2005, **308**, 63.

[4] R. H. Baughman, C. Cui, A. A. Zakhidov, *Z.* Iqbal, J. N. Barisci, G. M. Spinks, G. G. Wallace, A. Mazzoldi, D. De Rossi, A. G. Rinzler,O. Jaschinski, S. Roth, M. Kertesz, *Science* 1999, **284**, 1340.

[5] *Shape Memory Alloys*, H. Funakubo, Ed., Gordon and Breach, New York 1987.

[6] Y. Bar-Cohen, *Electroactive Polymer (EAP) Actuators as Artificial Muscles: Reality, Potential, and Challenges*, Y. Bar-Cohen, Ed., SPIE Press, Bellingham, WA, 2004.

[7] J. D. W. Madden, N. A. Vandesteeg, P. A. Anquetil, P. G. A. Madden, A. Takshi, R. Z. Pytel, S. R. Lafontaine, P. A. Wieringa, I. W. Hunter, *Oceanic Eng., IEEE Journal of* 2004, **29**, 706.

[8] Q. M. Zhang, H. Li, M. Poh, F. Xia, Z.-Y.Cheng, H. Xu, C. Huang, *Nature* 2002, **419**, 284.

[9] C. Huang, Q. M. Zhang, G. deBotton, K. Bhattacharya, *Appl. Phys. Lett.* 2004, **84**, 4391.

[10] B. Chu, X. Zhou, K. Ren, B. Neese, M. Lin, Q. Wang, F. Bauer, Q. M. Zhang, *Science* 2006, **313**, 334.

[11] S. M. Ha, W. Yuan, Q. Pei, R. Pelrine, S. Stanford, *Adv Mater* 2006, **18**, 887.

[12] R. Pelrine, R. Kornbluh, Q. Pei, J. Joseph, *Science* 2000, **287**, 836.

[13] R. Shankar, T. K. Ghosh, R. J. Spontak, *Adv. Mater.* submitted 2006.

[14] R. D. Kornbluh, R. Pelrine, J. Joseph, R. Heydt, Q. Pei, S. Chiba, *Proc. SPIE* 1999, **3669**, 149.

[15] Q. Pei, M. Rosenthal, S. Stanford, H. Prahlad, R. Pelrine, *Smart Mater. Struct.* 2004, **13**, N86.

[16] Q. Pei, R. Pelrine, S. Stanford, R. D. Kornbluh, M. S. Rosenthal, K. Meijer, R. J. Full, *Proc. SPIE* 2003, **4698**, 246.

[17] J. L. Pons, *Emerging Actuator Technologies A Micromechatronic Approach*, Wiley, Chichester, England ; Hoboken, NJ, 2005, 2, p. 731.

[18] H. R. Choi, K. Jung, N. H. Chuc, M. Jung, I. Koo, J. Koo, J. Lee, J. Lee, J. Nam, M. Cho, Y. Lee, *Proc. SPIE* 2005, **5759**, 283.

[19] I. W. Hamley, *The Physics of Block Copolymers,* Oxford University Press, New York, 1998.

[20] J. H. Laurer, J. F. Mulling, S. A. Khan, R. J. Spontak, R. Bukovnik, *J. Polym. Sci. Part B Polym. Phys.* 1998, **36**, 2379.

[21] S. Arora, T. Ghosh, J. Muth, *Sens. Actuator A* press 2006.

[22] T. L. Morkved, M. Lu, A. M. Urbas, E. E. Ehrichs, H. M. Jaeger, P. Mansky, T. P. Russell, *Science* 1996, **273**, 931.

[23] T. Xu, A.V. Zvelindovsky, G.J.A. Sevink, K.S. Lyakhova, H. Jinnai, T. P. Russell *Macromolecules* 2005, **38**, 10788.

[24] A. Boker, H. Elbs, H. Hansel, A. Knoll, S. Ludwigs, H. Zettl, A. V. Zvelindovsky, G. J. A. Sevink, V. Urban, V. Abetz, A. H. E. Muller, G. Krausch, *Macromolecules* 2003, **36**, 8078.

[25] J. H. Laurer, S.A. Khan, R. J. Spontak, M. M. Satkowski, J. T. Grothaus, S. D. Smith, J. S. Lin, *Langmuir* 1999, **15**, 7947.

[26] S.-G. Lee, H.-C. Park, S. D. Pandita, Y. Yoo, *Int. J. Cont. Automat. Syst.* 2006, **4**, 748.

[27] G. Kofod, R. Kornbluh, R. Pelrine, P. Sommer-Larsen, *Poc. SPIE* 2001, **4329**, 141.

[28] *Thermoplastic Elastomers*, Eds. G. Holden, H. R. Kricheldorf, R. P. Quirk, Hanser Gardner Pub, Cincinnati, Oh, USA, 3rd, 2004.

CHAPTER 6

6 Electrical and Mechanical Behavior of Electroactive Nanostructured Polymers

6.1 Abstract

Electroactive polymers (EAPs) can exhibit relatively large strain responses upon electrical stimulation. For this reason, in conjunction with their light weight, robust properties, low cost and facile processability, EAPs are of considerable interest in the development of next-generation organic actuators. Within this class of materials, dielectric elastomers (D-EAPs) have repeatedly exhibited the most promising and versatile properties. A new family of D-EAPs derived from swollen poly[styrene-*b*-(ethylene-*co*-butylene)-*b*-styrene] triblock copolymers has been recently found to undergo ultrahigh displacement at relatively low electric fields compared to previously reported D-EAPs. The present work examines the mechanical response of these electroactive nanostructured polymer (ENP) systems under quasi-static, dynamic and electromechanical loading conditions. Careful measurement of the quasi-static properties under tensile and compressive loading yield similar results that are significantly influenced by the introduction of in-plane strain, as well as by copolymer concentration or molecular weight. Blocking stress measurements reveal that the actuation effectiveness achieved by some of the ENPs is comparable to that of the VHB 4910 acrylic, thus providing a novel and efficient avenue to designer D-EAPs for advanced engineering, biomimetic and biomedical applications.

6.2 Introduction

Contemporary interest in "smart materials" that can respond to a variety of external stimuli such as temperature, pH, light, magnetic and electrical fields has dramatically increased due to the untapped potential of such functional materials in a diverse range of nano- and bio-related technologies.[1-3] Polymeric materials that can convert electrical energy to mechanical work are broadly classified as electroactive polymers (EAPs) and typically exhibit considerable stress and/or strain upon electrical stimulation.[4,5] Because of their electromechanical properties and the unique combination of general polymer attributes (e.g., low cost, robust properties, facile processability and light weight), EAPs have drawn

significant attention as suitable candidates in the development of organic actuators. Moreover, EAPs are superior to other actuator materials such as piezoelectric ceramics, shape memory alloys and carbon nanotubes in that they exhibit higher energy density, greater failure resistance, faster response speed and, maybe most importantly, commercial scalability.[4,6-9] On the basis of their resilience, large actuation strains, toughness and inherent vibration dampening, EAPs can be used to emulate the motion of animals and insects for fabricating biologically inspired (micro)robots and responsive prosthetics.[8, 10-12]

Of all the EAPs reported thus far, dielectric elastomers (D-EAPs) possess the most promising and versatile properties such as highest actuation strain, highest energy density, highest electromechanical coupling efficiency and the fastest actuation time.[4,13] Most D-EAPs of current relevance derive from chemically cross-linked acrylic, silicone and natural/synthetic rubber homopolymers,[4] as well as segmented polyurethane.[14] Recently, we have demonstrated[13,15] that the electromechanical response of electroactive nanostructured polymers (ENPs) is promising and, unlike conventional D-EAPs, tunable. These materials consist of a microphase-separated block copolymer that can spontaneously self-organize into (a)periodic nanostructures alone[16,17] or in the presence of other (macro)molecular or nanoscale species.[18,19] The resultant properties can be controllably altered by varying copolymer characteristics such as molecular composition, weight and architecture, in addition to the concentration and selectivity of the additive.[20,21] Incorporation of a midblock-selective oligomeric solvent into a triblock copolymer yields physically cross-linked molecular networks that exhibit high areal actuation strains (> 250 %) at low electric fields (~22 V/μm) with high electromechanical coupling efficiencies (> 90%).[13] We have also shown[15] that (*i*) these versatile systems undergo moderate actuation under 0% prestrain and (*ii*) the elastic energy density increases with decreasing copolymer molecular weight.

The actuation mechanism of a D-EAP can be most clearly explained by considering a planar film of pre-actuation thickness L, although such a geometry is not required for practical application. A voltage (V) is applied across the film, which is sandwiched between two compliant electrodes, as depicted in Fig. 6.1. The electrostatic force of attraction between the oppositely charged electrodes initiates a Maxwell stress that serves to compress the film in the transverse (z) direction.[4,22] Like charges along each film surface repel each other, resulting in further stretching of the film along the lateral (x and y) directions. The

effective actuation (Maxwell) stress is given[14] by $\varepsilon_o \varepsilon E^2$, where ε_o is the permittivity of free space, ε represents to the field-invariant dielectric constant of the D-EAP film and E denotes the electric field (= V/L). The normal actuation stress acting along z generates a transverse strain, as well as in-plane stresses along the x and y directions. The extent and distribution of the accompanying in-plane strains upon actuation are governed by the elastic modulus (E) of the D-EAP and any in-plane anisotropy, which can be introduced by prestraining the film. These two topics constitute the focus of the present work wherein the mechanical response of ENPs under quasi-static (compressive and tensile) and electromechanical loading with and without mechanical prestrain is systematically investigated.

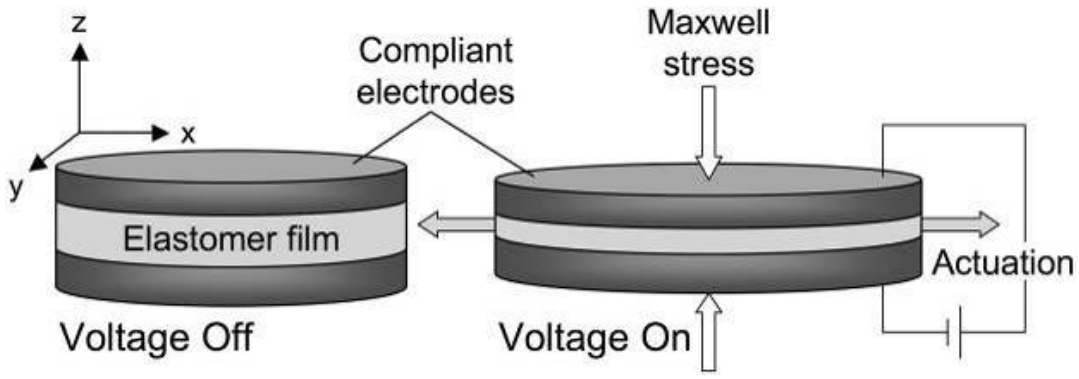

Figure 6.1 Schematic illustration of a D-EAP before (left) and after (right) electrical actuation. Electrostatic attraction between the negatively charged compliant electrodes applied to opposing surfaces of the D-EAP generates a normal Maxwell stress upon actuation and compresses the film in the transverse (z) direction. Under isochoric conditions, the film extends laterally along the x and y directions.

6.3 Experimental

Two poly[styrene-*b*-(ethylene-*co*-butylene)-*b*-styrene] (SEBS) triblock copolymers (GLS Corp., McHenry, IL) with number-average molecular weights of 161 and 217 kg/mol (designated SEBS161 and SEBS217, respectively) and S compositions ranging from 30-33 wt% were blended with an aliphatic/alicyclic white mineral oil (Witco Hydrobrite 380, Crompton Corp., Petrolia, PA) to prepare four ENP systems. Only two copolymer concentrations (5 and 30 wt%, which constitute the extreme concentrations from our previous study[13]) were examined here to illustrate the (electro)mechanical attributes of ENPs

varying in rigidity. It should be recognized at this juncture that these ENPs fundamentally differ from ionic polymer-metal composites (IPMCs) or hydrogels in that the oligomeric oil serves to swell the molecular network formed by the copolymer and does not assist in electrolyte transport. Each ENP was prepared by mixing either the SEBS161 or SEBS217 copolymer, oil and 1 wt% antioxidant in a Ross LDM double-planetary mixer under vacuum at 180 °C for 30 min. Films measuring 1-2.5 mm thick were prepared by compression-molding at 180 °C, followed by slow cooling to ambient temperature.[23]

Quasi-static uniaxial compression and tension tests were performed at ambient temperature with an MTS-30 unit operated at crosshead speeds of 5 and 127 mm/min, respectively. Results not presented here confirm that the stress response, including the tensile modulus (E_T), of the ENPs (with up to 30 wt% copolymer) to uniaxial tensile deformation is nearly independent of crosshead speed up to 500 mm/min, whereas other D-EAPs exhibit a conventional viscoelastic response, that is, the stress increases with increasing strain rate. Values of E_T were extracted from the initial linear region of stress-strain curves generated upon uniaxial tensile loading. Compressive modulus (E_C) values were measured under two different test conditions. In the first, the MTS-30 platen made direct contact with, and indented, the specimen. During indentation, however, non-linear shear forces arising from the viscoelastic nature of the specimens contributed to the measured E_C. To alleviate this complication, silicone oil, confirmed to be immiscible with all the polymeric species examined and the mineral oil used to prepare the ENPs, was applied to the platen prior to specimen contact. Values of E_C were extracted from the linear region of the resultant stress-strain curves after initial contact and indentation.

As-prepared elastomer films, as well as those biaxially prestrained (300% along x and y), were subjected to uniaxial compression loading. These tests were likewise performed on the VHB 4910 acrylic elastomer (1 mm thick, from 3M Co., Minneapolis, MN) and the PT6100S polyurethane (0.076 mm thick, from Deerfield Urethane, South Deerfield, MA) for comparative purposes. Blocking stresses were discerned with the test fixture illustrated in Fig. 6.2. This fixture differed from that previously reported by Kofod et al.[24,25] because it possessed equally spaced holes along its length to secure the prestrained D-EAP films. This modification was necessary since the ENPs do not exhibit the same level of tackiness as the acrylic adhesive. Each film was prestrained on a stage (Fig. 6.2a) that permitted accurate

biaxial deformation of an initially relaxed D-EAP film to predetermined (although not necessarily equal) extents along x and y. For example, two of the ENP films were prestrained to 500% (along x) and 200% (along y) and fixed in place with the new frame (Fig. 6.2b), which was then mounted on the MTS-30 so that the specimen could be further strained in the y direction (Fig. 6.2c) to a total prestrain of 350% in y.

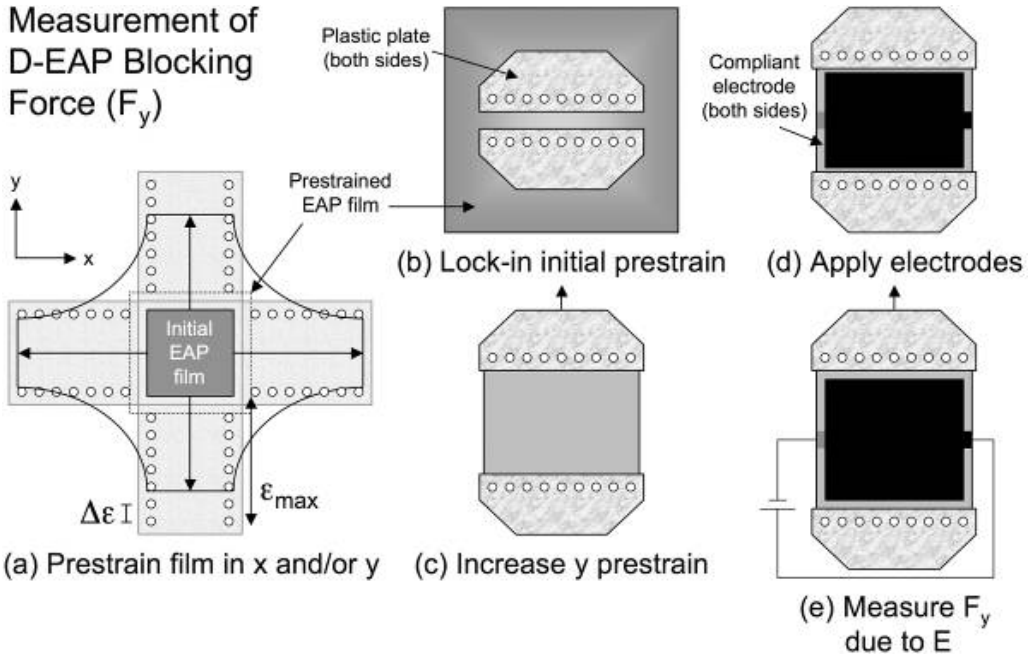

Figure 6.2 Process diagram depicting measurement of the blocking force generated by a D-EAP upon electrical actuation. In (a), a film is prestrained (an)isotropically along x and y at predetermined strain increments ($\Delta\varepsilon$ = 25%) up to ε_{max} = 275%. The plastic fixture shown in (b) is bolted on both sides of the prestrained film to lock-in the biaxial deformation, and the fixture is then subjected to uniaxial tensile loading along y to achieve a predetermined final anisotropic prestrain in (c). The specimen is then coated with a compliant electrode on both sides (d) and subsequently subjected to an external potential (e) to induce transverse compression and lateral actuation, which results in a measurable force reduction in the y direction.

A compliant electrode (Ag grease from Chemtronics Circuit Works, Kennesaw, GA) was subsequently coated on both sides of the prestrained film (Fig. 6.2d). Caution was exercised to avoid contacting the film edges. When the external voltage was applied, the actuation-induced load reduction along the y direction yielded the blocking force of the D-EAP (Fig.

6.2e). Unless otherwise indicated, all stresses reported here correspond to engineering stresses.

6.4 Results and Discussion

To understand the general response of dielectric elastomers under compressive loading, uniaxial compression tests have been performed on the VHB 4910 acrylic and ENP systems. The results of these tests are compared with data acquired during uniaxial tension in Fig. 6.3. In Fig. 6.3a, the stress-strain behavior of VHB 4910 is displayed and illustrates the general difference between the two deformation mechanisms. It is important to recognize that the initial stress-strain slope used to extract E_T and the post-indentation slope from which to extract E_C are comparable, signifying that the two moduli are of similar magnitude. Similarly, Figs. 6.3b and 3c show the compressive and tensile behavior of the SEBS217 and SEBS161 ENPs, respectively, at two different copolymer concentrations (5 and 30 wt%). The results presented in Fig. 6.3 indicate all the dielectric elastomers examined here possess quantitatively similar moduli under both compressive and tensile loading.

This trend has been reported[26] for other elastomers and is evident in Fig. 6.4, wherein E_T computed on the bases of both engineering and true stress is provided as a function of E_C. Values of E_T derived from the true stress are collectively in more favorable agreement with E_C than those computed from the engineering stress. All the compressive moduli included in Fig. 6.4 have been measured using the indirect-contact test protocol (with silicone oil) described in the Experimental section. Pelrine et al.[4] have, however, reported that the modulus for the VHB 4910 acrylic elastomer is significantly larger in magnitude (*ca*. 1-3 MPa) than either the compressive or tensile modulus measured in the present work. Since the type of modulus is not explicitly specified, we presume that it represents E_C, which is more prone to variation. If a direct-contact compression test (no silicone oil), which includes the effects of shear forces, is conducted, E_C is measured as 2.3 Mpa, which agrees well with the prior results listed above. In this case, the corresponding E_C values for the ENPs with 30 wt% SEBS217 and SEBS161 are 1.1 and 1.3 Mpa, respectively. A comparison of the compressive moduli measured for the acrylic and nanostructured D-EAPs under both sets of test conditions is displayed for completeness in Fig. 6.5 and establishes that the indirect-contact procedure, which yields results that are comparable to values of E_T and confirms that these

D-EAPs do not exhibit anisotropic mechanical properties, consistently yields a reduced E_C. This observation, in agreement with intuitive expectation, helps to explain variations in modulus documented for some D-EAPs.

Dielectric elastomer films are routinely and largely prestretched uniaxially or biaxially to improve their actuation performance.[4,27] Prestraining tends to reduce the dielectric constant while simultaneously enhancing the dielectric breakdown strength. An increase in the dielectric breakdown strength dominates the accompanying reduction in dielectric constant so that the actuation (Maxwell) stress generally increases with increasing prestrain.[28] If the prestrain is anisotropic, the local modulus increases in the higher prestrain direction, in which case the D-EAP film actuates to a greater extent in the lower prestrain (i.e., softer material) direction. Choi et al.[29] have observed that the elastic modulus of VHB 4910 does not change upon prestrain, which is contrary to other reports[30] that prestrain stiffens specimen films. In this section, we explore the effect of prestrain on the mechanical properties of the VHB 4910 acrylic adhesive and the ENPs that are capable of large actuation displacement (> 100%). Although polymeric materials subjected to biaxial strain have been thoroughly investigated[31-33] in independent experimental efforts, no studies have, to the best of our knowledge, elucidated the response of a biaxially prestrained elastomer to a uniaxial compressive stress superimposed along the transverse (z) direction. This is, however, precisely the set of strain conditions under which D-EAPs undergo displacement when a Maxwell stress develops upon electrical stimulation (cf. Fig. 6.1).

To explore differences in material properties due to such sequential mechanical deformation, several D-EAPs have been subsequently exposed to a compressive load after being biaxially prestrained to 300% in both x and y. In Fig. 6.6, the stress-strain responses of the VHB 4910 (Fig. 6.6a), SEBS217 ENP (Fig. 6.6b) and SEBS161 ENP (Fig.6.6c) elastomers reveal that mechanical prestrain consistently and dramatically reduces the compressive stress at a given strain level. It immediately follows that E_C correspondingly drops with biaxial prestrain. Values of E_C measured for the VHB 4910 acrylic and ENP elastomers by both the direct- and indirect-contact protocols discussed earlier are included for comparison in Fig. 6.5.

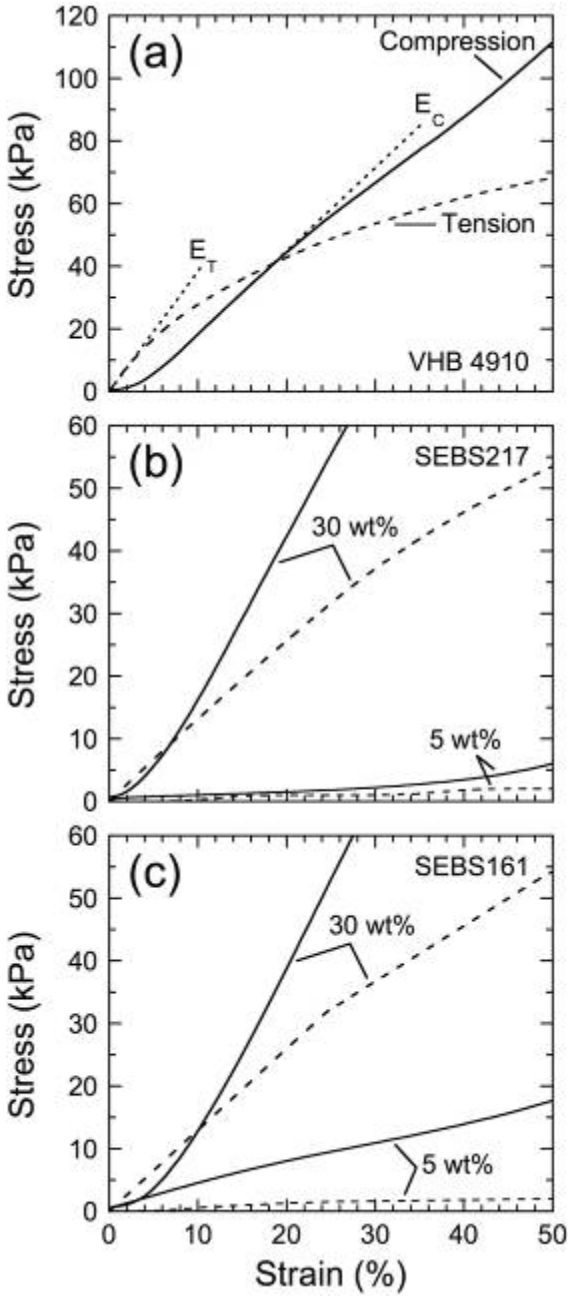

Figure 6.3 Stress-strain curves generated during uniaxial compression and tension loading, identified by the solid and dashed lines, respectively, at ambient temperature. The dotted lines in (a) identify the regions of the curves from which the compressive (E_C) and tensile (E_T) moduli are determined. Data acquired from the VHB 4910 acrylic elastomer are shown in (a), whereas the compositions of ENPs composed of the SEBS217 and SEBS161 copolymers are labeled in (b) and (c), respectively.

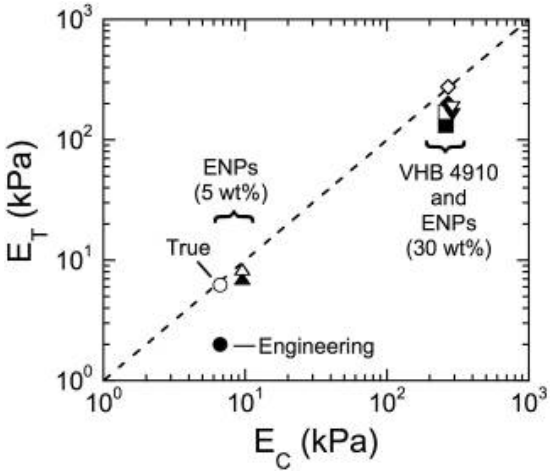

Figure 6.4 Engineering (filled symbols) and true (open symbols) tensile moduli (E_T) presented as a function of the compressive modulus (E_C) for several D-EAPs (in wt% copolymer where appropriate): SEBS217 ENP (5, circles; 30, squares), SEBS161 ENP (5, triangles; 30, inverted triangles) and VHB 4910 (diamonds). The dashed line identifies where $E_T = E_C$, and the E_C values were measured by the indirect-contact method described in the text.

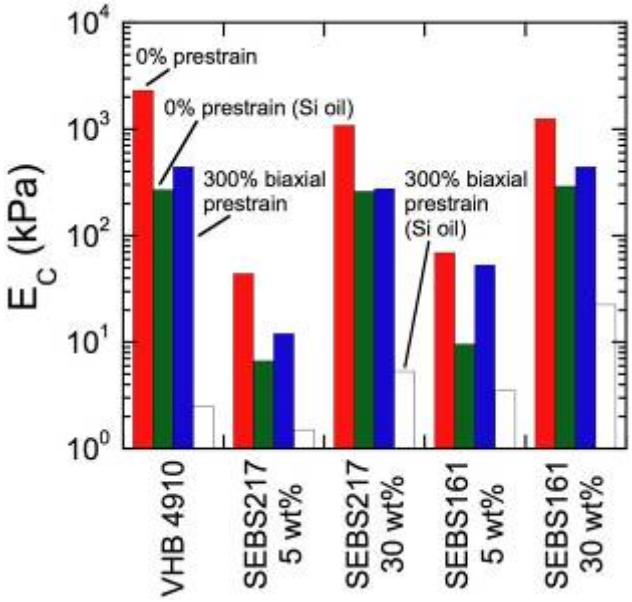

Figure 6.5 Values of E_C measured according to different testing protocols and specimen prestrain conditions: no prestrain, direct contact (red), no prestrain, indirect contact (green), 300% biaxial prestrain, direct contact (blue) and 300% biaxial prestrain, indirect contact (white).

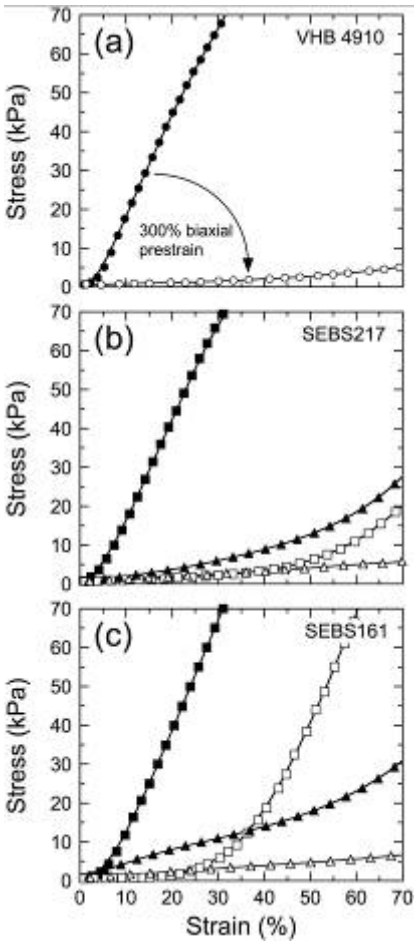

Figure 6.6 Stress-strain curves generated during uniaxial compression loading of D-EAPs before (filled symbols) and after (open symbols) 300% biaxial prestrain. The VHB 4910 acrylic elastomer is shown as circles, whereas the ENPs containing 5 and 30 wt% SEBS217 (b) and SEBS161 (c) are denoted by triangles and squares, respectively. The solid lines serve to connect the data.

In the case of direct-contact compression testing, E_C decreases by less than one decade due to biaxial prestrain. Results obtained by indirect-contact compression testing, however, show a more marked reduction, exceeding 2 orders of magnitude in some cases. For comparison, values of E_C measured by the indirect-contact method from a polyurethane before and after 300% biaxial prestrain are 9.5 and 2.3 kPa, respectively, which indicates that a prestrain-induced reduction in E_C is not restricted to the elastomers examined in this study. These findings establish that the mechanical behavior of biaxially prestrained EAPs can

differ significantly from that of the unstrained precursor along the transverse direction (the ENPs with 5 wt% copolymer do not show such prestrain sensitivity).

The in-plane electrostatic stress generated upon application of an electrical field across a D-EAP actuator is commonly referred to as the blocking stress (σ_B), since it defines the force required to return a fully energized actuator to zero displacement. This important performance metric can be measured under isometric (constant strain) conditions according to Kofod et al.,[24,25] who provided a detailed experimental procedure for assessing σ_B in the case of the VHB 4910 acrylic elastomer. In the context of their experiment, a specimen is prestrained in the x direction and then mounted on a test fixture to induce strain along the y direction prior to actuation. At the free ends of the fixture, however, the elastomeric specimen contracts in the x direction. This contraction is further exacerbated when the film is stretched upon actuation in the y direction and the effective strain in the x direction is further reduced. Use of the test fixture and protocol detailed in the Experimental section and illustrated in Fig. 6.2 alleviates this shortcoming. At every sequential step during film deformation, the lateral strains along x and y are controlled. The maximum and incremental prestrain values (ε_{max} and $\Delta\varepsilon$, respectively) identified in Fig. 6.2a are 275% and 25%, respectively. Once a film is (an)isotropically prestrained to predetermined extents in the x and y directions, the film is fully immobilized. Polycarbonate plates fitted on the top and bottom of the film and attached by screws (Fig. 6.2b) permit retention of the initial prestrain as further prestrain along y is applied (Fig. 6.2c) prior to coating with compliant electrodes (Fig. 6.2d) and eventual exposure to an external electric field (Fig. 6.2e).

Repeated attempts to replicate the blocking stress of 1.2 Mpa reported by Kofod et al.[24,25] for the VHB 4910 acrylic biaxially prestrained to 500% in x and 300% in y have been unsuccessful due to failure of the elastomer at strain levels beyond 400% in x and 300% in y. Comparable biaxial prestrain levels are, however, routinely achieved with the ENPs, which can be stretched to over 2000% strain without failure under uniaxial tensile loading.

For comparative purposes, the biaxial prestrain imposed upon the VHB 4910 acrylic elastomer in this study is the maximum attained (i.e., 400% in x and 300% in y), whereas the ENPs are prestrained to 500% in x and 350% in y. The variation in tensile force along y with increasing time upon final prestrain is presented in Fig. 6.7 for the VHB 4910 acrylic (Fig. 6.7a) and the ENP composed of 30 wt% SEBS217 (Fig. 6.7b). The response of each material

to isometric conditions reveals an important difference: the acrylic initially undergoes substantial stress relaxation. Fitting the initial reduction in measured tensile force (or, equivalently, stress) to the Zener model with two relaxation time (τ) constants (a single relaxation element is insufficient to represent the data) yields a short τ of 34.7 ± 2.3 s and a long τ of 4600 ± 290 s, indicating that multiple molecular relaxation processes in the material occur, and the stress state of the acrylic elastomer continually changes, over the time scale of the blocking force experiment. In marked contrast, the ENP possesses a single, long τ of over 15000 s, confirming that this D-EAP is mechanically stable and reliable.

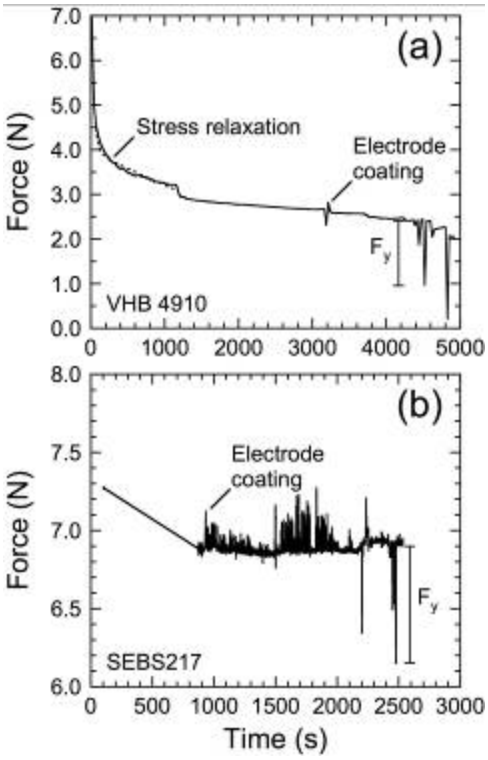

Figure 6.7 Force-time curves of (a) the VHB 4910 acrylic elastomer and (b) the ENP composed of 30 wt% SEBS217 upon final prestrain before and after electrical actuation. Regressions of the Zener stress-relaxation model to the data are shown by the dotted lines. Noise in the data reflects hand application of the compliant electrode on each side of the D-EAP film. Sharp downward spikes correspond to the blocking force (F_y, identified in each part) during actuation under an external electric field.

The blocking force exerted along the y direction upon electrical actuation (F_y) is observed as a sharp downward spike (labeled in Fig. 6.7), since the tensile force is sharply reduced

when the film actuates and consequently compresses along the transverse direction, while expanding laterally along both x and y. Several spikes are evident in Fig. 6.7 due to the occurrence of several different actuation tests within the time frame examined. The noise in the data (especially pronounced in the case of the ENP) corresponds to changes in tensile force upon hand application of the compliant electrode. Values of σ_B, deduced from F_y and the cross-sectional film area after the final prestrain step and before actuation, are listed in Table 6.1. These results confirm that the σ_B values discerned for the VHB 4910 acrylic elastomer and the two ENPs with 30 wt% copolymer are comparable in magnitude. Additional prestrain is anticipated to decrease the film thickness further and, thus, increase σ_B, which is consistent with the higher value of σ_B reported[24,25] for the acrylic elastomer. Included in Table 6.1 is the dielectric breakdown strength, which is lower for the VHB 4910 D-EAP than that documented elsewhere.[22,25] This difference may likewise reflect differences in prestrain level,[24,25] since the breakdown strength tends to increase with increasing prestrain. [4,27] Table 6.1 also confirms that the values of dielectric breakdown strength for the ENPs with 30 wt% copolymer are similar to that of the acrylic elastomer.

Table 6.1D-EAP Blocking Stresses Measured in this Study.

D-EAP	Polymer fraction (wt%)	Lateral prestrain (x%, y%)	Breakdown electric field (V/μm)	Blocking stress (kPa)
VHB 4910 acrylic elastomer	100	400,300 500,300	134 190	556 1200[a]
ENP elastomers				
SEBS161	30	500,350	203	442
SEBS217	30	500,350	195	357

[a] Reported in refs. 24 and 25.

6.5 Conclusions

The performance evaluation of D-EAPs depends on the intrinsic properties of the material(s) under investigation, as well as on the conditions and protocols of the tests employed. In this study, we have investigated the mechanical properties of the benchmark D-EAP, namely, the VHB 4910 acrylic elastomer,[4] and novel ENPs composed of swollen triblock copolymers[13,15] before and after mechanical prestrain. Careful measurement of the response of these elastomers to uniaxial compressive loading under indirect-contact conditions yields compressive moduli that are comparable in magnitude to the corresponding tensile moduli. Biaxial prestrain followed by compression testing, designed to emulate electrical actuation conditions between compliant electrodes, reveals that the compressive moduli of prestrained specimens are considerably lower than those of their unstrained precursors. Measured blocking stresses upon actuation are exquisitely sensitive to the level of existing prestrain and, thus, to the method by which prestrain is induced. In this work, we have proposed a modification to an existing procedure[24,25] for measuring the blocking stresses of D-EAPs. This modification alleviates complications associated with uncontrolled lateral prestrain and provides a means by which to discern the mechanical stability of D-EAP films under prolonged (an)isotropic biaxial strain. Blocking stresses measured for the ENPs with 30 wt% copolymer are comparable to those discerned for the acrylic elastomer, suggesting that the ENP platform may serve as an equally responsive, but more robust and tunable, alternative to conventional D-EAPs.[12,34]

6.6 Acknowledgments

This work was supported by the U. S. Department of Commerce through the National Textiles Center.

6.7 Notes

This chapter was submitted in *Sensors and Actuators A,* published under the authorship of Ravi Shankar,[§†] Tushar K. Ghosh[%] and Richard J. Spontak[†‡] ([§]Fiber and Polymer Science Program and Departments of [†]Materials Science & Engineering, [%]Textile & Apparel Technology & Management and [‡]Chemical & Biomolecular Engineering, North Carolina State University, Raleigh, NC 27695, USA).

6.8 References

1. W. B. Jr. Spillman, J. S. Sirkis and P. T. Gardiner, Smart materials and structures: what are they?, *Smart Mater. Struct.*, 5 (1996) 247.
2. Z. L. Wang and Z. C. Kang, *Functional and Smart Materials: Structural Evolution and Structure Analysis,* Plenum, New York, 1998, p. 523.
3. J. L. Pons, *Emerging Actuator Technologies A Micromechatronic Approach*, Wiley, Hoboken, NJ, 2005, p. 731.
4. R. Pelrine, R. Kornbluh, Q. Pei and J. Joseph, High-speed electrically actuated elastomers with strain greater than 100%, *Science*, 287 (2000) 836.
5. J. D. W. Madden, N. A. Vandesteeg, P. A. Anquetil, P. G. A. Madden, A. Takshi, R. Z. Pytel, S. R. Lafontaine, P. A. Wieringa and I. W. Hunter, Artificial muscle technology: physical principles and naval prospects, *IEEE J. Ocean. Eng.*, 29 (2004) 706.
6. M. Zupan, M. F. Ashby and N. A. Fleck, Actuator classification and selection: The development of a database, *Adv. Eng. Mater.*, 4 (2002) 933.
7. Q. M. Zhang, H. Li, M. Poh, F. Xia, Z.-Y. Cheng, H. Xu and C. Huang, An all-organic composite actuator material with a high dielectric constant, *Nature,* 419 (2002) 284.
8. S. Ashley, Artificial muscles, *Sci. Am.*, October (2003) 53.
9. Y. Bar-Cohen (ed.), *Electroactive Polymer (EAP) Actuators as Artificial Muscles: Reality, Potential, and Challenges*, SPIE Press, Bellingham, WA, 2004.
10. R. H. Baughman, Playing nature's game with artificial muscles, *Science*, 308 (2005) 63.
11. Y. Bar-Cohen, Current and future development in artificial muscles using electroactive polymers, *Expert Rev. Med. Dev.*, 6 (2005) 731.

12. R. Shankar, T. K. Ghosh and R. J. Spontak, Dielectric elastomers as next-generation polymeric actuators, *Soft. Mater.* (in press).
13. R. Shankar, T. K. Ghosh and R. J. Spontak, Electroactive nanostructured polymers as tunable actuators, *Adv. Mater.* (in press).
14. R. Kornbluh, R. Pelrine, J. Joseph, R. Heydt, Q. Pei and S. Chiba, High-field electrostriction of elastomeric polymer dielectrics for actuation, *Proc. SPIE*, 3669 (1999) 149.
15. R. Shankar, T. K. Ghosh and R. J. Spontak, Electromechanical response of nanostructured polymer systems with no mechanical pre-strain, *Macromol. Rapid. Commun.* (in press).
16. I. W. Hamley, *The Physics of Block Copolymers*, Oxford University Press, New York, 1998.
17. M. Lazzari, G. Liu and S. Lecommandoux (eds.), *Block Copolymers in Nanoscience*, Wiley-VCH, Weinheim, 2007.
18. P. Alexandridis and R. J. Spontak, Solvent-regulated ordering in block copolymers, *Curr. Opin. Coll. Interface Sci.*, 4 (1999) 130.
19. S. Jain and F. S. Bates, On the origins of morphological complexity in block copolymer surfactants, *Science*, 300 (2003) 460.
20. R. J. Spontak and N. P. Patel, Phase behavior of block copolymer blends, in I. W. Hamley (ed.), *Developments in Block Copolymer Science and Technology*, Wiley, New York, 2004, pp. 159-212.
21. R. J. Spontak, R. Shankar, M. K. Bowman, A. S. Krishnan, M. W. Hamersky, J. Samseth, M. R. Bockstaller and K. Ø. Rasmussen, Selectivity- and size-induced segregation of

molecular and nanoscale species in microphase-ordered triblock copolymers, *Nano Lett.*, 6 (2006) 2115.

22. R. Pelrine, R. Kornbluh and G. Kofod, High-strain actuator materials based on dielectric elastomers, *Adv. Mater.*, *12* (2000) 1223.
23. J. H. Laurer, J. F. Mulling, S. A. Khan, R. J. Spontak and R. Bukovnik, Thermoplastic elastomer gels. I. effects of composition and processing on morphology and gel behavior, *J. Polym. Sci. B: Polym. Phys.*, 36 (1998) 2379.
24. G. Kofod, R. Kornbluh, R. Pelrine and P. Sommer-Larsen, Actuation response of polyacrylate dielectric elastomers, *Proc. SPIE*, 4329 (2001) 141.
25. G. Kofod, P. Sommer-Larsen, R. Kornbluh and R. Pelrine, Actuation response of polyacrylate dielectric elastomers, *J. Intell. Mater. Syst. Struct.*, 14 (2003) 787.
26. J. LeBras, in I. E. Berck, (ed.), *Rubber: Fundamentals of its Science and Technology*, Chemical Publishing Co. Inc., New York, 1957, pp. 464-100.
27. R. Palakodeti and M. R. Kessler, Influence of frequency and prestrain on the mechanical efficiency of dielectric electroactive polymer actuators, *Mater. Lett.*, 60 (2006**)** 3437.
28. A. O'Halloran and F. O'Malley, in P. J. Prendergast and P. E. McHugh (eds.), *Topics in Bio-Mechanical Engineering*, Trinity Centre for Bioengineering & the National Centre for Biomedical Engineering Science, Dublin & Galway, 2004, pp. 184-215.
29. H. R. Choi, K. Jung, N. H. Chuc, M. Jung, I. Koo, J. Koo, J. Lee, J. Lee, J. Nam and M. Cho, Effects of prestrain on behavior of dielectric elastomer actuator, *Proc. SPIE*, 5759 (2005) 283.
30. X. Zhang, C. Löwe, M. Wissler, B. Jähne and G. Kovacs, Dielectric elastomers in actuator technology, *Adv. Eng. Mater.*, **7** (2005) 361.

31. R. Kleppinger, M. van Es, N. Mischenko, M. H. J. Koch and H. Reynaers, Physical gelation in a triblock copolymer solution: in situ study of stress-strain behavior and structural development, *Macromolecules*, 31 (1998) 5805.
32. S. Ramaswamy and A. J. Lesser, Microscopic damage and macroscopic yield in acrylonitrile–butadiene–styrene (ABS) resins tested under multi-axial stress states, *Polymer*, 43 (2002) 3743.
33. S. Ramaswamy and A. J. Lesser, Generic crack patterns in rubber-modified polymers under biaxial stress states, *J. Polym. Sci. B: Polym. Phys.*, 41 (2003) 2248.
34. T. Mirfakhrai, J. D. W. Madden and R. H. Baughman, Polymer artificial muscles, *Mater. Today*, 10 (2007) 30.

CHAPTER 7

7 Triblock Copolymer Organogels as High-Performance Dielectric Elastomers

7.1 Abstract

Block copolymers and nanostructured materials derived therefrom are becoming increasingly ubiquitous in a wide variety of (nano)technologies. Recently, we have demonstrated that triblock copolymer organogels composed of physically cross-linked copolymer networks swollen with a midblock-selective solvent exhibit excellent electromechanical behavior as dielectric elastomers. In-plane actuation of such organogels, collectively referred to as electroactive nanostructured polymers (ENPs) to reflect the existence of a self-organized copolymer morphology, is attributed to the development of an electric field-induced surface-normal Maxwell stress. In this study, we examine the composition and molecular weight dependence of the electromechanical properties afforded by organogels prepared from poly[styrene-*b*-(ethylene-*co*-butylene)-*b*-styrene] (SEBS) triblock copolymers selectively swollen with EB-compatible aliphatic oligomers. These materials undergo ultrahigh actuation displacement at significantly reduced electric fields relative to previously reported dielectric elastomers, and possess electromechanical coupling efficiencies, which relate the conversion from electrical input to mechanical output, greater than 90%. The design of ENPs with broadly tunable electromechanical properties represents an attractive route to responsive materials for advanced engineering, biomimetic and biomedical applications.

7.2 Introduction

Triblock copolymers consisting of chemically distinct homopolymers that are covalently linked in an ABA sequence are capable of spontaneous self-organization into a variety of classical nanoscale morphologies such as lamellae, cylinders on a hexagonal lattice and spheres on a body-centered-cubic lattice,[1-3] as well as spatially complex morphologies such as the gyroid[4] and sponge,[5] alone or in the presence of a solvent, homopolymer or another copolymer. Generally speaking, nanostructured block copolymers provide a remarkably broad platform for the development of multifunctional materials targeted for various

(nano)technologies[6,7] including, for instance, nanotemplates,[8] membranes,[9] nanoporous media[10] and biomaterials.[11] Most notably, ABA triblock copolymers have been used extensively as thermoplastic elastomers[2,12] (TPEs) due to their shape-memory attributes. Addition of an organic solvent to a microphase-separated AB diblock[13] or ABA triblock[14] copolymer provides a straightforward route by which to controllably modify copolymer morphologies and accompanying properties. Unlike their AB diblock counterparts, however, ABA molecules are capable of forming bridges between neighboring microdomains and thus generating physically cross-linked molecular networks, as schematically depicted in Fig. 7.1a, in the presence of a B-selective solvent.[15-22] At relatively high concentrations of a B-selective solvent, the incompatible A blocks of the ABA molecules aggregate to form micelles (*cf*. Fig. 7.1b), which serve to stabilize the copolymer network and thereby generate an organogel.

Organogels derived from commercial TPEs are ideally suited for diverse applications ranging from personal care and other consumer products to vibration-dampening media and adhesives. Recently, we have reported[23-25] that such organogels likewise exhibit excellent electromechanical behavior as dielectric elastomers. Dielectric elastomers comprise one class of electroactive polymers (EAPs), macromolecules that respond to external electrical stimulation by displaying a significant change in shape or size and thus converting electrical energy into mechanical force and movement.[39] Because of their light weight, mechanical resilience, low cost and facile processability, EAPs constitute excellent candidates for use in micro air vehicles, microrobotics, microfluidic/haptic devices, active displays and responsive prosthetics.[40] Actuators derived from EAPs possess higher energy density, response speed and electromechanical coupling efficiency than inorganic actuators such as piezoelectric ceramics.[41] Common EAPs include conductive,[41,42] electrostrictive[43] and ferroelectric[44,45] polymers, in addition to dielectric elastomers. Of all the EAPs investigated thus far, though, dielectric elastomers exhibit the largest actuation displacement, but typically require high electric fields (*ca*. 50-250 V/μm) to achieve full actuation. These elastomers are traditionally produced from chemically cross-linked homopolymers, and the two most promising EAPs in this genre derive specifically from acrylic and silicone elastomers, with the former serving as the benchmark due to its exceptional electromechanical properties.[39,46]

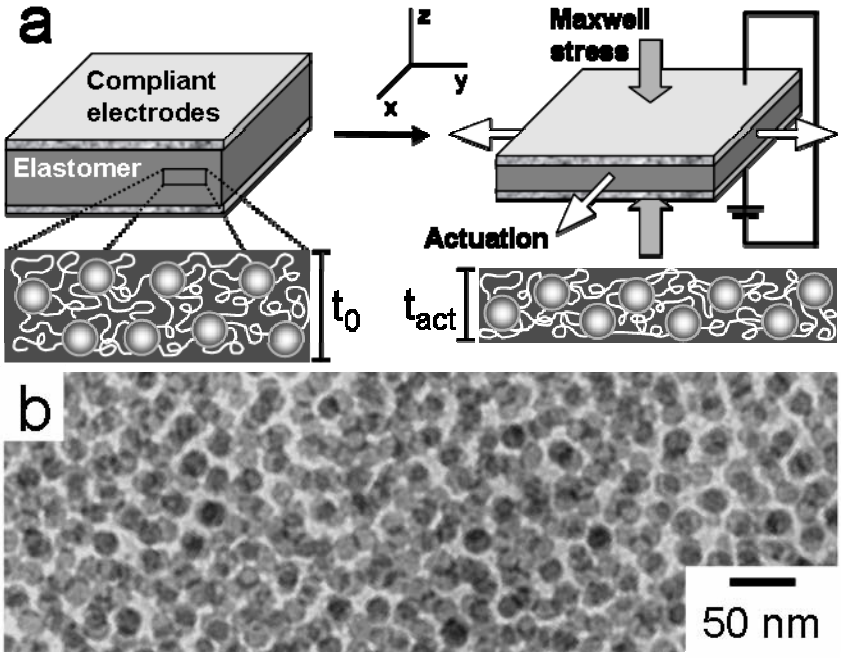

Figure 7.1 In (a), a schematic diagram of the mechanism by which a dielectric elastomer actuates upon electrical stimulation. The electric field-induced Maxwell stress and resulting in-plane actuation (along x and y) are labeled. Included are pre- and post-actuation illustrations of the micellar morphology present in selectively swollen triblock copolymer organogels introduced as electroactive nanostructured polymers (ENPs). In (b), a TEM image of the micellar morphology generated in a 10/90 w/w SEBS/MO blend. The styrenic units comprising the micellar core are stained with the vapor of RuO_4(aq) and appear dark.

Although experimental and theoretical studies have endeavored to elucidate the response of microphase-separated block copolymers to an applied electric field, these efforts have focused exclusively on (re)alignment of the copolymer nanostructure in both thin[26] and bulk[27] films with and without solvent. In our previous study,[23] we have demonstrated that organogels composed of nonpolar poly[styrene-*b*-(ethylene-*co*-butylene)-*b*-styrene] (SEBS) triblock copolymers (each with glassy S endblocks and a rubbery EB midblock) swollen with an EB-selective (aliphatic) solvent exhibit ultrahigh actuation displacement as dielectric elastomers, exceeding the performance benchmarks established by the acrylic elastomer. To distinguish the difference between chemically cross-linked homopolymer-based dielectric elastomers and physically cross-linked copolymer-based elastomers, we refer to the latter as electroactive nanostructured polymers (ENPs) in light of the existing copolymer morphology. The functional effectiveness of ENPs is primarily attributed to their intrinsically low

modulus. Moreover, organic functionalities possessing delocalized π-electrons (e.g., the phenyl rings located on the S repeat units of the SEBS copolymer) are known[28] to exhibit nonlinear optical properties and, unlike the EB units and solvent, are polarizable in the presence of a high electric field. The objective of the present study is to interrogate, in systematic fashion, ENPs varying in copolymer molecular weight and concentration to assess the extent to which their electromechanical properties are physically tunable.

7.3 Theoretical Background

The actuation response of a dielectric elastomer film is attributed to the development of a Maxwell stress (σ_M) acting normal to the film surface upon electrical stimulation.[39] This predominantly uniaxial compressive stress, or pressure, arises in response to the electrostatic force of attraction between compliant electrodes applied to the opposing surfaces of the film, and promotes in-plane (lateral) expansion of the film. According to Pelrine *et al.*,[39] the effective electrostatic pressure (P) acting along the transverse (z) direction defined in Fig. 7.1 is given by

$$P = \frac{1}{A_{xy}} \frac{dU}{dz} \tag{1}$$

where U denotes the electrostatic potential, and A_{xy} is the lateral surface area undergoing compression. For perfectly elastic materials, dU/dz is equal to the mechanical work that can be performed by an actuator. When a potential is applied across the elastomer film, the dielectric elastomer construct depicted in Fig. 7.1a is analogous to a parallel-plate capacitor for which

$$U = \frac{Q^2}{2C} \tag{2}$$

where Q represents the charge on the plate and the capacitance (C) is given by $\in_0 \in A_{xy}/z$. Here, $\in_0$ is the permittivity of free space, and $\in$ corresponds to the dielectric constant of the elastomer. The change in potential (dU) accompanying concurrent changes in film thickness (dz) and area (dA_{xy}) due to actuation can be determined directly from Eq. 2, in which case

$$dU = \frac{Q^2}{2 \in \in_0} \left(\frac{dz}{A_{xy}} - \frac{z dA_{xy}}{A_{xy}^2} \right) \tag{3}$$

If the deformation due to actuation is isochoric, $dV = zdA_{xy} + A_{xy}dz = 0$ and Eq. 3 simplifies to

$$dU = \frac{Q^2}{\in \in_0} \frac{dz}{A_{xy}} \tag{4}$$

Substitution of Eq. 4 into Eq. 1 yields

$$P = \frac{Q^2}{\in \in_0 A_{xy}^2} \tag{5}$$

Since the electric field (E) is given by $Q/\in_0 \in A_{xy}$, the electrostatic pressure, or equivalently σ_M, can be conveniently written as

$$P = \in_0 \in E^2 \tag{6}$$

Equation 6 establishes that the field-induced electrostatic stress introduced during actuation is proportional to E^2 and $\in$ of the elastomer, the latter of which distinguishes these actuators from other electrostatic materials because the magnitude of $\in$ for a polymer can be readily altered (by chemical or physical means) to increase σ_M without increasing the operating voltage. Alternatively, σ_M can be similarly increased by decreasing the thickness of the film (through, for instance, mechanical pre-strain) and thus increasing E, which can be equivalently expressed as U/t_0 where t_0 represents the film thickness prior to actuation (*cf.* Fig. 7.1a). Since σ_M acts normal to the film surface, it serves to compress the film along its thickness (z) and stretch the film laterally (along x and y in Fig. 7.1). Repulsive like charges accumulate along both film surfaces and further increase the extent to which the film stretches laterally.[25,39] The resulting transverse strain (s_z) is defined as $(t_{act} - t_0)/t_0$, where t_{act} denotes the dielectric elastomer film thickness after actuation. At sufficiently small strains (< 20%), the deformation due to actuation can be presumed to be linearly elastic, and Hooke's law in compression ($\sigma_M = -Ys_z$) can be used to directly relate s_z to the applied electric field, *viz.*,

$$s_z = - \in \in_0 \frac{E^2}{Y} \tag{7}$$

At large strains routinely encountered with dielectric elastomers, however, Y becomes a function of strain so that Eq. 7 is no longer valid. In the limit of large in-plane (lateral) strains, s_z can be discerned from constitutive relations.[39] Under isochoric conditions, the in-

plane and transverse strains are related by $(1 + s_x)(1 + s_y)(1 + s_z) = 1$. If the actuation-induced deformation is laterally isotropic, then $s_x = s_y = s_{xy}$ and

$$s_z = (1 + s_{xy})^{-2} - 1 \quad (8)$$

Actuation of dielectric elastomers is frequently measured using a circular test geometry,[39] which yields the in-plane actuation strain (s_{act}) expressed in terms of the electric field-induced change in electrode area, $(A_{act} - A_0)/A_0$. Again assuming isotropic in-plane actuation, this commonly reported strain is related to s_{xy} by $s_{act} = (1 + s_{xy})^2 - 1$, which consequently requires that

$$s_z = (1 + s_{act})^{-1} - 1 \quad (9)$$

Although s_z has been measured[47,48] by Doppler interferometry, it is typically computed from s_{act}.

7.4 Experimental

7.4.1 Materials

Three SEBS triblock copolymers with comparable compositions (30-33 wt% S) and different molecular weights (75, 161 and 217 kDa) were used to produce the ENPs investigated in this study. These copolymers were obtained from the GLS Corporation (McHenry, IL), and the corresponding ENPs are hereafter designated as ENP*M*, where *M* (75, 161 and 217) denotes the copolymer molecular weight in kDa. Two EB-selective oligomeric solvents, one an aliphatic/ alicyclic white mineral oil (MO, Witco Hydrobrite 380, Crompton Corporation, Petrolia, PA) with a molecular weight of 503 Da and the other an α-olefin (αO, Durasyn D166, Amoco Corp., Chicago, IL) with a molecular weight of 529 Da, were both used as-received. A double-sided acrylic adhesive commercialized as VHB-4910 was obtained by 3M Company (St. Paul, MN).

7.4.2 Methods

Each organogel was prepared by mixing the copolymer with an EB-selective solvent at a predetermined block copolymer concentration (w_{BC}, in wt%), along with 1 wt% antioxidant, for 30 min in a Ross LDM double-planetary mixer under vacuum at 180 °C. The ENP75 systems were produced over the w_{BC} interval from 25 to 50 wt% in 5 wt% increments,

whereas w_{BC} in the ENP161 and ENP217 systems ranged from 5 to 30 wt% also in 5 wt% increments. The difference in concentration ranges was due to the melt viscosity of the organogel and the operational limitation of the mixer. A portion of each organogel was compression-molded at 180 °C and then slowly cooled to ambient temperature, yielding films measuring 0.5-2.5 mm thick.

7.4.2.1 Mechanical Property Characterization

Since the actuation response of elastomers is strongly influenced by their mechanical properties, each of the ENPs prepared during the course of this study, as well as the acrylic dielectric elastomer, was subjected to uniaxial compression and tension testing performed at ambient temperature with an MTS-30G unit operated at crosshead speeds of 5 and 127 mm/min, respectively. Free compression tests were conducted under indirect-contact conditions wherein silicone oil (which is immiscible with the copolymers and solvents employed in ENP preparation) was applied to the top and bottom platen prior to measurement. This procedure, which alleviates the development of shear forces during compression, was previously found[29] to yield compressive moduli (Y_C) that were much closer in magnitude to the corresponding tensile moduli (Y_T) than Y_C values measured by direct specimen contact. Another consideration examined here was mechanical hysteresis, which constitutes an important issue in the general design of EAPs intended for cyclic applications (e.g., flapping). The ENPs and acrylic elastomer were cycled up to 400% tensile strain for 100 cycles at a fixed extension rate of 500 mm/min. After 100 cycles, the non-recoverable strain due to permanent material deformation was determined.

7.4.2.2 Electromechanical Property Characterization

The dielectric constants of the ENPs and acrylic elastomer were measured on an Agilent dielectric test fixture 16451B with HP4284A LCR meter operated over a frequency range of 20 Hz to 1 MHz at 25 °C. The actuation response of the dielectric elastomers to an external electric field was investigated under no-pre-strain and 300% biaxial pre-strain conditions in the conventional circular test configuration. Pre-strain was necessary to decrease film thickness and thus increase the magnitude of the electric field at manageable electric

potentials. Compliant electrodes (Ag silicone grease from Chemtronics Circuit Works, Kennesaw, GA) were applied in a circular pattern (the active area) to the top and bottom surfaces of each film. To avoid boundary effects, this active region was kept small relative to the inactive region of the film. The quality of selected electrode/ENP/electrode constructs (illustrated in Fig. 7.1a) was evaluated by fracturing the constructs in liquid nitrogen. Cross-sectional backscattered electron (BSE) images were acquired by variable-pressure scanning electron microscopy performed with a Hitachi S-3200N microscope operated under a He atmosphere (100 Pa) at 20 kV. Upon application of a voltage across the electrodes, the active circular region expanded due to transverse film compression. Electric field-induced actuation was evaluated using a manual voltage trigger, followed by frame-by-frame analysis of captured real-time video images. Image analysis software (Matrox Inspector 4.1) was used to measure the in-plane (lateral) actuation strain (s_{act}) and discern the transverse actuation strain (s_z) under the assumption of isochoric displacement. To discern the extent of hysteresis due to actuation cycling, the voltage across a specimen was ramped from zero to an applied voltage in 10 s, and no noticeable lag was observed between voltage ramping and full specimen actuation. Afterward, the specimen was held at voltage for 10 s before the voltage was returned to zero for 10 s to permit discharge. This process was repeated for 100 cycles, and image analysis was used to compare the size of the active area in the initial image frame with that after 100 cycles.

7.5 Results and Discussion

While the ability of an elastomer to show evidence of actuation depends on the dielectric constant of the elastomer and the magnitude of the external electric field by Eq. 6, the extent to which the elastomer is able to respond to electrical stimulation is sensitive to the inherent mechanical properties of the elastomer. Previous studies[14-22] of triblock copolymer organogels containing either MO or squalene have relied almost exclusively on dynamic rheology conducted in the linear viscoelastic limit (at low strain amplitudes) to extract dynamic shear moduli as functions of chemistry, copolymer concentration and molecular weight for comparative purposes. Limited extensional rheometry has been reported[22,30,31] for selectively swollen copolymer networks. In this work, however, high deformation levels resulting from electrical actuation are anticipated, in which case we first turn our attention to

tension and compression testing of ENPs varying in copolymer concentration and molecular weight.

7.5.1 Nonlinear Mechanical Behavior

Representative stress-strain curves measured for triblock copolymer organogels varying in molecular weight and concentration, as well as the acrylic elastomer, under uniaxial tension are presented in Fig. 7.2a. At the highest copolymer concentration displayed (30 wt% SEBS in MO), the organogels and acrylic elastomer exhibit qualitatively similar characteristics: a rapid initial rise that is gradually followed by a less pronounced monotonic increase in stress with increasing strain. The extensional behavior of the acrylic elastomer shows evidence of a second change in slope in the vicinity of 350% strain, but is certainly comparable in magnitude to the ENP75 and ENP161 systems containing 30 wt% copolymer. At this concentration, which is common to all three copolymers, the mechanical behavior of the ENP75, ENP161 and ENP217 systems can be examined more closely to discern the molecular weight dependence. Since classic rubberlike (neo-Hookean) elasticity[32] fails to capture the stress-strain signatures evident in Fig. 7.2a, we elect to analyze the data in terms of the modified Mooney-Rivlin model,[33] which is given by

$$\sigma = 2\left(C_1 + \frac{C_2}{\varepsilon+1}\right)\left(\varepsilon + 1 - \frac{1}{(\varepsilon+1)^2}\right) f(\phi,\Phi) \qquad (10)$$

Here, σ is the engineering (nominal) stress, ε is the tensile strain given by $(L - L_0)/L_0$ (with L_0 and L denoting the specimen length before and after uniaxial tensile deformation, respectively), and C_1 and C_2 are material-dependent empirical constants. In the limit of rubberlike elasticity, $C_1 = G/2$, where G represents the shear modulus, and $C_2 = 0$. For a solvent-swollen thermoplastic elastomer containing a dispersed solid filler, $f(\phi,\Phi)$ is a function of both filler concentration (ϕ) and copolymer volume fraction ($\Phi \approx w_{BC}$).[34,35] In the present case, however, ϕ is fixed by the copolymer composition (S content), which is nearly constant for the three copolymers in the SEBS series employed (30-33 wt% S), and Φ is necessarily constant since w_{BC} in the ENP series under investigation is set (at 30 wt% SEBS). Thus, $f(\phi,\Phi)$ is effectively a constant denoted here by f. Fitting Eq. 10 to the stress-strain data

shown in Fig. 7.2a yields excellent agreement and the regressed values of C_1f and C_2f provided in Fig. 7.2b, which reveals that C_1 decreases slightly but monotonically with increasing copolymer molecular weight, whereas C_2 is less sensitive to changes in copolymer molecular weight. Recent efforts by Rubinstein and Panyukov[36] have yielded a more physically realistic slip-tube network model, for which σ in the present case can be alternatively expressed as

$$\sigma = \left(G_c + \frac{G_e}{g(\varepsilon)} \right) \left(\varepsilon + 1 - \frac{1}{(\varepsilon+1)^2} \right) f(\phi, \Phi) \tag{11}$$

where

$$g(\varepsilon) = 0.74(\varepsilon+1) + 0.61(\varepsilon+1)^{-1/2} - 0.35 \tag{11a}$$

Within the context of this model, G_c and G_e represent contributions to G due to the existence of both permanent cross-links (glassy micelles) and transient entanglements, respectively. Regressed values of G_cf and G_ef are included in Fig. 7.2b and confirm that G_c decreases, whereas G_e increases slightly, with increasing copolymer molecular weight at constant f. More importantly, however, the relative magnitudes of G_c and G_e indicate that entanglements, not cross-links, dominate G at 30 wt% copolymer. At lower w_{BC}, cross-links dominate and $G_c > G_e$. The results of both nonlinear elasticity models, which are included here for comparative purposes only, establish that the ENPs under investigation in this study become increasingly stiffer due to their physically cross-linked networks as the copolymer molecular weight, which translates into the molecular weight between cross-links, decreases at constant copolymer concentration. This trend is likewise apparent in Fig. 7.3, which displays the dependence of the Young's tensile modulus on both copolymer concentration and molecular weight at ambient temperature.

Conversely, as the copolymer concentration is reduced in any of the three ENP series, Y_T decreases accordingly. Note that the ENP75 series does not form stable molecular networks at w_{BC} below ~20 wt% copolymer. In all cases, however, it is important to recognize that the moduli values measured for the ENPs are consistently lower than that for the acrylic elastomer. Another important aspect of dielectric elastomers that can be gleaned from uniaxial tension testing is the mechanical hysteresis induced by cyclic deformation. Results acquired by subjecting the ENP161 and ENP217 systems with 10 and 30 wt% copolymer to 400% strain for 100 cycles are presented for illustrative purposes in Fig. 7.4 to demonstrate

that the present ENPs do not generally exhibit pronounced hysteresis (< 18% nonrecoverable strain) upon mechanical cycling at ambient temperature. The ENP161 system with 5 wt% copolymer, which is close to the critical gel concentration required for network formation, fails prematurely (after 65 cycles), whereas the comparable ENP217 system remains intact with ~1% nonrecoverable strain. Although the value of Y_T changes slightly with extension rate (from 100 to 500 mm/min), the corresponding degrees of hysteresis do not. In marked contrast, the permanent strain induced in the acrylic elastomer under identical cyclical conditions is 38%.

While the results from uniaxial tension testing provide insight into the molecular networks generated by triblock copolymer organogels under nonlinear elastic deformation conditions, compression testing is more indicative of the electromechanical response of dielectric elastomers subjected to electrical actuation. Values of Y_C, discerned from the first linear region of the stress-strain curve after the initial transient arising from non-uniform contact between the platen and specimen surface, are presented as a function of copolymer concentration and molecular weight in Fig. 7.5a and closely resemble the trends exhibited by Y_T in Fig. 7.3. A direct comparison between Y_C and Y_T is included in Fig. 7.5b and reveals that Y_C is consistently larger than Y_T by about 75% on average due to the use of engineering stress in the calculation of Y_T. If, however, Y_T is determined from the true stress, the measured values of Y_C and Y_T are in substantially closer agreement. The curves included in Fig. 7.5a signify power-law fits of the form $Y_C = Y_C^0(w_{BC}/100)^n$, where Y_C^0 is the compressive modulus of the neat copolymer in the melt and n is a scaling exponent. The overall best-fit value for n is 2.0 (shown in Fig. 7.5a), but regressed values range slightly from 1.9 to 2.3.

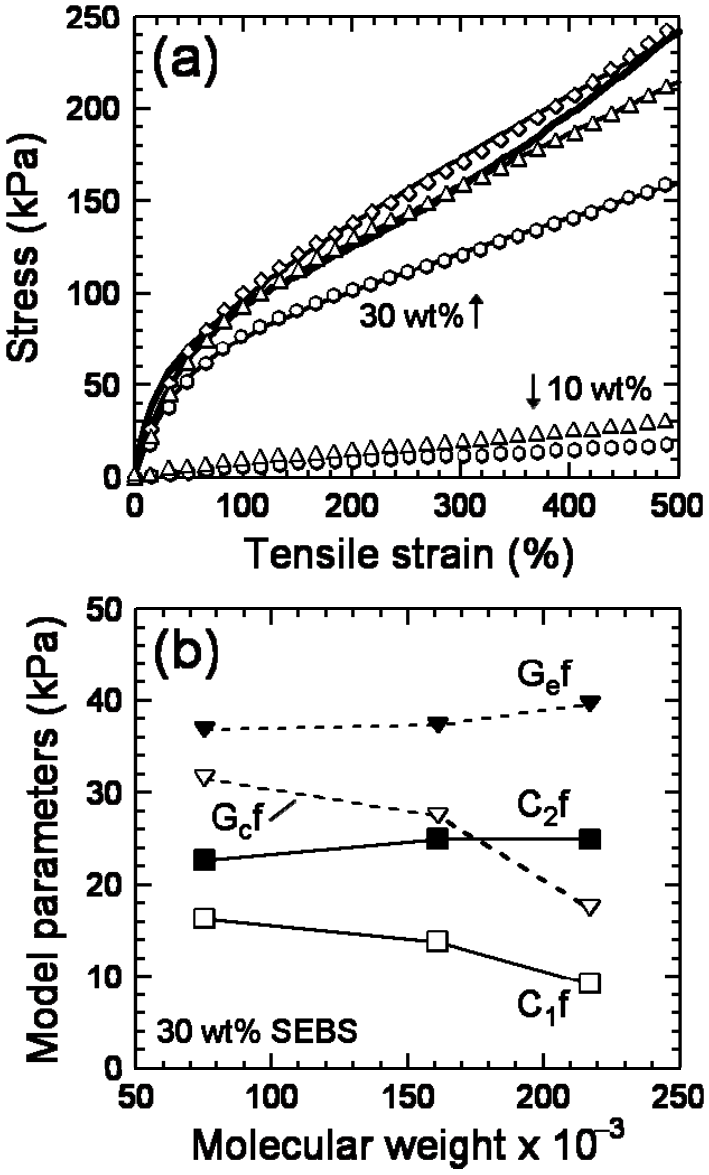

Figure 7.2 In (a), nominal (engineering) tensile stress-strain curves of three ENP systems — ENP75 (◇), ENP161 (△) and ENP217 (○) — evaluated at two copolymer concentrations: 10 and 30 wt% (labeled). In all cases, the extension rate was constant at 127 mm/min. The light solid lines correspond to regressed fits of the modified Mooney-Rivlin model (Eq. 10) to the data, whereas the heavy solid line denotes the stress-strain response of the acrylic dielectric elastomer. In (b), parameters extracted from the modified Mooney-Rivlin and slip-tube network models (labeled) as functions of copolymer molecular weight at a constant copolymer concentration of 30 wt%. The solid and dashed lines serve to connect the data.

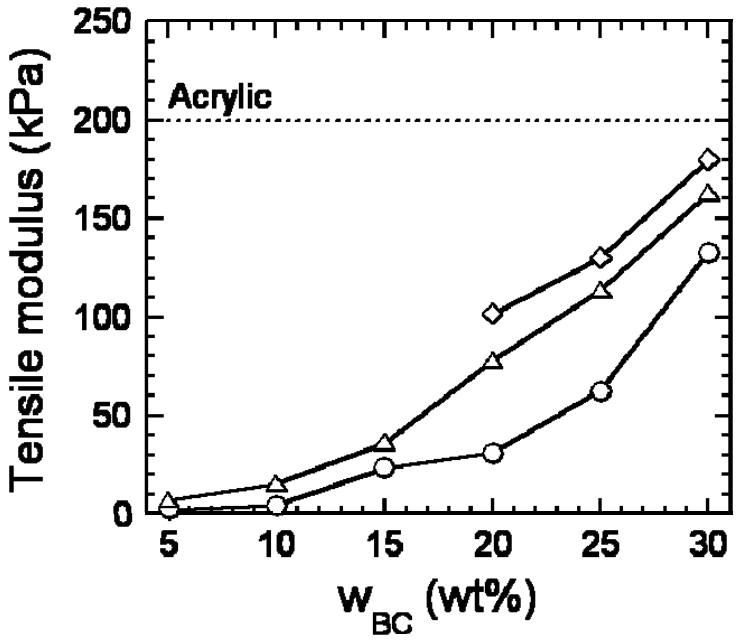

Figure 7.3 Dependence of the tensile modulus (Y_T) on copolymer concentration in the ENP75 (◇), ENP161 (△) and ENP217 (○) systems at ambient temperature. The solid lines connect the data, whereas the dashed line identifies the modulus for the acrylic elastomer.

For semidilute polymer solutions in the presence of a θ or good solvent, n is theoretically expected to range from 2.25 to 2.33, but has been experimentally measured from 2.0 to 2.5,[20,22,37] which is consistent with the data reported here. Corresponding values of Y_C^0 range from 2.02 to 3.77 MPa. Under the condition that Poisson's ratio is ½, $Y_C \approx 3G$, which implies that the plateau shear modulus (G_N^0) of poly(ethylene-*co*-butylene), neglecting contributions from the S microdomains in the copolymer matrix, should be in the vicinity of 0.67 - 1.26 MPa at ambient temperature. This range agrees reasonably well with the measurements of Fetters et al.,[38] who report that G_N^0 for poly(ethylene-*alt*-butylene) is 0.58 MPa, but increases to 0.69 - 1.12 MPa if the number of ethyl branches/100 carbon atoms along the backbone is less than 25, at 25°C.

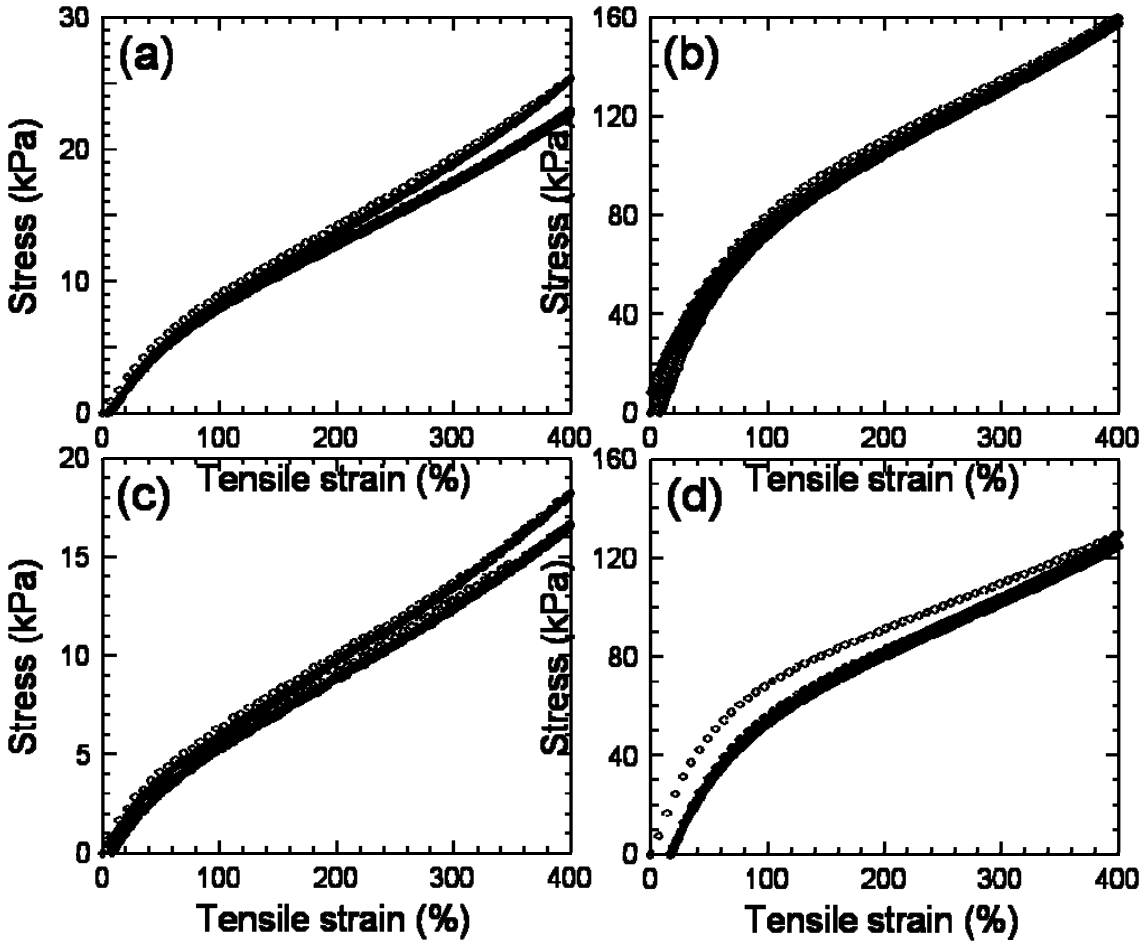

Figure 7.4 Nominal (engineering) tensile stress-strain curves measured from the ENP161 and ENP217 systems at 10 and 30 wt% copolymer concentrations (labeled) upon cycling 100 times to 400% strain. The degree of hysteresis is given by the nonrecoverable strain, the permanent deformation (shown as a shift in the data along the abscissa) introduced upon repeated extension.

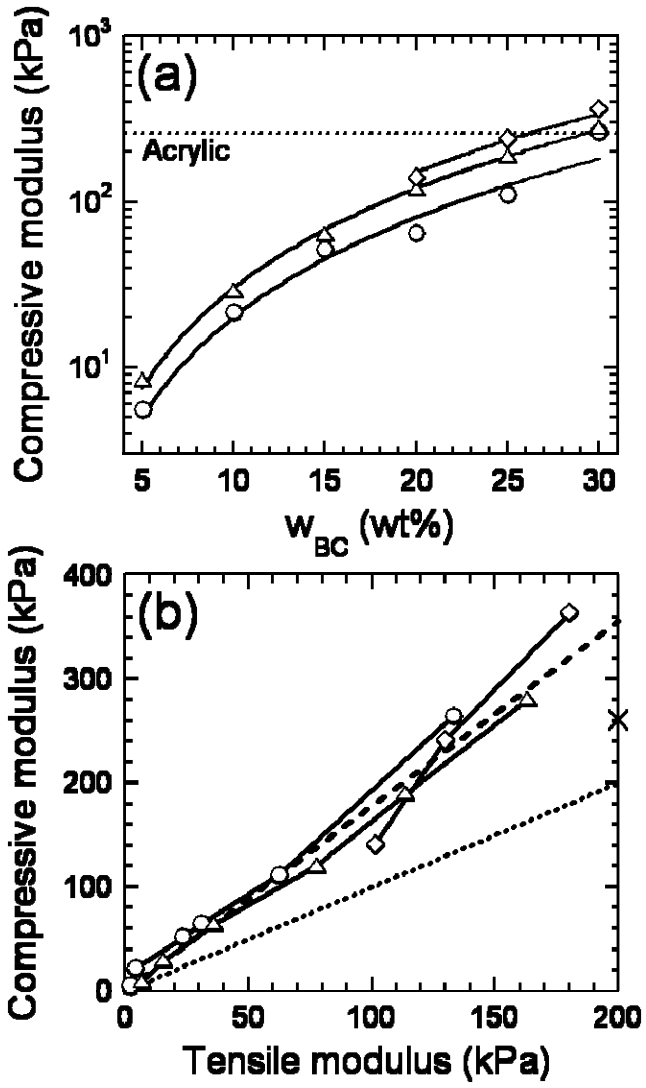

Figure 7.5 In (a), the compressive modulus (Y_C) presented as a function of copolymer concentration for the ENP75 (◇), ENP161 (△) and ENP217 (○) series. The solid lines are power-law fits to the data (with a scaling exponent of 2). The dashed line corresponds to the modulus measured for the acrylic dielectric elastomer. In (b), the compressive modulus is displayed in terms of the nominal (engineering) tensile modulus for the same ENP series as in (a). The solid lines serve to connect the data, whereas the dashed and dotted lines identify the best linear fit of the data and the condition where $Y_C = Y_T$, respectively. Included for comparison is a single datum point measured for the acrylic elastomer (x).

The data presented in Figs. 7.3-7.5 clearly indicate that the mechanical properties of ENPs can be readily tailored over a relatively broad range by judicious choice of copolymer

molecular weight and concentration. This inherent versatility is in marked contrast to conventional dielectric elastomers derived from homopolymers, although we recognize that systematic changes in cross-link density in silicone elastomers, for instance, can likewise provide limited tunability (usually at the cost of detrimentally affecting electroresponsive behavior or stability). In addition, the very high tensile strains (2000-4000%) and strain energies achieved at failure for some of the ENPs further attest to the superior potential of triblock copolymer organogels as actuator materials. Since the Maxwell stress is compressive in nature, the electromechanical property evaluations reported in the next section will utilize the compressive modulus as required.

7.5.2 Electromechanical Behavior

As previously mentioned, a commercial acrylic adhesive presently constitutes the benchmark dielectric elastomer,[39] in which case direct comparisons between the ENPs and the acrylic elastomer will be provided throughout this section. Because of their lower rigidity, only the ENP161 and ENP217 systems will be considered further at this point. According to Eq. 6, electric field-induced actuation depends on $\in$ of the material, as well as the applied electric field strength. Values of $\in$ measured for the ENP161 and ENP217 series at ambient temperature are presented as a function of w_{BC} in Fig. 7.6 and exhibit no discernible concentration dependence. These values are lower than those measured here for the acrylic elastomer and reported elsewhere[39] for both acrylic and silicone dielectric elastomers. Unlike the acrylic elastomer, however, $\in$ determined for the ENPs is virtually independent of frequency.[24] On the basis of the comparison provided in Fig. 7.6 and the parameters required to generate a Maxwell stress (Eq. 6), the electromechanical response of the ENPs is naïvely anticipated to be lower than that of the acrylic and silicone elastomers. An important concept to recall before assessing actuation efficacy is that all dielectric elastomers are mechanically pre-strained prior to electrical actuation to reduce specimen thickness and thus increase the magnitude of the electric field at constant voltage. (Prior studies[49] further indicate that $\in$ can likewise be decreased through the use of mechanical pre-strain, but this result remains open to general confirmation.) In keeping with this practice,

the data reported below have been acquired from ENPs and the acrylic elastomer upon 300% biaxial pre-strain using a home-built straining stage.[29]

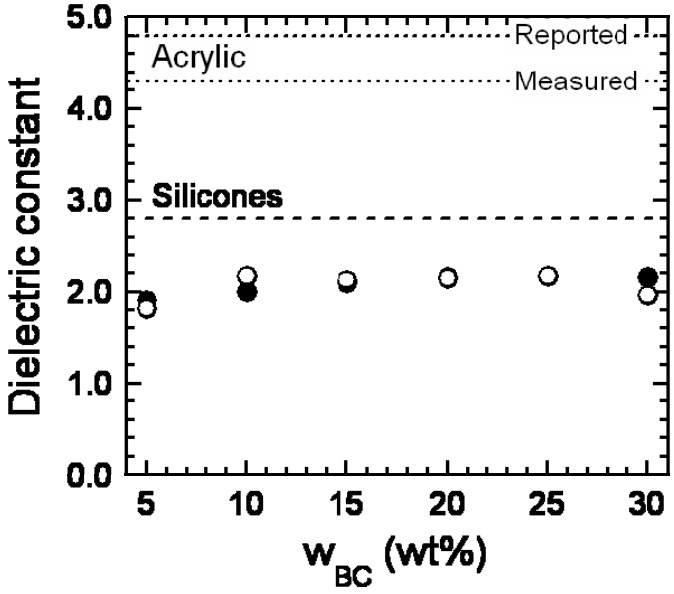

Figure 7.6 Dependence of the dielectric constant ($\in$) measured for the ENP161 (●) and ENP217 (○) series as a function of copolymer concentration. Included are data previously reported[50] and measured here for the acrylic dielectric elastomer, as well as data provided elsewhere[50] for silicone elastomers.

After pre-straining, compliant electrodes are applied to both sides of the film. A cross-sectional BSE image of the top portion of this layered construct is provided in Fig. 7.7 and reveals that the electrode, which consists mainly of aggregated Ag particles (each measuring ~0.3 μm in diameter), is about 15-20 μm thick. The sharp delineation between the silicone-based electrode and the swollen copolymer film verifies that the electrode does not diffuse to any discernible extent into the copolymer film. Recall that s_{act} is measured directly from real-time images, such as the ones displayed for the ENP217 system with 5 wt% copolymer collected at initial and near dielectric breakdown (where the specimen fails) conditions in Fig. 7.8. In this figure, s_{act} is also presented as a function of applied electric field for ENP217 systems differing in copolymer concentration.

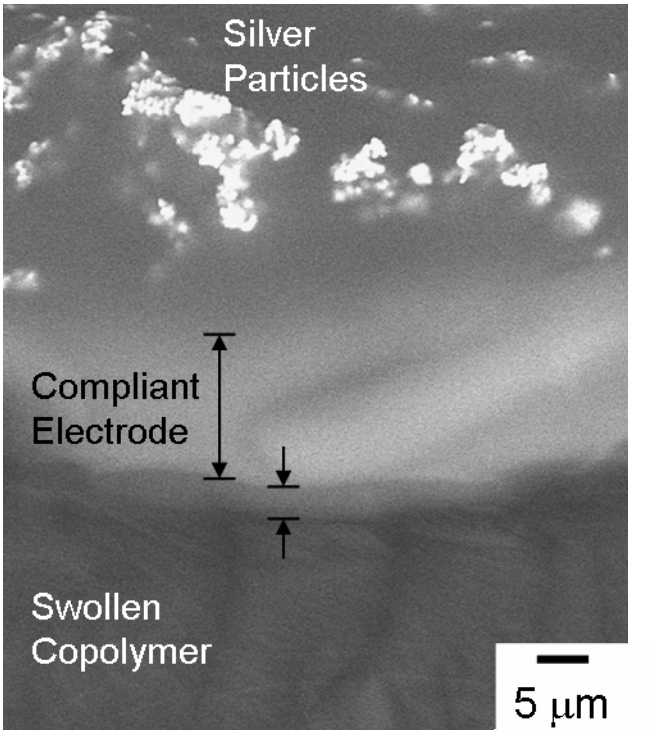

Figure 7.7 Cross-sectional BSE image of the ENP75 system with 35 wt% copolymer coated with a compliant electrode (Ag particles embedded in silicone). The MO-swollen copolymer is completely carbonaceous (dark), whereas the more electron-dense compliant electrode (arrow) appears light and the Ag particles within the electrode are bright. During fracture under liquid nitrogen, the pliable silicone layer formed protrusions, an example of which is seen in this image (arrowheads).

Several features of these data are particularly noteworthy. The first is that copolymer concentration has a systematic effect on the electromechanical response of the ENPs. At low w_{BC} (and correspondingly low modulus values), ultrahigh actuation strains (> 200 area%) are achieved at relatively low electric field strengths (< 40 V/μm). As w_{BC} is increased, however, the maximum s_{act} attained decreases, but the dielectric breakdown strength markedly improves. Complementary results provided in Fig. 7.9 confirm that (*i*) the polarity of the applied electric potential has no effect on the magnitude of the ENP actuation response and, coupled with images such as those shown in Fig. 7.8, (*ii*) these ENPs actuate isotropically along their lateral and transverse directions. The images portrayed in Fig. 7.8 illustrate that the active region of the ENP enlarges because the film thickness decreases due to the electric

field-induced development of a Maxwell stress. Maximum σ_M values, evaluated at the dielectric breakdown strengths measured from real-time video sequences in conjunction with Eq. 6, are displayed as a function of w_{BC} for the ENP161 and ENP217 series in Fig. 7.10 and typically measure on the same order as the Y_C values in Fig. 7.5.

Included in this figure is the maximum σ_M value discerned for the acrylic elastomer. The electric fields shown in Fig. 7.8 and used to compute the σ_M values presented in Fig. 7.10 are determined by dividing the applied voltage by the initial film thickness prior to actuation (t_0 in Fig. 7.1a). While this is a standard convention, several efforts[39,46] have previously documented dielectric breakdown strengths on the basis of the true film thickness (t in Fig. 7.1a). Corresponding σ_M values computed in this fashion by Eq. 9 and the definition of s_z are also provided in Fig. 7.10. Since the method by which the dielectric breakdown field is calculated can account for more than an order of magnitude difference in σ_M at large actuation strains (low w_{BC}), caution must be exercised in drawing quantitative comparisons among actuation data tabulated for dielectric elastomers in the literature. Throughout the remainder of this study, all electric fields are reported relative to t_0.

The dependence of the maximum actuation and transverse strains on w_{BC} for the ENP161 and ENP217 series containing MO is shown in Figs. 7.11a (s_{act}) and 7.11b ($|s_z|$). In both cases, the electric field-induced displacements decrease monotonically with increasing w_{BC} and, at the lowest w_{BC} examined here, exceed the actuation performance of both the acrylic and silicone dielectric elastomers.

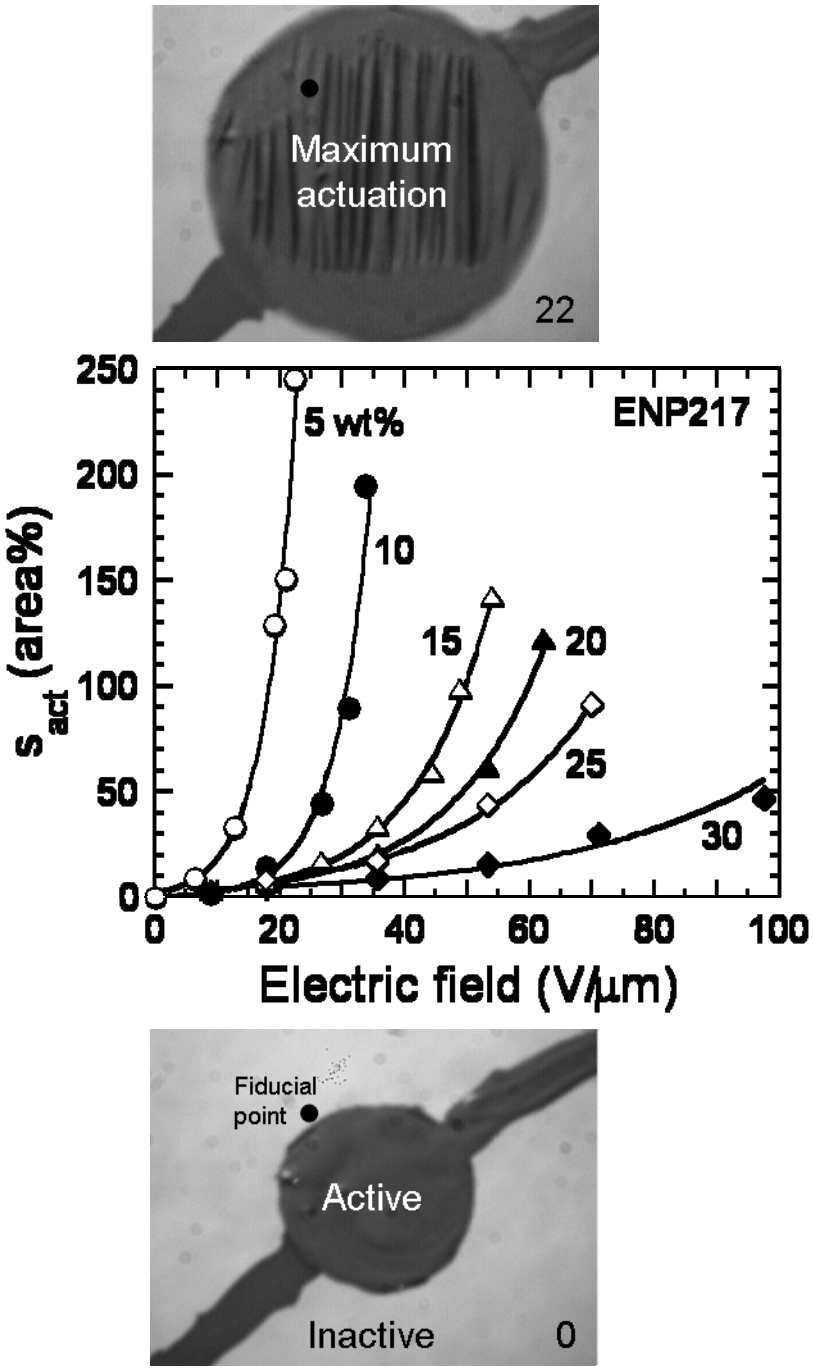

Figure 7.8 Actuation strain (s_{act}) measured for the ENP217 series (300% biaxial pre-strain) as functions of applied electric field and copolymer concentration (labeled). The solid lines serve as guides for the eye. The images of the ENP217 systems containing 5 wt% copolymer correspond to pre-actuation (0 V/μm, bottom) and maximum actuation (22 V/μm, top). The active and inactive actuation areas, as well as a reference feature to facilitate comparison between the two images, are displayed in the bottom image.

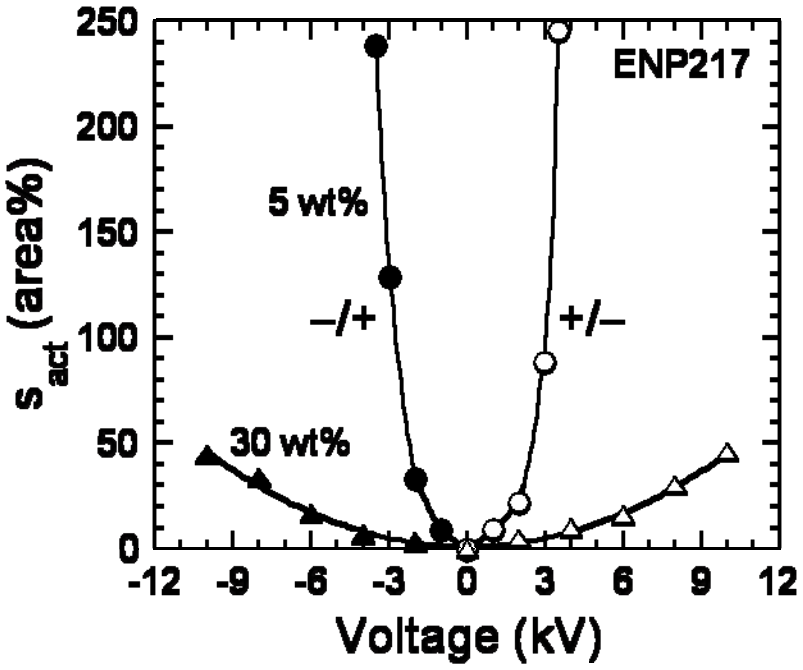

Figure 7.9 Dependence of the actuation strain (s_{act}) measured for the ENP217 series (300% biaxial pre-strain) with 5 and 30 wt% copolymer (circles and triangles, respectively) at opposite electric polarities (labeled). The solid lines serve as guides for the eye.

The MO employed in all the organogels discussed thus far contains a small alicyclic fraction that may exhibit limited compatibility with the S endblocks of the copolymers and consequently locate within (and plasticize) the glassy micelles.[15] To discern the effect of such plasticization on actuation behavior, the ENP217 series has also been prepared with a purely aliphatic αO (see the Experimental section). According to Fig. 7.11, the field-induced lateral and transverse displacement levels achieved with the αO-derived organogels is significantly lower than those realized with the corresponding ENP217 systems containing MO, but is nonetheless comparable at low w_{BC} to the actuation performance exhibited by silicone elastomers. This pronounced difference, coupled with the generally low (electro)mechanical hysteresis behavior of these ENPs, suggests that slightly plasticized micelles capable of

reversible deformation (or possibly limited chain pullout) upon mechanical pre-strain or electrical actuation may be required to achieve large lateral and transverse strains upon electrical stimulation. The extent of micelle deformation during pre-strain and actuation in ENPs is currently under investigation. The results presented in Fig. 7.11 indicate that the ENP217/MO series consistently attains greater electric field-induced displacement than the ENP161/MO series, thereby establishing that the ENP series with the lower modulus exhibits the larger electromechanical response.

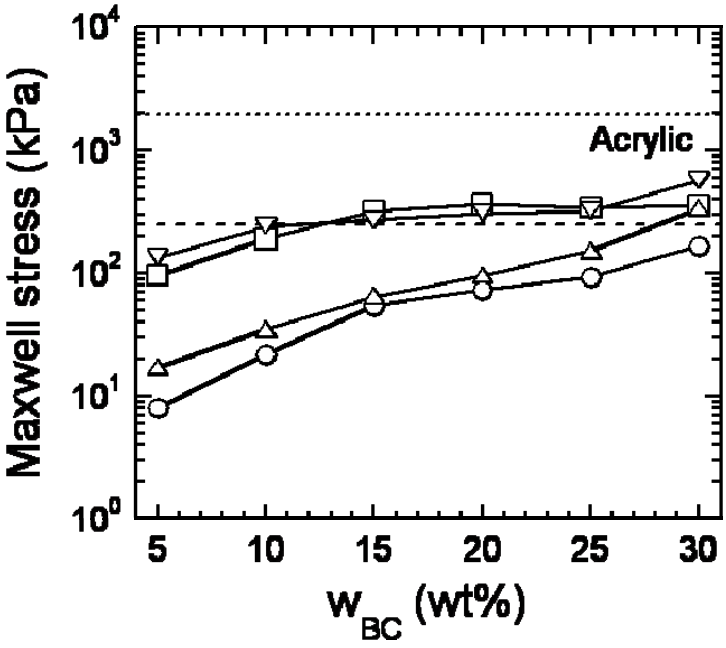

Figure 7.10 The Maxwell stress (σ_M) as a function of copolymer concentration for the ENP161 (△, ◇) and ENP217 (○, ■) series (300% biaxial pre-strain) evaluated at the dielectric breakdown field computed in terms of the initial specimen thickness (△, ○) and the true specimen thickness (◇, ■). Corresponding values measured for the acrylic elastomer (300% biaxial pre-strain) are displayed as dashed and dotted lines, respectively.

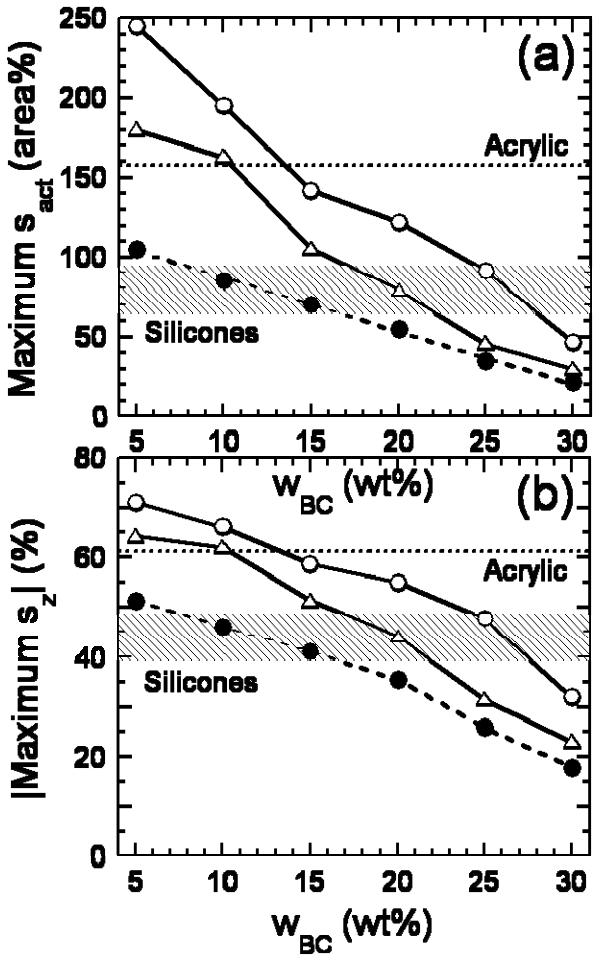

Figure 7.11 Maximum actuation and transverse strains (s_{act} and $|s_z|$, respectively) presented as functions of copolymer concentration for the ENP161/MO (△), ENP217/MO (○) and ENP217/αO (●) series (300% biaxial pre-strain) in (a) and (b), respectively. The solid and dashed lines serve to connect the data, whereas the dotted line and shaded region correspond to acrylic (300% biaxial pre-strain) and silicone[39] dielectric elastomers, respectively.

Conversely, the series achieving larger actuation displacement displays the lower dielectric breakdown field, as evidenced in Fig. 7.12a. At high w_{BC}, the breakdown fields measured for both ENP series are comparable in magnitude to those previously reported for silicone and acrylic dielectric elastomers. At low w_{BC}, however, the glassy micelles are separated by greater distance due to a higher degree of swelling, and the breakdown fields of

both ENP series are considerably lower. Replacement of MO by αO in the ENP217 series reduces the breakdown field over the entire copolymer concentration range examined here.

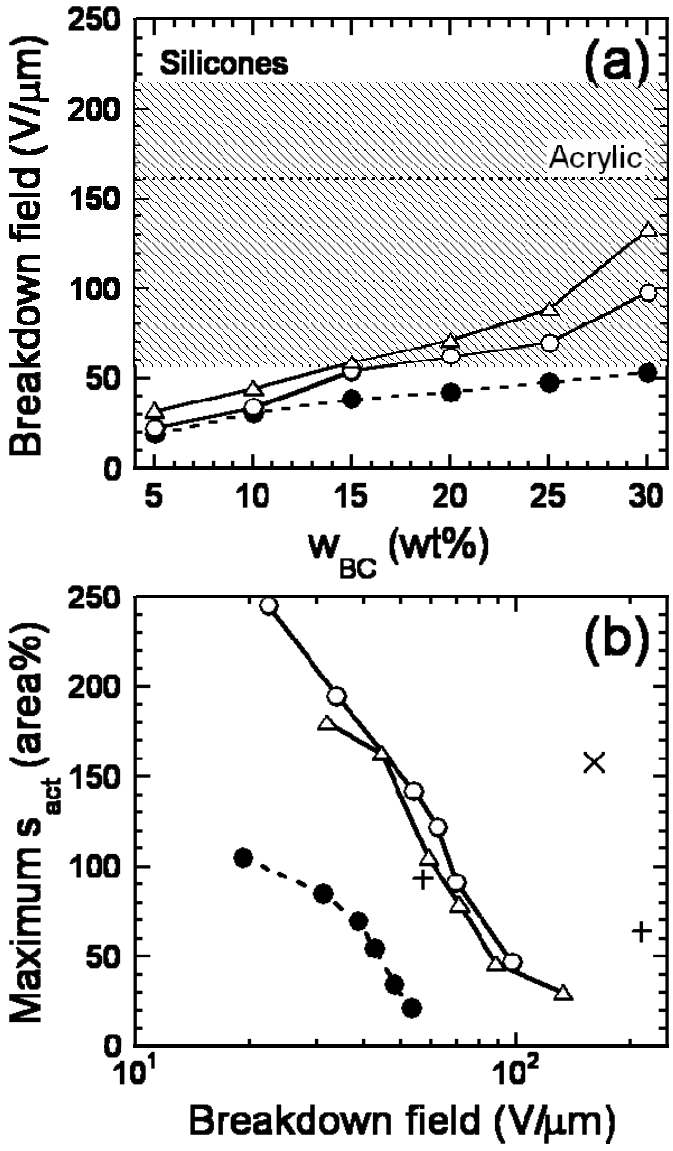

Figure 7.12 In (a), the dielectric breakdown field (relative to the initial specimen thickness) displayed as a function of copolymer concentration for the ENP161/MO (Δ), ENP217/MO (○) and ENP217/αO (●) series (300% biaxial pre-strain). The solid and dashed lines serve to connect the data, whereas the dotted line and shaded region correspond to acrylic (300% biaxial pre-strain) and silicone[39] dielectric elastomers, respectively. In (b), the maximum actuation strain shown in terms of the dielectric breakdown field for the same series as in (a). The acrylic (x) and silicone (+) elastomers are included for comparison.

For completeness, the maximum s_{act} is provided as a function of breakdown field for the ENP161/MO series, the ENP217 series with both MO and αO, the acrylic elastomer and two different silicone elastomers in Fig. 7.12b. It is interesting to note that results from the ENP series containing MO overlap, whereas those from the ENP217 series containing αO are translated to lower displacement and lower breakdown field due presumably to the absence of alicyclic compounds. This result suggests that the actuation behavior of ENPs can be controllably shifted by judiciously altering solvent quality.[19] Included in Fig. 7.12b are data reported for the acrylic elastomer[39] (at high displacement, 158 area%, and high field, 161 V/μm) and a silicone elastomer[39] (at low displacement and high field).

Another metric of dielectric elastomer actuation performance is the electromechanical coupling efficiency (K^2), defined[25,39] as the ratio of stored mechanical energy to input electrical energy. This parameter provides a measure of energy conversion efficiency and is related to s_z by

$$K^2 = -2s_z - s_z^2 \qquad (12)$$

The dependence of K^2 on w_{BC} for the ENP161/MO series and the ENP217 series with MO and αO, along with both acrylic and silicone elastomers, is displayed in Fig. 7.13 and reveals that K^2 generally decreases with increasing w_{BC}. The results shown in this figure confirm that the ENPs introduced here attain efficiencies that are comparable, if not superior, to existing dielectric elastomers. The low-modulus ENPs with the largest s_{act} achieved possess the highest K^2 values reported to date (for the ENP217 system containing 5 wt% copolymer, $K^2 \approx 92\%$). Moreover, K^2 is found to decrease with (*i*) decreasing copolymer molecular weight (increasing modulus) and (*ii*) replacement of MO by αO in the ENP217 series over the entire copolymer concentration range examined. The energy density (F) complements K^2 by providing a measure of the work generated per actuation cycle per unit volume of actuator (exclusive of overhead peripherals).[50] At large actuation strains such as those observed with the present ENPs, as well as acrylic and silicone elastomers, F is given by

$$F = -\sigma_M \ln(1 + s_z) \qquad (13)$$

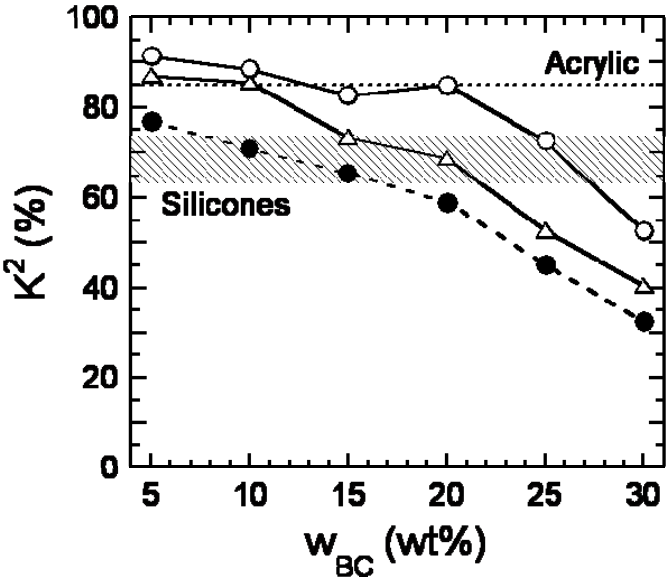

Figure 7.13 Dependence of the electromechanical coupling efficiency (K^2) on copolymer concentration for the ENP161/MO (△), ENP217/MO (○) and ENP217/αO (●) series (300% biaxial pre-strain). The solid and dashed lines serve to connect the data, whereas the dotted line and shaded region correspond to acrylic (300% biaxial pre-strain) and silicone[39] dielectric elastomers, respectively.

Values of F determined for both ENP series with MO are provided as a function of w_{BC} in Fig. 7.14 and compare favorably with those reported for silicone elastomers. It should be noted, however, that these values are substantially lower than those exhibited by the acrylic elastomer: previously reported[39] as 3.4 MJ/m^3 and measured here as 1.9 MJ/m^3. All the ENPs discussed thus far require large pre-strains to realize their superior actuation performance. As alluded to elsewheree,[24] though, pre-straining an elastomer film can alternatively promote a reduction in the quality of actuation performance (due to stress relaxation) and the life of the dielectric elastomer (due to greater wear at the elastomer/solid frame interface). We have recently demonstrated that, due to its intrinsic rigidity (*cf*. Figs. 7.3 and 7.5), the ENP75 series (with MO) undergoes moderate actuation (s_{act} < 20 area% and K^2 < 30%) without mechanical pre-strain prior to electrical stimulation. At such small actuation strain levels, F can be determined directly from Hooke's law, in which case[24,25]

$$F = Y_C s_z^2/2 \qquad (14)$$

Included in Fig. 7.14 to illustrate the importance of mechanical pre-strain in the actuation efficacy of dielectric elastomers are values of F measured for the ENP75 series and acrylic elastomer without mechanical pre-strain prior to actuation. While a considerable reduction in F is evident in the absence of mechanical pre-strain, the ENP75 series nonetheless outperforms the acrylic elastomer over most of the copolymer concentration range explored. The abrupt decrease in F in the ENP75 series with increasing w_{BC} may reflect an increase in the extent of entangled loops along the coronas of the glassy micelles or the onset of microphase ordering, both of which could inhibit deformation of the copolymer network upon actuation. While this feature remains under investigation, the results displayed in Fig. 7.14 confirm that a trade-off in ENP actuation performance exists: ultrahigh s_{act} and K^2 both increase at the expense of F and vice-versa.

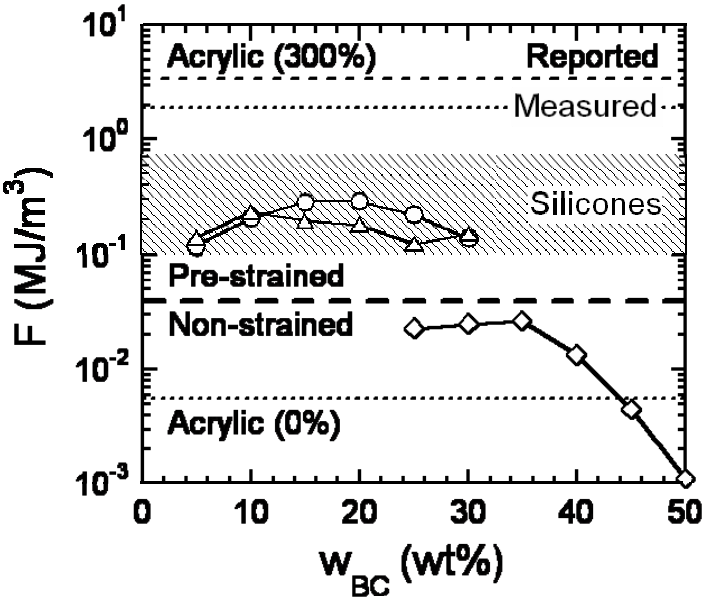

Figure 7.14 Energy density (F) values displayed as a function of copolymer concentration for the ENP161/MO (△) and ENP217/MO (○) series. The light dashed and dotted lines (labeled) and the shaded region correspond to acrylic and silicone[39] dielectric elastomers, respectively. Dielectric elastomers shown above the heavy dashed line have been subjected to mechanical pre-strain (300% biaxial for both the ENP and acrylic elastomers) prior to actuation. At conditions included below the heavy dashed line, the ENP75 (◇) and acrylic elastomers are relaxed (0% pre-strain) prior to actuation. The solid lines serve to connect the data.

7.6 Conclusions

Due primarily to their exceptional adhesive, shape-memory and vibration-dampening attributes, triblock copolymer organogels have found tremendous use in a wide range of present-day technologies. In this work, we demonstrate that they are likewise stimulus-responsive materials that can be used as dielectric elastomers in the light-weight, flexible and efficient actuators required in the ongoing development of microrobotic systems (e.g., micro air vehicles), microfluidic/haptic/biomedical devices (e.g., active Braille and steerable catheters) and smart prosthetics. The electromechanical data reported here confirm the robust mechanical properties (e.g., low hysteresis, high strain cycling and very high failure strains) and broadly tunable actuation performance of ENPs. Unlike conventional dielectric elastomers derived from chemically cross-linked homopolymers, the present ENPs rely on the microphase-separated network morphology afforded by selectively swollen triblock copolymers, the electromechanical properties of which can be systematically altered through variation in copolymer parameters (e.g., molecular composition, organogel concentration and molecular weight) and/or solvent quality. In this regard, further studies are clearly warranted to elucidate the underlying nanostructure-property relationships governing actuation performance. The relatively nonpolar ENP systems investigated in this work exhibit high actuation strains and coupling efficiencies at relatively low electric fields, which makes them particularly suited for energy-efficient applications requiring substantial displacement with little pushing or pulling. Equally important, these materials compare favorably relative to the benchmark acrylic dielectric elastomer, as well as to various silicone elastomers, and even show evidence of modest actuation in the absence of mechanical pre-strain. The ENP design strategy described herein provides an attractive and viable route to high-performance dielectric materials with physically tunable properties.

7.7 Acknowledgments

This work was supported by the U. S. Department of Commerce through the National Textiles Center.

7.8 Notes

This chapter is submitted to *Macromolecules* for publication. It will be published under the authorship of Ravi Shankar,[§†] Arjun S. Krishnan, [‡] Tushar K. Ghosh[%] and Richard J. Spontak[†‡] ([§]Fiber and Polymer Science Program and Departments of [†]Materials Science & Engineering, [%]Textile & Apparel Technology & Management and [‡]Chemical & Biomolecular Engineering, North Carolina State University, Raleigh, NC 27695, USA).

7.9 References

1. Hamley, I. W. In *The Physics of Block Copolymers;* Oxford University Press: New York, 1998; p 221.

2. Holden, G., Legge, N. R., Quirk, R. P. and Schroder, H. E., Eds.; Thermoplastic Elastomers; Hanser: Munich, 1998; Vol. 2, pp 336-364.

3. Mayes, A M; Olvera de la Cruz ; *J. Chem. Phys.* **1991**, 95, 4670-4677.

4. Laurer, J. H.; Bukovnik, R.; Spontak, R. J. *Macromolecules* **1996,** *29*, 5760-5762;

5. Schulz, M. F.; Bates, F. S.; Almdal, K.; Mortensen, K. *Phys. Rev. Lett.* **1994**, 73, 86.

6. Hamley, I. W. *J. Phys.: Condens. Matter.* **2001**, 13, R643-R671.

7. Ueyama, N.; Harada, A., Eds.; Macromolecular Nanostructured Materials; Kodansha: Tokyo, 2004; pp 66-150.

8. Finnefrock, A.C.; Ulrich, R.; Toombes, G.E.S.; Gruner, S.M.; Wiesner, U. *J. Am. Chem. Soc.* **2003**, 125, 13084-13093.

9. Arnold, M. E.; Nagai, K.; Spontak, R. J.; Freeman, B. D.; Leroux, D.; Betts, D. E.; DeSimone, J. M.; DiGiano, F. A.; Stebbins, C. K.; Linton, R. W. *Macromolecules* **2002**, *35*, 3697-3707.

10. Hedrick, J. L.; Miller, R. D.; Hawker, C. J.; Carter, K. R.; Volksen,W.; Yoon, D. Y.; Trollsås, M. *Adv. Mater*. **1998**, *10*, 1049.

11. La, S. B.; Okano, T.; Kataoka, K. *J. Pharm. Sci.* **1996**, *85*, 85-90.

12. Spontak, R. J.; Patel, N. P. *Current Opinion in Colloid & Interface Science* **2000**, *5*, 333-340.

13. Hanley, K. J.; Lodge, T. P. J. Polym. Sci., Part B: Polym. Phys. **1998**, 36, 3101.

14. Laurer, J. H.; Khan, S. A.; Spontak, R. J.; Satkowski, M. M.; Grothaus, J. T.; Smith, S. D.; Lin, J. S. *Langmuir* **1999**, *15*, 7947-7955.

15. Laurer, J. H.; Mulling, J. F.; Khan, S. A.; Spontak, R. J.; Lin, J. S.; Bukovnik, R. *Journal of Polymer Science Part B-Polymer Physics* **1998**, *36*, 2513-2523; Laurer, J. H.; Mulling, J. F.; Khan, S. A.; Spontak, R. J.; Bukovnik, R. *J. Polym. Sci. B: Polym. Phys.* **1998**, *36*, 2379-2391.

16. Jackson, N. R.; Wilder, E. A.; White, S. A.; Bukovnik, R.; Spontak, R. J. *Journal of Polymer Science Part B-Polymer Physics* **1999**, *37*, 1863-1872; van Maanen, G. J.; Seeley, S. L.; Hartmann, J.; Bukovnik, R.; Spontak, R. J. *Macromol. Rapid Commun.* **submitted**.; van Maanen, G. J.; Seeley, S. L.; Capracotta, M. D.; White, S. A.;

Bukovnik, R. R.; Hartmann, J.; Martin, J. D.; Spontak, R. J. *Langmuir* **2005**, *21*, 3106-3115.

17. Soenen, H.; Berghmans, H.; Winter, H. H.; Overbergh, N. *Polymer* **1997**, *38*, 5653-5660.

18. Reynders, K.; Mischenko, N.; Mortensen, K.; Overbergh, N.; Reynaers, H. *Macromolecules* **1995**, *28*, 8699-8701; Mischenko, N.; Reynders, K.; Mortensen, K.; Scherrenberg, R.; Fontaine, F.; Graulus, R.; Reynaers, H. *Macromolecules* **1994**, *27*, 2345-2347; Mortensen, K. *Journal of Polymer Science Part B-Polymer Physics* **2004**, *42*, 3095-3101; Mortensen, K.; Theunissen, E.; Kleppinger, R.; Almdal, K.; Reynaers, H. *Macromolecules* **2002**, *35*, 7773-7781; Mischenko, N.; Reynders, K.; Koch, M. H. J.; Mortensen, K.; Pedersen, J. S.; Fontaine, F.; Graulus, R.; Reynaers, H. *Macromolecules* **1995**, *28*, 2054-2062.

19. Quintana J.R.; Janez M.D.; Katime I. *Polymer*, **1998**, 39, 2111-2117.

20. Vega, D. A.; Sebastian, J. M.; Loo, Y. -.; Register, R. A. *Journal of Polymer Science Part B: Polymer Physics* **2001**, *39*, 2183-2197.

21. Patel, N. P.; Spontak, R. J. Macromolecules 2004, 37, 2829.

22. Webber, R. E.; Shull, K. R.; Roos, A.; Creton, C. *Phys Rev E.* **2003**, *68*, 021805.

23. Shankar, R.; Ghosh, T. K.; Spontak, R. J. *Adv. Mater.* **2007**.

24. Shankar, R.; Ghosh, T. K.; Spontak, R. J. *Macromol. Rapid Commun.* **2007**, *28*, 1142-1147.

25. Shankar, R.; Ghosh, T. K.; Spontak, R. J. *Soft Matter.* **2007**, 3, 1.

26. Morkved, T. L.; Lu, M. ; Urbas, A. M.; Ehrichs, E. E.; Jaeger, H. M.; Mansky, P.; Russell, T. P. *Science* **1996**, *273*, 931.

27. Böker, A.; Elbs, H.; Hansel, H.; Knoll, A.; Ludwigs, S.; Zettl, H.; Zvelindovsky, A. V.; Sevink, G. J. A.; Urban, V.; Abetz, V.; Muller, A. H. E.; Krausch, G. *Macromolecules* **2003**, *36*, 8078-8087; Böker, A.; Elbs, H.; Hänsel, H.; Knoll, A.; Ludwigs, S.; Zettl, H.; Urban, V.; Abetz, V.; Müller, A. H.; Krausch, G. *Phys. Rev. Lett.* **2002**, *89*, 135502

28. Cheng, L. -T.; Tam, W.; Marder, S. R.; Stiegman, A. E.; Rikken, G.; Spangler, C. W. *J. Phys. Chem.* **1991**, *95*, 10643-10652.

29. Shankar, R.; Ghosh, T. K.; Spontak, R. J. *Sens. Actuators A* **submitted**.

30. Levitt, L.; Macosko, C. W.; Schweizer, T.; Meissner, J. *J. Rheol.* 1997, 41, 671-685.

31. Winey, K. I.; Gobran, D. A.; Xu, Z.; Fetters, L. J.; Thomas, E. L. *Macromolecules* **1994**,27, 2392-2397.

32. Treloar, L. R. G. In *The Physics of Rubber Elasticity*, Clarendon Press: Oxford; 2005; p 60.

33. Mooney, M. *J. Appl. Phys.* **1940**, 11, 582-595.

34. Song, M.S.; He, Z.R. *Rheol Acta*, **1990,** 29, 31-45.

35. Diamant, J.; Williams,M.C. *Polym. Eng. Sci.*, **1989**, 29, 235-243.

36. Rubinstein, M.; Panyukov, S. *Macromolecules*, **1997**, 30, 8036 -8044.

37. De Gennes, P. G. *Macromolecules*, **1976**, 9, 587-593

38. Ashbaugh, H. S.; Guo, X.; Schwahn, D.; Prud'homme, R. K.; Richter, D.; Fetters, L. J. *Energy & Fuels*, **2005**, 19, 138-144.

39. Pelrine, R.; Kornbluh, R.; Pei, Q.; Joseph, J. *Science* **2000**, *287*, 836-839.

40. Bar-Cohen, Y. In *Biomimetics Biology inspired technologies;* Bar-Cohen, Y., Ed.; Taylor & Francis Group: Boca Raton, FL, 2005; pp 527.

41. Pons, J. L. In *Emerging Actuator Technologies A Micromechatronic Approach;* Wiley: Chichester, England ; Hoboken, NJ, 2005; Vol. 2, pp 731.

42. Baughman, R. H.; Cui, C.; Zakhidov, A. A.; Iqbal, Z.; Barisci, J. N.; Spinks, G. M.; Wallace, G. G.; Mazzoldi, A.; De Rossi, D.; Rinzler, A. G.; Jaschinski, O.; Roth, S.; Kertesz, M. *Science* **1999**, *284*, 1340-1344.

43. Madden, J. D. W.; Barisci, J. N.; Anquetil, P. A.; Spinks, G. M.; Wallace, G. G.; Baughman, R. H.; Hunter, I. W. *Adv Mater* **2006**, *18*, 870-873.

44. Berdichevsky, Y.; Lo, Y. H. *Adv. Mater.* **2006**, *18*, 122-125.

45. Baughman, R. H. *Synth. Metals* **1996**, *78*, 339-353.

46. Pelrine, R.; Kornbluh, R.; Kofod, G. *Adv. Mater.* **2000**, *12*, 1223-1225.

47. Yang, G.; Yao, G.; Ren, W.; Akhras, G.; Szabo, J. P.; Mukherjee, B. K. *Proc.SPIE* **2005**, *5759*, 134-143.

48. Yang, G.; Ren, W.; Mukherjee, B. K.; Szabo, J. P. *14th IEEE Int. Symp.* **2004**, 237-240.

49. Choi, H. R.; Jung, K.; Chuc, N. H.; Jung, M.; Koo, I.; Koo, J.; Lee, J.; Lee, J.; Nam, J.; Cho, M. *Proc. SPIE-Int. Soc. Optical Eng.* **2005**, *5759*, 283-291.

50. Madden, J. D. W.; Vandesteeg, N. A.; Anquetil, P. A.; Madden, P. G. A.; Takshi, A.; Pytel, R. Z.; Lafontaine, S. R.; Wieringa, P. A.; Hunter, I. W. *Oceanic Engineering, IEEE Journal of* **2004**, *29*, 706-728.

CHAPTER 8

8 Conclusions and Future Work

8.1 Summary of Present Work

Electroactive polymers (EAPs) offer a new class of actuator materials, which display physical response to electrical excitation[1,2]. They can generate stains as high as two orders of magnitude greater than rigid piezoelectric ceramics[1]. They exhibit superior performance than shape memory alloys (SMA) in terms of their resilience, response speed, and lower density. EAPs can be used to design mechanical devices without traditional components such as pneumatic/hydraulic pistons, gears, and bearings. However, low actuation force and robustness are concerns that continue to constrain their practical application. EAPs can be classified in two groups, electronic and ioninc, based on their response mechanism[3]. Electronic EAPs respond due to electrostatic or Coulomb forces developed on application of an electric field, however ionic EAPs are driven by mobility or diffusion of ions. Ionic EAPs require low voltage for their excitation compared to the electronic EAPs. In general, electronic EAPs display better properties than ionic EAPs in terms of their high actuation strain, reliability and durability, efficiency, and response time. Unlike ionic EAPs, electronic EAPs can operate for a long time in ambient condition and do not require any electrolyte medium for actuation. Another important advantage of electronic EAPs over ionic EAPs is that they can hold strain under DC activation. Among electronic EAPs, dielectric elastomers such as acrylic foams, various silicones, polyurethanes, ethylene propylene, fluroelastomers, and isoprene, have shown the most promising properties. Dielectric electroactive polymers or D-EAPs produce large actuation strain on application of an electric field due to Maxwell stress effect. In general, D-EAPs show superior performance than other EAPs, in terms of high actuation strain, fast response time, high energy density, and high efficiency[3,4]. Acrylic elastomer is known to be superior amongst electric EAPs due to its highest areal actuation strain (~160 %), highest elastic energy density (3.4 MJ/m^3), and highest actuation pressure (7 MPa)[4]. However, almost all the D-EAPs reported in the literature are homopolymers based materials such as acrylic, silicone, and polyurethane. As a result, they offer limited potential

for manipulation of key electrical and mechanical properties. In addition, all of the D-EAPs require very high electric field for actuation. Nevertheless, D-EAPs offer wide range of potential applications in the areas of robotics, aerospace, automotive, entertainment, haptic and tactile interface, biomimetic, and smart structures[1].

In this work (in chapter 4), we have demonstrated that physically cross-linked micellar networks, known as, thermoplastic elastomer gels (TPEG) produced by incorporation of a low-volatility, aliphatic-rich solvent (mineral oil) into a nanostructured poly[styrene-b-(ethylene-co-butylene)-b-styrene] (SEBS) triblock copolymer respond to applied electrical field by changing their dimensions. This discovery of electroactive behavior of a nanostructured thermoplastic elastomer based system with highly tunable electromechanical behavior can meet a wide variety of contemporary and potential future applications. TPEGs of different triblock molecular weights and corresponding to different copolymer fractions are investigated. It is observed that as the solvent content and molecular weight of the copolymer increases, the elastic modulus of the resulting nanostructured systems decreases. These nanostructured materials exhibit excellent displacement under an external electric field, and can be collectively referred to as electroactive nanostructured polymers (ENP). Performance characteristics such as areal actuation strain, thickness strain, energy density, and electromechanical coupling efficiency of ENPs are evaluated under 300% biaxial prestrain condition. Ultrahigh areal actuation strains (~250%), observed for some ENPs at significantly reduced electric fields (22 V/μm), reflect solvent-induced reductions in matrix viscosity and nanostructural order. Comparison of the ENPs investigated here with EAPs previously reported confirms that the ENP217 system with 5 wt% copolymer yields the highest areal actuation of all dielectric EAPs currently known. It is also evident that the areal actuation decreases (exponentially over most of the copolymer concentration range explored) for both ENP series (copolymer molecular weights 161 and 217 kDa) as the modulus increases. Dielectric strength of both ENPs increases with increasing copolymer fraction.

Electromechanical coupling efficiencies, which relate the conversion from electrical input to mechanical output, have been calculated from experimental data. The ENPs introduced here exhibit coupling efficiencies that are comparable, if not superior, to existing EAPs. In particular, the ENP217 system with 5 wt% copolymer possesses the highest

coupling efficiency reported thus far (92%). In addition to energy conversion, another important dielectric EAP characteristic is mechanical and electrical hysteresis. The mechanical hysteresis behavior of the ENPs reveals that under cyclic loading/unloading at constant strain (100 cycles at 400% strain) these materials exhibit far less nonrecoverable strain than acrylic elastomer, which suffers from high viscoelastic losses[1]. In fact, ENPs with 5 wt% copolymer does not show any nonrecoverable strain. Similar result is recorded for the ENPs subjected to cyclic actuation cycling (i.e. 100 cycles), which is of considerable importance in the application of EAPs.

Comparison of ENPs with homopolymer based EAPs demonstrates that these ENPs exhibit a broad range of composition-tunable electromechanical behavior. An increase in copolymer molecular weight (i.e., the population of polarizable phenyl rings within each micelle and correspondingly the length of the swollen EB midblock) or, conversely, a reduction in copolymer concentration significantly improves actuation strain at low electric field in both ENP series.

ENPs investigated in the present work exhibit highly tunable alternative to conventional homopolymer-based dielectric elastomers (explained in details in the Chapter 4). However, these polymeric actuator materials currently require mechanical prestrain prior to actuation, which restricts their practical application. In the Chapter 5, we demonstrate that ENPs of a relatively low-molecular-weight SEBS75 triblock copolymer, swollen in the presence of a primarily aliphatic mineral oil, can produce significant actuation strain with no (0%) mechanical prestrain. This ENP converts a large fraction of input energy into useful mechanical work more effectively than either (i) ENPs containing high-molecular-weight copolymers of comparable composition, or (ii) EAPs based on acrylic dielectric elastomers under no mechanical pre-strain condition. One such ENP exhibits a high elastic energy density (26 kJ/m^3) at 0% prestrain relative to other dielectric EAPs investigated thus far. Under these conditions, the ENPs afford higher electromechanical coupling efficiencies than the benchmark acrylic elastomer. In addition, the ENPs provide frequency-independent dielectric behavior, which is suitable for high-frequency microrobotic applications that require, for instance, flapping wings.

Mechanical and actuation response of these ENP systems is determined under quasi-static and dynamic electromechanical loading conditions and are present in Chapter 6. This chapter

describes effect of type of loading such as tensile and compressive on the mechanical response of ENPs and acrylic. It is observed that the response of VHB 4910 acrylic elastomer and ENPs to uniaxial compressive loading under free compression test conditions, wherein interfacial shear stresses are released, yields compressive moduli that are comparable in magnitude to the corresponding tensile moduli. Biaxial prestrain (300%) followed by compression testing, designed to emulate electrical actuation test conditions, shows that the compressive moduli of prestrained specimens are considerably lower than those of their no-prestrain precursors. Response of the ENPs under quasi-static tensile and compressive loading is similar, and depends on copolymer concentration and triblock molecular weight. Blocking stress measurements reveal that the actuation stress produced by ENPs with 30 wt% copolymer is comparable to that of the VHB 4910 acrylic D-EAP, suggesting that the ENP platform consisting of selectively swollen block copolymer networks may serve as an equally responsive, but more robust and tunable, alternative to conventional D-EAPs

In Chapter 7, electromechanical response of ENPs of three molecular weights (MW) is presented. It is observed that areal actuation of ENPs under no-prestrain condition does not show large variation with the molecular weight of ENPs. It is found that tunable electromechanical behavior can be achieved by not only changing the copolymer MW and their fraction but also by changing the oil type. Alpha olefins are used as a midblock selective solvent instead of mineral oil. It is observed that mineral oil containing ENPs show better performance than that with alpha olefins. It is attributed to the plasticization of the styrenic micelles, due to the presence of alicylic compounds in the mineral oil containing ENPs.

8.2 Future work

As suggested to earlier, the key material parameters that determine performance of EAPs are their dielectric constant and dielectric strength. Fundamental research toward improving these characteristics by both physical and chemical means is very important. Before commencing on ENP modification, a detail fundamental understanding of the current ENPs is required.

8.2.1 Fundamental behavior of nanostructured EAPs

The results of the electromechanical response of ENPs presented here reveal that these materials are superior to the conventional D-EAPs[5]. We hypothesized that the electrical response of ENPs is due to Maxwell stress buildup and/or due to polarization of phenyl rings on the styrenic units located within the glassy micelles. Examination of the literature of solvated copolymers suggests that the micelles are slightly plasticized by the solvent, which thereby imparts limited mobility to the styrenic units[6]. It remains unclear, however, how these units or the supramolecular micelles in which they reside respond to applied electric field. Therefore, it is important to examine the response of the micelles in-situ by synchrotron small-angle x-ray scattering (SAXS). SAXS has been used to probe in the microstructure of block copolymer and their gels under similar conditions such as tensile loading[7,8]. This way dimensional and shape changes could be correlated with the applied electric field and the expected mechanical properties of the micelles to explicate the operational mechanism of the ENPs as functions of copolymer molecular weight and concentration.

8.2.2 Physical Modification of ENPs

It is well documented in the literature that solvents and homopolymers[9] and, more recently, inorganic and organic species[10] can easily modify properties of block copolymers. In this regard, high dielectric and conductive fillers can be judiciously incorporated into the micelles of the ENPs. One such example is homopolystyrene (hPS), which will provide more phenyl rings and, presumably, greater electrostrictive response. To ensure that hPS, as well as other macromolecules, is imbibed within the micelles, design rules regarding chain length and compatibility must be followed. Other additives to be considered include Au and TiO_2 nanoparticles surface-modified with oligostyrene that are conductive in nature.

Experimentally, it has been observed that addition of the conductive filler such as carbon nanotubes and carbon nanofibers to an insulting matrix increases the permittivity in the vicinity of the percolation threshold[11,12]. It is possible to enhance the dielectric properties of the ENP systems by incorporation of these fillers below their percolation threshold.

8.2.3 Design of novel polar blocks containing EAPs

New systems based on polar blocks (either midblock or endblocks) should exhibit higher electrostrictive behavior due to the presence of the polar groups. To improve the elevated temperature properties of SEBS, sulfonation of styrene in the SEBS has been carried out[13,14]. One such modified triblock could be used to enhance the dielectric properties of ENPs. Furthermore, another interesting approach could be the use if sulfonated midblocks. In this case, polar liquid can be used as midblock selective solvents, which could increase dielectric response of the proposed ENPs.

8.3 References

1. Y. Bar-Cohen (ed.), *Electroactive Polymer (EAP) Actuators as Artificial Muscles: Reality, Potential, and Challenges*, SPIE Press, Bellingham, WA, 2004.
2. J. D. W. Madden, N. A. Vandesteeg, P. A. Anquetil, P. G. A. Madden, A. Takshi, R. Z. Pytel, S. R. Lafontaine, P. A. Wieringa and I. W. Hunter, Artificial muscle technology: physical principles and naval prospects, *IEEE J. Ocean. Eng.*, 29 (2004) 706.
3. R. Shankar, T. K. Ghosh and R. J. Spontak, Dielectric elastomers as next-generation polymeric actuators, *Soft. Mater.* (in press).
4. R. Pelrine, R. Kornbluh, Q. Pei and J. Joseph, High-speed electrically actuated elastomers with strain greater than 100%, *Science*, 287 (2000) 836.
5. R. Shankar, T. K. Ghosh and R. J. Spontak, Electroactive nanostructured polymers as tunable actuators, *Adv. Mater.* (in press).
6. J. H. Laurer, J. F. Mulling, S. A. Khan, R. J. Spontak and R. Bukovnik, Thermoplastic elastomer gels. I. effects of composition and processing on morphology and gel behavior, *J. Polym. Sci. B: Polym. Phys.*, 36 (1998) 2379.

7. R. Kleppinger, R., M. van Es, N. Mischenko, M. H. J. Koch and H. Reynaers, Physical gelation in a triblock copolymer solution: In situ study of stress-strain behavior and structural development, *Macromolecules,* 31 (1998) 5805.
8. E. Prasman and E. L. Thomas, High-Strain Tensile Deformation of Sphere-Forming Triblock Copolymer/Minearl Oil Blend, *J. Polym. Sci. B: Polym. Phys.*, 36 (1998) 1625.
9. R. J. Spontak and N. P. Patel, Phase behavior of block copolymer blends, in I. W. Hamley (ed.), *Developments in Block Copolymer Science and Technology*, Wiley, New York, 2004, pp. 159-212.
10. R. J. Spontak, R. Shankar, M. K. Bowman, A. S. Krishnan, M. W. Hamersky, J. Samseth, M. R. Bockstaller and K. Ø. Rasmussen, Selectivity- and size-induced segregation of molecular and nanoscale species in microphase-ordered triblock copolymers, *Nano Lett.*, 6 (2006) 2115.
11. C. G. Cameron, R. S. Underhill, M. Rawji and J. P. Szabo, Conductive filler-elastomer composites for Maxwell stress actuator applications, *Proc. SPIE*, 5385 (2004) 51.
12. R. Shankar, T. K. Ghosh and R. J. Spontak, Percolation Behavior in Conducting Polymer Composites and Nanocomposites: Fundamental Principles to New Opportunities, *Mater. Sci. Eng. R.* (submitted).
13. R. A. Weiss, A. Sen, C. L. Willis and L. A. Pottick, Block Copolymer Ionomers .1. Synthesis and Physical-Properties of Sulfonated Poly(styrene Ethylene/butylene Styrene), *Polymer*, 32 (1991) 1867.
14. R.I. Blackwell and K. A. Mauritz, Mechanical creep and recovery of poly(styrene-b-ethylene/butylene-b-styrene)(SEBS), sulfonated SEBS (sSEBS), and sSEBS/siticate nanostructured materials, *Polym.Adv.Technol.*, 16 (2005) 212.